AD-A034 942 AIR FORCE INST OF TECH WRIGHT-PATTERSON AFB OHIO SCH--ETC F/G 1/2
SYSTEM SIMULATION IN AIRCRAFT LANDING GEAR AND TIRE DEVELOPMENT--ETC(U)
DEC 76 J A SKORUPA

UNCLASSIFIED GAE/MC/76D-7 NL

1 OF 2
ADA034942

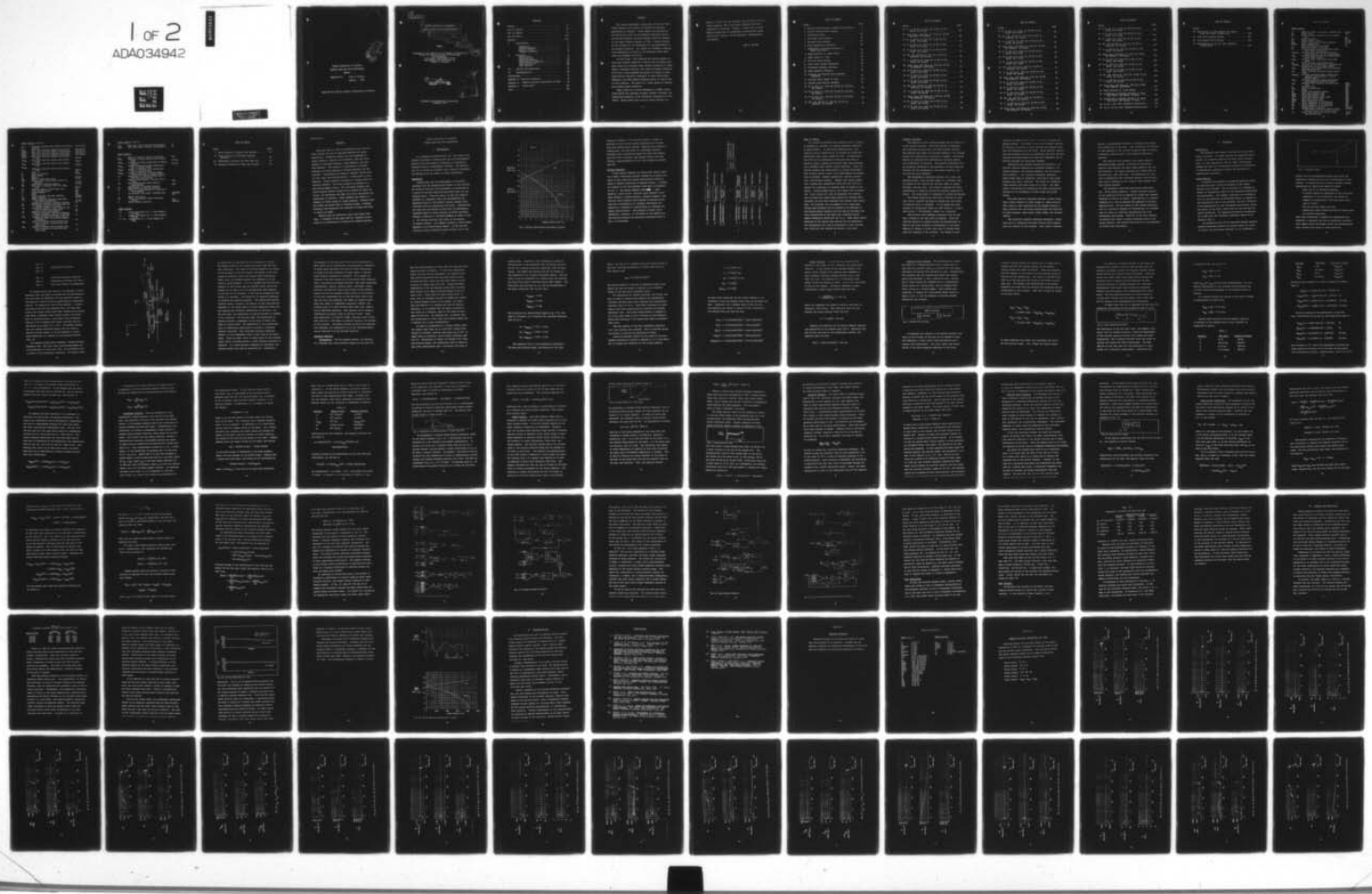

SYSTEM SIMULATION IN AIRCRAFT LANDING GEAR AND TIRE DEVELOPMENT

THESIS

GAE/MC/76D-7 John A. Skorupa

Captain USAF

(17)

GAE/MC/76D-7

(6)

SYSTEM SIMULATION IN AIRCRAFT LANDING GEAR AND TIRE DEVELOPMENT.

(9) Master's Thesis,

(11) Dec 76

(12) 140 p.

THESIS

Presented to the Faculty of the School of Engineering
of the Air Force Institute of Technology
Air University
in Partial Fulfillment of the
Requirements for the Degree of
Master of Science

(10) by

John Anthony Skorupa ~~B.S.~~

~~Captain~~ ~~USAF~~

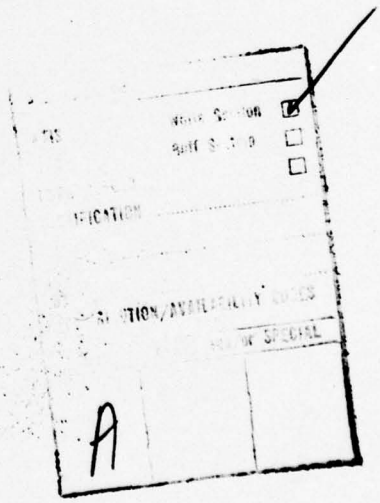

Graduate Aero-Mechanical Engineering
December 1976

012225

B

Contents

Preface

This thesis represents a small part of the Air Force Flight Dynamics Lab's effort to improve the stopping performance of aircraft. Major impetus was provided by the sensitivity study of the stopping parameters done by the Boeing Commercial Aircraft Company under the auspices of the Combat Traction program in 1974. A major finding of this program was the importance of tire performance in the stopping equation. This thesis is intended to improve tire performance by improving the procedure under which tires are designed and tested.

In this study I have employed the analog computer to solve the aircraft equations of motion and to predict main gear loads of an aircraft under varying conditions of gross weight, touchdown velocity, sink rate and runway condition. To do this I have comgined the efforts of Boeing in their Brake Control Simulator, McDonnell in their Motion Base Simulator, and NASA Langley Research Center in their study of tire traction. The result is a three degree of freedom, pure analog system simulation.

Major thanks go to Jerry Schumacher of AFFDL, Mechanical Branch for providing valuable insight, contacts, and information essential to the successful completion of this effort. Major thanks also go to my thesis advisor, Dr.

Robert A. Calico for his guidance and assistance with the analog computer, and to my thesis committee for their constructive criticism. Finally, I would like to thank Barbara Barnes for her assistance in editing and typing and my wife, Barbara, for her patience, understanding, and support.

John A. Skorupa

List of Figures

List of Figures

List of Figures

List of Figures

List of Figures

List of Symbols

Roman Symbols

a	Speed of sound, sea level, standard day	ft/sec
BF	Brake force	lbf
BP	Brake pressure modified by 0.1 second lag	psi.
BP´	Brake pressure	psi.
BT	Brake torque, total	ft-lbf
BT_1	Brake torque due to brake pressure	ft-lbf
BTemp	Brake temperature	°F
$\bar{c}$	Mean aerodynamic wing chord	ft
cg	Aircraft center of gravity	
C_D	Total aircraft drag coefficient minus drag chute contribution	
$C_{D_{BASIC}}$	Aircraft drag coefficient, approach configuration, oat of ground effect	
$C_{D_{ge}}$	Aircraft drag coefficient contribution from ground effect	
$C_{D_{dc}}$	Aircraft drag coefficient from drag chute	
C_L	Total aircraft lift coefficient	
$C_{L_{BASIC}}$	Aircraft lift coefficient, approach configuration; out of ground effect	
$C_{L_{ge}}$	Aircraft lift coefficient contribution from ground effect	
C_M	Total aircraft pitching moment coefficient	
$C_{M_{BASIC}}$	Aircraft pitching moment coefficient, approach configuration, out of ground effect	
$C_{M_{ge}}$	Aircraft pitching moment coefficient contributiondue to ground effect	
C_{p_b}	Specific heat capacity of brake heat sink	BTU/ lbm°F
D	Aircraft drag	lbf
D_{dc}	Drag of drag chute	lbf
F	Force	lbf
F_d	Force from dynamic effects	lbf
$F_{d_{mg}}$	Main gear dynamic load	lbf
$F_{d_{ng}}$	Nose gear dynamic load	lbf
F_s	Force from quasi static load	lbf
$F_{s_{mg}}$	Main gear static load	lbf
$F_{s_{ng}}$	Nose gear static load	lbf
F_x	Force component in x-direction	lbf
F_y	Force component in y-direction	lbf
F_z	Force component in z-direction	lbf
g	Acceleration of gravity	ft/sec^2
GT	Ground torque caused by braking force acting through the rolling radius	ft-lbf
I_w	Wheel mass moment of inertia about the rolling axis	$ft\text{-}lb\text{-}sec^2$

Roman Symbols (cont'd)

I_{yy}	Aircraft pitching mass moment of inertia	ft-lb-sec^2
K	Constant	
$K_{d_{mg}}$	Main gear vertical damping coefficient	lbf-sec/ft
$K_{d_{mg_H}}$	Main gear fore-aft damping coefficient	lbf-sec/ft
$K_{d_{ng}}$	Nose gear vertical damping coefficient	lbf-sec/ft
$K_{d_{ng_H}}$	Nose gear fore-aft damping coefficient	lbf-sec/ft
$K_{s_{mg}}$	Main gear vertical spring rate coefficient	lbf/ft
$K_{s_{mg_H}}$	Main gear fore-aft spring rate coefficient	lbf/ft
$K_{s_{ng}}$	Nose gear vertical spring rate coefficient	lbf/ft
$K_{s_{ng_H}}$	Nose gear fore-aft spring rate coefficient	lbf/ft
L	Lift	lbf
M	Mass of aircraft	slugs
M	Mach number	
M	Moment	ft-lbf
M_b	Mass of brake heat sink	slugs
M_{cg}	Moment about the aircraft center of gravity	ft-lbf
M_p	Aerodynamic pitching moment	ft-lbf
M_s	Main gear, unsprung strut and wheel mass	slugs
R_r	Rolling radius of main gear tire	ft
S	Wing planform area	ft^2
T	Engine thrust	lbf
t	Time	sec
V	True airspeed; aircraft velocity	ft/sec
V_w	Wheel velocity	ft/sec
V_{ws}	Wheel velocity component from fore-aft strut oscillation	ft/sec
X	Horizontal distance; landing distance	ft
X_A	Horizontal distance from main gear to aircraft center of gravity	ft
X_B	Horizontal distance from aircraft center of gravity to nose gear	ft
X_s	Fore-aft strut displacement	ft
Z	Vertical distance; vertical displacement of aircraft center of gravity	ft
Z_{dc}	Vertical distance from drag chute attachment point to aircraft center of gravity	ft
Z_{mg}	Vertical distance from aircraft center of gravity to main gear contact point	ft
Z_{ng}	Vertical distance from aircraft center of gravity to nose gear contact point	ft

Roman Symbols (cont'd)

Z_{smg}	Main gear strut vertical displacement	ft
Z_{sng}	Nose gear strut vertical displacement	ft

Greek Symbols

α	Angle of attack, angle of incidence	deg
ΔBT_F	Decrease in brake torque due to brake fade	ft-lbf
ΔBT_{TP}	Increase in brake torque due to torque peaking	ft-lbf
ΔC_{Dge}	Change in aircraft drag coefficient due to ground effect	
ΔC_{Lge}	Change in aircraft lift coefficient due to ground effect	
ΔC_{Mge}	Change in aircraft pitching moment coefficient due to ground effect	
$\Delta\mu$	Correction in braking coefficient of friction for velocity	
θ	Angular displacement, aircraft pitch angle	rad
θ_w	Main landing gear wheel angular displacement	rad
μ	Coefficient of braking friction	
μ_r	Coefficient of rolling friction	
π	Ratio of circumference of a circle to its diameter	
ρ	Air density, sea level, standard day	$lb\text{-}sec^2/ft^4$
σ	Wheel slip ratio	
Φ_T	Thrust inclination angle from horizontal	deg
ω	Wheel angular velocity	rad/sec

Other Symbols

$\dot{(\ )}$	First derivative of ( ) with respect to time
$\ddot{(\ )}$	Second derivative of ( ) with respect to time
$\int(\ )\,dt$	Integration of ( ) with respect to time

List of Tables

Abstract

Main gear load vs. time is predicted for an F-4E aircraft through the use of subsystem modeling and analog computation. Subsystems modeled are the aerodynamics, engine dynamics, vertical strut dynamics, fore-aft strut dynamics, tire/wheel dynamics, brake dynamics, and antiskid dynamics. The problem is restricted to a landing sequence with three degrees of freedom permitted for the aircraft. Aerodynamics are based on constant coefficients of lift, drag, and pitching moment. A drag chute is also employed. Engine dynamics are based on a linear thrust vs. velocity schedule. The strut dynamics are modeled by a mass-spring-damper system. The tire/wheel dynamics subsystem applies Newton's Second Law to derive the wheel velocity, and calculates the wheel slip ratio and ground-tire coefficient of friction. Brake dynamics are based on a schedule of brake torque vs. brake pressure. Antiskid dynamics model the Hytrol Mark II antiskid system. Stopping distances from simulation are compared to flight test data to verify the model.

Results from the simulation agree with flight test data. A schedule of main gear load vs. velocity is proposed as an alternative to current tire testing practice.

SYSTEM SIMULATION IN AIRCRAFT LANDING GEAR AND TIRE DEVELOPMENT

I. Introduction

In a theoretical-experimental vein, this thesis will explore one aspect of landing gear and tire developmental practice with the purpose of proposing an alternative procedure based on experimental findings. The approach will be to divide the aircraft into a group of subsystems and determine the net effect of their interaction.

Background

Landing gear and tire development is critically concerned with the operating environment of the aircraft. For military aircraft this environment is determined by a series of military specifications which spell out performance goals. These mil specs, as they are commonly referred to, supposedly take into consideration the operating limits of the various aircraft systems which interface with the landing gear and tires. Historically, mil specs for the design of tires have set performance standards based on static analysis of forces projected through a velocity vs. distance schedule as shown in Fig. 1. The glaring omission with these is the absence of dynamic effects. For example, consider a brake system dependent on antiskid system inputs. If the two were designed without considering brake pressure lag or the

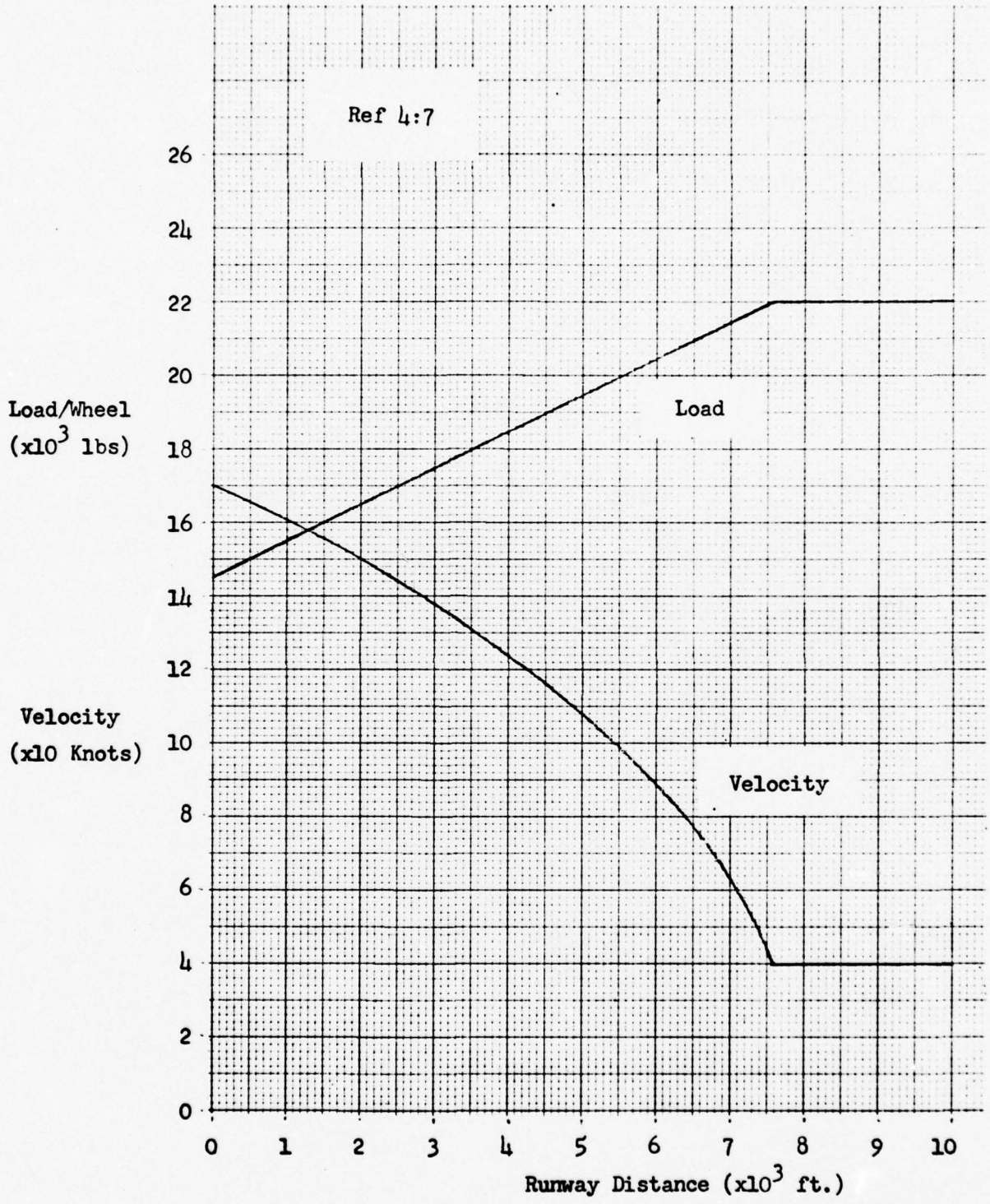

Fig. 1. Military Specification Load/Velocity Schedule

frequency response of the antiskid system, it might be possible to have the two systems operating out of phase such that braking never occured! Applying this analogy to landing gear, the test pilot of a prototype aircraft developed under existing mil specs for tires and landing gear has little assurance that dynamic effects will not interact catastrophically on the first landing or aborted take off.

Problem Statement

A more logical approach to landing gear design would be to model interacting aircraft systems on an analog computer so that realistic design specifications could be based on dynamic simulation of expected forces. A schematic diagram of how this approach could work is presented in Fig. 2. The analog computer simulation of aerodynamics, engine thrust, vertical strut dynamics, tire/wheel dynamics, braking dynamics, antiskid dynamics, and fore-aft strut dynamics would combine to provide either real-time load/velocity vs. distance information for testing or a schedule of load/velocity vs. distance for design specifications. The problem of dynamic force simulation, therefore, is achievable if the modeling of the aircraft dynamics and pertinent subsystems shown in Fig. 2 is performed.

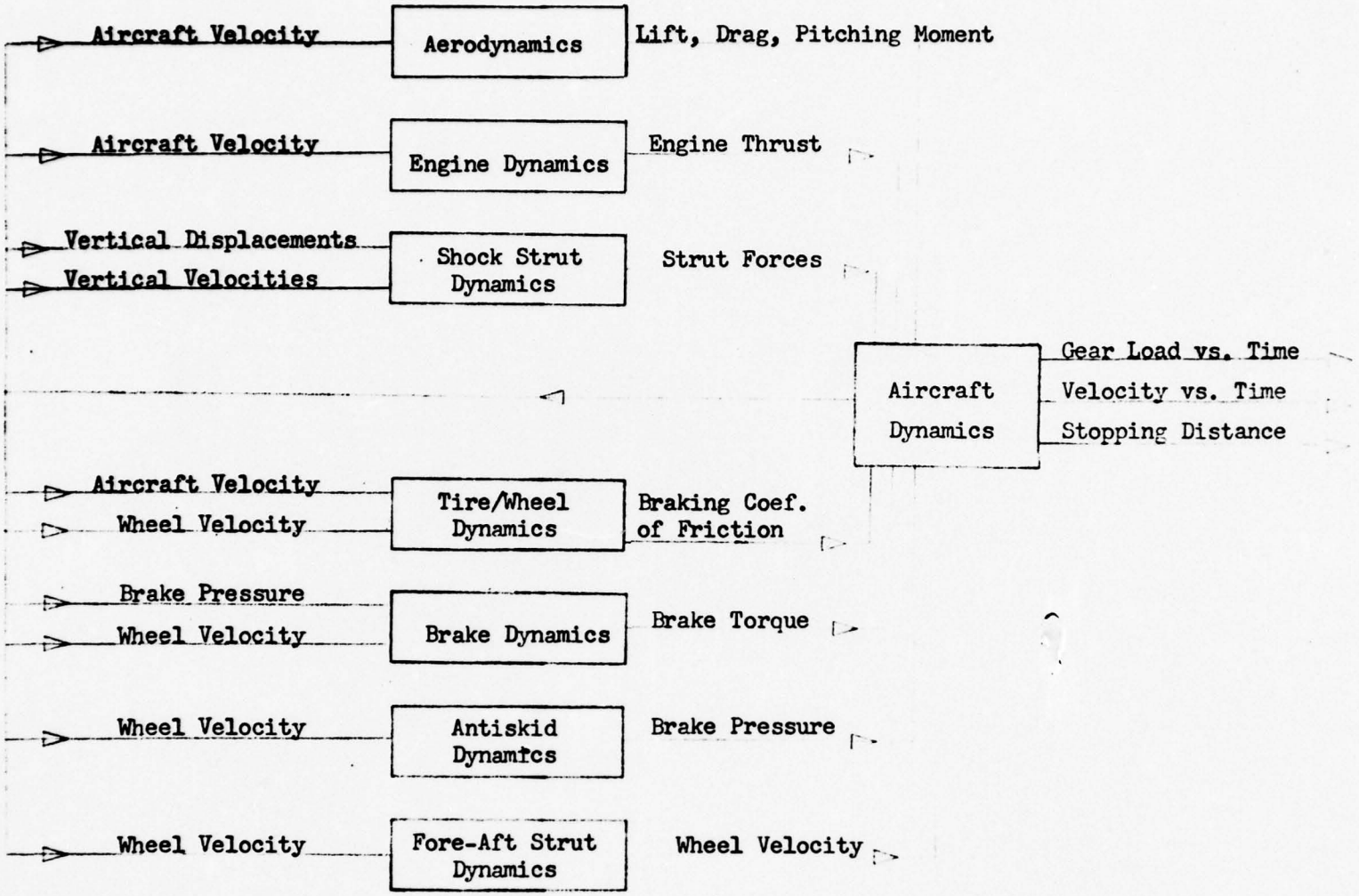

Fig. 2 Aircraft System Block Diagram

Scope of Effort

As a proof of principle this analysis will be limited to studying an aircraft in a landing sequence, operating in ground effect. To facilitate gathering data, this analysis will be restricted to an aircraft for which well accumulated data exists, namely an F-4E. In particular, the F-4E will be considered to have gear down with no external stores, leading and trailing edge flaps deployed and a boundary layer control system operating. Since the landing dynamics are constrained to a runway environment with limited lateral travel, only three degrees of freedom will be assumed: forward translation, vertical translation, and pitching rotation. Despite this latter assumption, landing gear compression limits for the F-4E also warrant the assumption of constant angle of attack on the runway. Pitching moment due to idle thrust will be neglected. Pilot inputs will also be neglected; the controls will be fixed with brakes being applied two seconds after touchdown and drag chute deployed four seconds after touchdown. The aircraft will be assumed to be a rigid body. Landing gear dynamics will be assumed to be analogous to mass-spring-damper dynamics with the mass of the wheel and strut concentrated in the wheel and a massless spring-damper combination simulating the strut. Small angle static deviation of the struts from vertical will be neglected. Tire deformation will also be neglected, so that vertical gear loads will act through the center of the wheel.

Proposed Procedure

The modeling of this landing sequence can be broken into two related sections. The first section is concerned with producing the main gear load and aircraft velocity. This section would model the aircraft dynamics if an average ground-tire coefficient of friction is assumed. The second section is concerned with calculating a variable ground-tire coefficient of friction. The aircraft subsystems that are primarily concerned in the generation of gear loads and velocity are the aerodynamics, the engine dynamics, and the vertical strut dynamics.

The aerodynamics subsystem produces lift, drag, and pitching moment, which are each equal to a constant times the square of the velocity for constant angle of attack, altitude, and wing area. The velocity required for these calculations is found by solving the aircraft equations of motion. The acceleration is integrated to obtain the velocity.

The engine dynamics are also only a function of velocity since a constant altitude is assumed and idle thrust is selected prior to touchdown. At low speeds the relationship is essentially linear, so that (thrust) = (static idle thrust) + (K)(velocity), where K is a constant.

The vertical strut dynamics simulation will be such that a change in the gear load is produced. Since the aircraft dynamics is summing forces and accelerations in each of the three directions corresponding to the three degrees of freedom, a static gear load is already known, given the geometry of the aircraft. The change in gear

load will be added to the static gear load to correct for dynamic effects. The inputs to the strut dynamics required to calculate the change in gear load are the vertical velocity and displacement at the strut. Since vertical translation and pitching rotation are permitted, the strut vertical velocity and displacement will both have components due to vertical movement and rotational movement.

Calculating the variable ground-tire coefficient of friction requires modeling the tire/wheel dynamics, the braking dynamics, the antiskid dynamics, and the fore-aft strut dynamics. The antiskid subsystem, basically, senses wheel speed to determine a skid and to vent brake pressure when one is detected. The output is a modified brake pressure with wheel speed as an input. The wheel speed is determined by integrating the wheel acceleration produced by the difference in brake torque and ground torque.

The brake dynamics subsystem produces a brake torque from a known schedule of brake torque vs. brake pressure. This torque is then corrected for the dynamic effects of fade, pressure lag, and torque peaking which are functions of brake pressure, wheel speed, brake torque, and antiskid cycling.

The tire/wheel dynamics subsystem calculates a wheel slip ratio by comparing the wheel velocity after braking with the velocity of the aircraft. This value is matched

against a preprogrammed schedule to determine the ground-tire coefficient of friction. This coefficient of friction is then supplied to the aircraft dynamics model to provide a corrected braking force in the foreward translation equation.

The fore-aft strut dynamics, once again, employ a mass-spring-damper analogy to produce an oscillatory velocity that modifies the wheel speed sensed at the runway interface. The inputs required are a coefficient of friction and a main gear load. The coefficient of friction is produced by the tire/wheel dynamics, and the main gear load is produced by the vertical strut dynamics and the aircraft dynamics.

The simulation used three Electronics Associates, Inc., TR-48 analog computers. Landing distance produced by the simulation will be compared to flight test stopping distances to verify the model. Load/velocity vs. distance schedules will then be prepared and compared to military specifications. The net result of this system simulation will be a realistic schedule of load/velocity vs. distance that can serve as a military specification for tire development and testing. Since all of the data required to complete this model is easily generated early in the design sequence, this method could serve as a new procedure in landing gear development.

II. Procedure

Introduction

The procedure used herein is divided into four basic areas of concern: (1) force analysis and subsystem designation; (2) subsystem modeling and total system integration; (3) data acquisition; and (4) model verification. Assumptions made will be discussed followed by formulation of mathematical equations of motion and conversion to computational equations.

Force Analysis

To achieve the benefits of subsystem modeling a natural starting point is with an analysis of the forces acting on the aircraft. For an aircraft in a landing sequence, an appropriate choice of the coordinate system will aid considerably. For example, selecting the x-direction to be in the direction of horizontal motion, as opposed to the longitudinal axis of the aircraft, and the z-direction to be perpendicular to the x-direction and pointing toward the center of the earth, forces such as lift and drag are easily reconciled. The remaining y-direction corresponds to a right hand rule Cartesian coordinate system as depicted in Fig. 3.

By recognizing that the no-crosswind landing sequence properly performed involves no rotation about the z-axis or x-axis, nor any motion side-ways, it is reasonable to

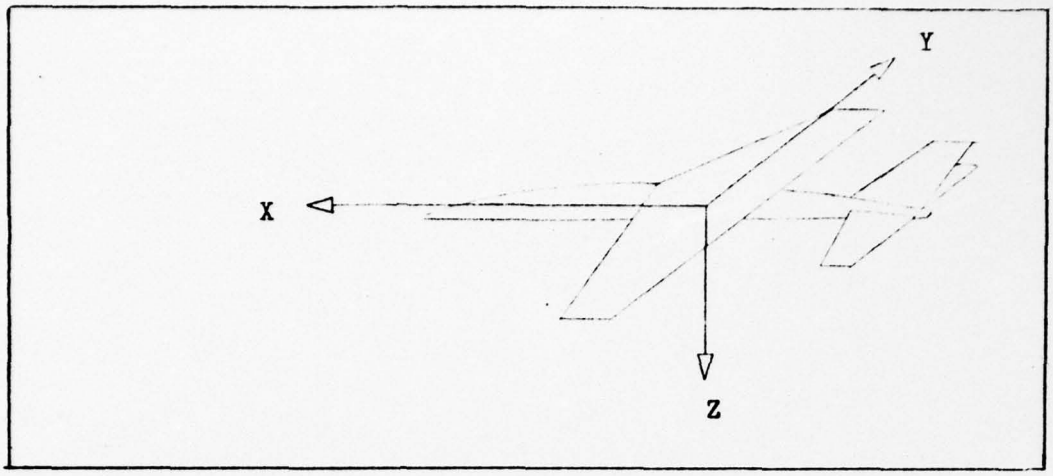

Fig. 3. Coordinate System

assume that the corresponding moments and forces are perpetually balanced and are of no significance to this problem. In specifying this, however, several relevant assumptions are implied and should be stated.

- There can be no crosswind component.
- No forces should be transmitted to the tires with components in the y-direction, nor should any moments be transmitted to the tires about the x-axis or z-axis.
- The yaw and bank angles are zero.
- Symmetrical runway conditions exist on either side of aircraft centerline.

With these assumptions a symmetrical landing/roll-out condition is specified and the six equations, resulting from summing forces and moments about the aforementioned axes, uncouple and reduce to three equations.

$$\Sigma F_x = 0$$

$$\Sigma F_z = 0 \qquad \text{Longitudinal Equations}$$

$$\Sigma M_y = 0$$

$$\Sigma F_y = 0 \qquad \text{Lateral-Directional Equations}$$

$$\Sigma M_x = 0 \qquad \text{(Perpetually balanced, not rele-}$$

$$\Sigma M_z = 0 \qquad \text{vant with respect to assumptions)}$$

To further define the forces it is necessary to know something about the type of aircraft and its configuration. For this study the McDonnell F-4E was selected, based on availability of data and future applicability of potential results. By referring to the F-4E we specify: a single nose gear strut with two unbraked tires, two main gear struts with single braked tires each; leading and trailing edge flaps; a boundary layer control system; the Hytrol Mark II antiskid system; a drag chute; and two General Electric J-79-17 engines with thrust inclined from the horizontal at an angle, $\Phi_T = 5.25°$. By further assuming that the landing simulation begins with the tires in contact with the runway, it is now possible to locate force components on a profile of the selected aircraft (Fig. 4).

By lumping related forces together, several distinct groupings form. The lift, drag, and pitching moment all are aerodynamic in origin and, thus, are considered to be a product of the aerodynamic subsystem. The engine thrust

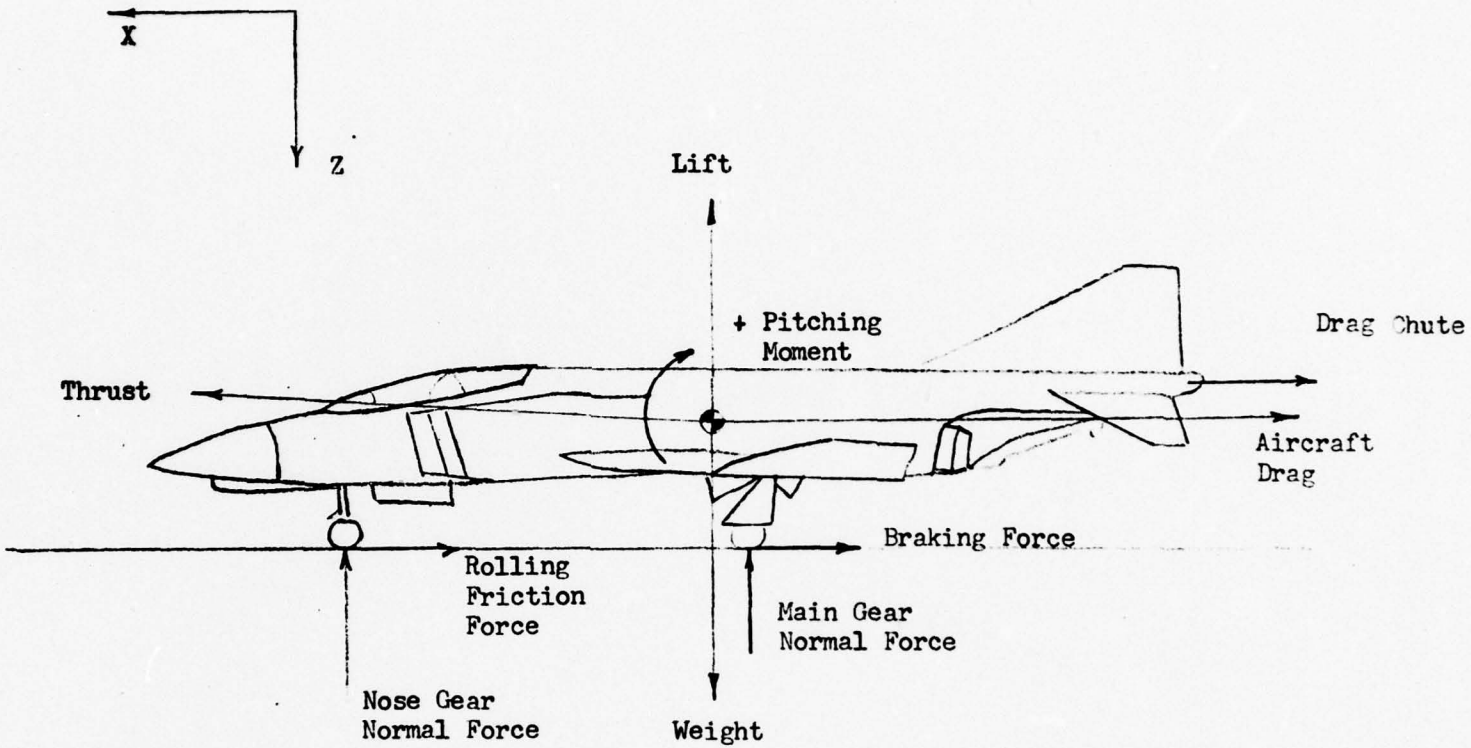

Fig. 4. Free Body Force Diagram

is unique and is considered to be a subsystem in itself. The normal forces on the landing gear arise from two separate mechanisms. The first is the load caused by the weight of the aircraft as the lift decays; the second is the load caused by touchdown impact and dynamic force interaction. These, then, are grouped together and referred to as the vertical strut dynamics. If it is assumed that the fuel consumption at idle thrust and tire surface losses during the landing are so small as to be insignificant when compared to the mass of the aircraft, it can then be assumed that the weight is a constant. This being so, no separate subsystem is required for modeling purposes. The braking and rolling friction forces, likewise, are similar in that they both are dependent on the normal force of their respective struts and the respectively different coefficients of friction. For the nose gear, the coefficient of rolling friction is assumed to be a constant. For the main gear, the coefficient of braking friction is dependent on the ratio of wheel slip speed to ground speed. The computation of this coefficient then is sufficiently complicated to warrant a tire/wheel dynamics subsystem. This tire/wheel dynamics subsystem, however, is not independent since it must rely on the wheel speed. Since the wheel speed is rarely equal to the aircraft speed, owing to braking action, a brake dynamics subsystem is required. If a brake dynamics subsystem is considered, the antiskid system must also be accounted for. Considering

the geometry of the main gear strut and the importance of wheel speed to the calculations, one recognizes a component of wheel speed resulting from fore-aft strut oscillation. To account for this component of wheel speed, a fore-aft strut dynamics subsystem is required. If we assume the surface of the earth serves as an inertially fixed reference point, considering the speeds involved, then these subsystems (aerodynamics, engine, vertical strut, tire/wheel, brake, antiskid, and fore-aft strut) plus weight of the aircraft account for all the external forces acting on the aircraft. If the only requirement was to find the total load on the nose and main gear combined, the number of unknowns would equal the number of independent equations; however, the ultimate goal is to know the main gear load, thus, requiring an additional equation. This equation can be found by considering the static loads on the gear struts. Since this proportion is 0.1396 to 0.8604, nose gear load to main gear load for a $.33\bar{c}$ center of gravity location, the problem is now solvable. The actual solving of these four equations will represent the integration of all the subsystem models and be referred to as the aircraft dynamics.

Subsystem Modeling

Aerodynamics. For the landing problem, the altitude is a constant and, since planform changes do not occur for

the F-4E from touchdown to stop, the wing area and chord length are also a constant. If the strut compression limits for the F-4E are considered, one observes that from static equilibrium the main gear travel is plus or minus one inch, while the nose gear travel is plus or minus 12 inches (Ref 8:V2, V5). Taking the worst combination of the two extremes acting over the wheel base results in an angle of attack change of plus or minus 2.66°. Since this will most likely occur, if ever, only at touchdown and will be damped out rapidly by viscous damping action of the struts, its effect over the duration of a landing roll will be minimal. Therefore, it is assumed that the angle of attack on the runway is a constant, equal to the angle of incidence of the wing. By assuming this, it follows that the coefficients of lift, drag, and pitching moment are a constant for a given configuration.

In terms of configuration, a normal landing calls for leading edge flaps set to 0°/60°/60° running from inboard to outboard, trailing edge flaps set to 60°, no speed brake, no spoilers, and no thrust reversing (Ref 11:4.2). Furthermore to obtain the correct lift, drag, and pitching moment, the coefficients must be based on gear down configuration with a correction for being in

ground effect. Implied in this assumption of constant configuration is the assumption that the flight controls are set at a constant position, untrimmed, with no pilot inputs. The rudder and ailerons are set to neutral by the assumption of no lateral-directional forces. The elevator is set to correspond to a slight stick aft position for which data exists--nominally minus eight degrees. The drag polar that provides C_L, C_D, and C_M corresponding to the above conditions (Ref 11:5.4) sets

$$C_{L_{BASIC}} = 0.195$$

$$C_{D_{BASIC}} = 0.140$$

$$C_{M_{BASIC}} = 0.025$$

The correction for ground effect based on $\delta_E = -8°$, and angle of incidence of 1° provides the following equations (Ref 11:14.2)

$$C_L = C_{L_{BASIC}} + 0.077 = 0.272$$

$$C_D = C_{D_{BASIC}} - 0.023 = 0.117$$

$$C_M = C_{M_{BASIC}} - 0.004 = 0.021$$

The remaining term in the aerodynamic subsystem is the drag and pitching moment contribution of the drag

chute. For the 16 ft. diameter ring-slot chute carried by the F-4E, the drag coefficient is 0.1875 (Ref 9:7.12.2). This implies that

$$D_{dc} = (0.1875)(1/2)\rho SV^2$$

The pitching moment is derived by multiplying D_{dc} by the moment arm from the center of gravity to the vertical height of the drag chute attachment point.

For computation of landing distances, the flight test data is based on brakes being applied two seconds after touchdown and drag chute fully deployed four seconds after touchdown (Ref 9:7.12.2). Drag chute initiation is simultaneous with brake application but requires two seconds deployment time. Drag chute effectiveness is assumed to be a step input based on pilot critique of the McDonnell Motion Base Simulator's one second ramp fade-in procedure (Ref 3:58).

The only unknown in the four aerodynamic equations is V, the aircraft true airspeed. This is provided during the process of solving the equations of motion.

Given the physical values for the terms in the aerodynamic equations as listed in Appendix A, it is now possible to arrange the equations for the analog computer.

$$L = 0.1714\dot{x}^2 \text{ lbs.}$$

$$D = 0.0737\dot{x}^2 \text{ lbs.}$$

$$M_p = 0.2123\dot{x}^2 \text{ ft-lbs.}$$

$$D_{dc} = 0.1182\dot{x}^2$$

$$Z_{dc}D_{dc} = 0.4302\dot{x}^2$$

To scale these equations for the analog computer it is necessary to know the maximum value that the variables can have. Assuming $\dot{x}$ has a maximum value of 280 ft./sec., the equations are scaled in terms of $\dot{x}$ as a fraction of its maximum value and take the form

$$[L/1] = 0.1714[\dot{x}/280]^2 280^2 = 13437.76[\dot{x}/280]^2$$

$$[D/1] = 0.0737[\dot{x}/280]^2 280^2 = 5778.08[\dot{x}/280]^2$$

$$[M_p/1] = 0.2123[\dot{x}/280]^2 280^2 = 16644.32[\dot{x}/280]^2$$

$$[D_{dc}/1] = 0.1182[\dot{x}/280]^2 280^2 = 9266.88[\dot{x}/280]^2$$

$$[Z_{dc}D_{dc}/1] = 0.4302[\dot{x}/280]^2 280^2 = 33,727.68[\dot{x}/280]^2$$

Engine Dynamics. Thrust from the two GE J-79-17 engines at idle power is not a constant, but varies with velocity. In the context of the landing sequence, the thrust varies linearly with velocity from touchdown to stop, assuming a maximum landing velocity of M = 0.25 (Ref 9:5.1.38). At velocity of M = 0 the static idle thrust of 470 lbs./engine is cited. At M = 0.2, the thrust is only 50 lbs./engine. Therefore, assuming a linear relationship, single engine thrust takes the form

$$T = \frac{(50-470)}{(0.2-0)\ (a)}\ \dot{x} + 470 \text{ lbs}$$

where (a) represents the speed of sound at sea level or, nominally, 1115 ft/sec. This being the case, for two engines the thrust equation takes the form

$$T = -3.7668\dot{x} + 940 \text{ lbs.}$$

Scaling this equation for the analog computer requires the recognition of the maximum value for $\dot{x}$. Recalling that 280 ft./sec. was used in the aerodynamics section, the equation takes the form

$$[T/1] = -1054.704[\dot{x}/280] + 940 \text{ lbs.}$$

Vertical Strut Dynamics. For controlability reasons the impact of a landing aircraft with a runway must be such that the aircraft remains in contact with the runway throughout the period from touchdown to stop. Accomplishing this requires that the landing gear absorb the landing energy and dissipate it over a period of time. Usually this is done through the combined use of a compressible fluid, acting as a spring force, and an incompressible fluid, acting as a viscous damper. Each landing gear, therefore, is modeled as a mass-spring damper system as shown in Fig. 5, with two degrees of relative freedom allowed for the aircraft.

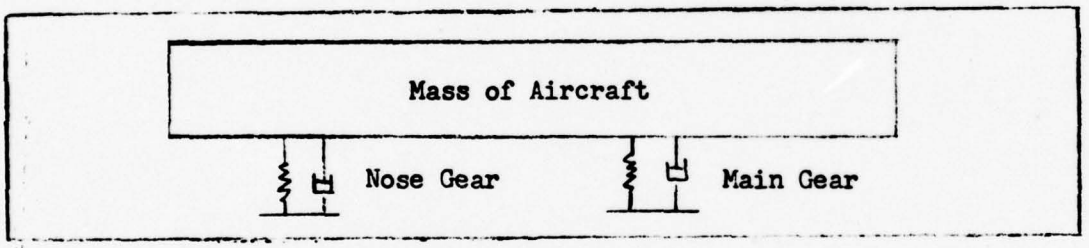

Fig. 5. Vertical Strut Analogy

In applying this concept to the landing aircraft, the force of the aircraft on the gear can be assumed to have two components, a quasi static load contribution and a dynamic load contribution. The quasi static load contribution is the first mechanism described in the force

analysis section whereby the landing gear is loaded and it accounts for all the external forces on the aircraft acting through the center of gravity. These are distributed with respect to the location of the aircraft center of gravity and the landing gear. The result is 86.04% of the load is on the main gear and 13.96% of the load is on the nose gear. The dynamic load contribution is the second mechanism and stems from the vertical and rotational motion/displacement of the aircraft. With this in mind the forces on the gear become

$$F_{z_{mg}} = F_{s_{mg}} + F_{d_{mg}}$$

$$= (0.8604 \text{ load}) + (K_{d_{mg}} \dot{Z}_{s_{mg}} + K_{s_{mg}} Z_{s_{mg}})$$

$$F_{z_{ng}} = F_{s_{ng}} + F_{d_{ng}}$$

$$= (0.1396 \text{ load}) + (K_{d_{ng}} \dot{Z}_{s_{ng}} + K_{s_{ng}} Z_{s_{ng}})$$

In these equations the (load) term represents the sum of all the vertical loads: lift, weight and engine thrust.

To maintain a constant attitude on the runway for changing gross weights, the nose gear and main gear are designed to displace equally for changing external forces acting through the aircraft center of gravity. Since the static gear loads result from forces acting through the aircraft center of gravity and the force on the gear from these sources is already accounted for, the strut displacements from static load sources are neglected. Instead, only the dynamic strut displacements are considered. Thus the simulation begins with the aircraft in a three point contact with the runway, with a sink rate, and the dynamic strut displacements at equilibrium.

To model each strut it is important to take into consideration the geometry of the aircraft as seen in Fig 6.

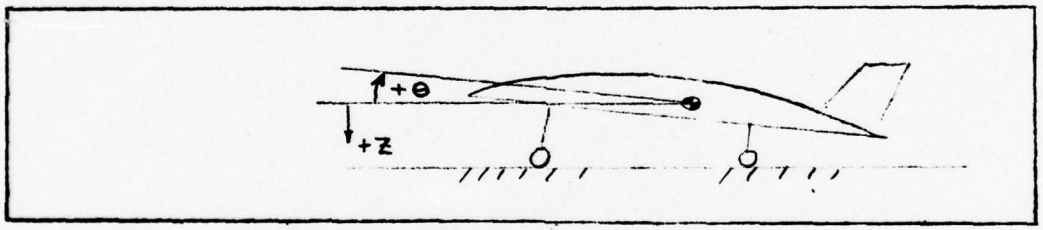

Fig. 6. Strut Compression Mechanics

The compression of the main gear strut, for example, will result from two separate motions; a vertical displacement of the aircraft center of gravity will change the strut displacement, and a pitching rotation about the center of gravity will change the strut displacement. The same applies for the nose gear with the exception of a sign change for a rotational displacement. Expressing this

in equation form, one arrives at

$$Z_{s_{mg}} = X_A\theta + Z \text{ ft.}$$

$$Z_{s_{ng}} = -X_B\theta + Z \text{ ft.}$$

where $Z_{s_{mg}}$ and $Z_{s_{ng}}$ are the strut displacements, θ is the angular displacement of the aircraft from horizontal and Z is the vertical displacement of the aircraft center of gravity.

In a similar fashion one arrives at the rate of change of displacement for each strut.

$$\dot{Z}_{s_{mg}} = X_A\dot{\theta} + \dot{Z} \text{ ft./sec.}$$

$$\dot{Z}_{s_{ng}} = -X_B\dot{\theta} + \dot{Z} \text{ ft./sec.}$$

Scaling these equations for the computer requires an estimate of the maximum value of each variable, as summarized in Table I.

Table I

Variable	Max Value	Computer Variable
Z	10 ft	$[Z/10]$
$\dot{Z}$	100 ft/sec	$[\dot{Z}/100]$
θ	0.25 rad	$[\theta/0.25]$
$\dot{\theta}$	2.5 rad/sec	$[\dot{\theta}/2.5]$

Variable	Max Value	Computer Variable
$z_{s_{mg}}$	1 ft	$[z_{s_{mg}}/1]$
$\dot{z}_{s_{mg}}$	10 ft/sec	$[\dot{z}_{s_{mg}}/10]$
$z_{s_{ng}}$	10 ft	$[z_{s_{ng}}/10]$
$\dot{z}_{s_{ng}}$	50 ft/sec	$[\dot{z}_{s_{ng}}/50]$

Arranging these equations in terms of computer variables leads to

$$[z_{s_{mg}}/1] = X_A[\theta/0.25]0.25 + [Z/10]10 \text{ ft.}$$

$$[z_{s_{ng}}/10]10 = -X_B[\theta/0.25]0.25 + [Z/10]10 \text{ ft.}$$

$$[\dot{z}_{s_{mg}}/10]10 = X_A[\dot{\theta}/2.5]2.5 + [\dot{Z}/100]100 \text{ ft./sec.}$$

$$[\dot{z}_{s_{ng}}/50]50 = -X_B[\dot{\theta}/2.5]2.5 + [\dot{Z}/100]100 \text{ ft./sec.}$$

Dividing through by the coefficients of the left side, substituting for X_A and X_B, and simplifying leads to

$$[z_{s_{mg}}/1] = 0.8125\ [\theta/0.25] + 10[Z/10] \text{ ft.}$$

$$[z_{s_{ng}}/10] = -0.5006[\theta/0.25] + [Z/10] \text{ ft.}$$

$$[\dot{z}_{s_{mg}}/10] = 0.8125[\dot{\theta}/2.5] + 10[\dot{Z}/100] \text{ ft./sec.}$$

$$[\dot{z}_{s_{ng}}/50] = -1.001[\dot{\theta}/2.5] + 2[\dot{Z}/100] \text{ ft./sec.}$$

The variables θ, $\dot{\theta}$, Z and $\dot{Z}$ are determined by solving the three equations of motion of the aircraft and the static load distribution equation, simultaneously, for $\ddot{X}$, $\ddot{\theta}$, and $\ddot{Z}$.

Once the respective strut displacements and rates of displacement are known, the dynamic force contribution to the gear can be determined. If one assumes that the maximum dynamic main gear load is 100,000 lbs. and the maximum dynamic nose gear load is 50,000 lbs., one arrives at

$$[F_{d_{mg}}/100{,}000]100{,}000 = K_{d_{mg}}[\dot{z}_{s_{mg}}/10]10 + K_{s_{mg}}[z_{s_{mg}}/1]$$

$$[F_{d_{ng}}/50{,}000]50{,}000 = K_{d_{ng}}[\dot{z}_{s_{ng}}/50]50 + K_{s_{ng}}[z_{s_{ng}}/10]10$$

To complete the above equations it is necessary to determine the spring-rate and damping coefficient. The spring rate coefficients may be determined by linearizing the load vs. displacement schedule for each strut about the static equilibrium displacement value. For the F-4E the main gear and nose gear spring rates are respectively 120,000 lbs./ft. and 19,500 lbs./ft. (Ref 8:V2,5). The viscous damping coefficients for each main gear and the nose gear as determined by the manufacturer are respectively 5100 lb.-sec./ft. and 1170 lb.-sec./ft. (Ref 15:18). Considering that there are two main gear struts, the above equations can be simplified by dividing through with the left side coefficients.

$$[F_{d_{mg}}/10^5] = 1.020[\dot{z}_{s_{mg}}/10] + 2.4[z_{s_{mg}}/1]$$

$$[F_{d_{ng}}/5X10^4] = 1.170[\dot{z}_{s_{ng}}/50] + 3.9[z_{s_{ng}}/10]$$

To determine the static force on the landing gear it is necessary to sum the external vertical forces on the aircraft and proportion the load according to the formula

$$F_{smg} = \frac{X_A}{(X_A + X_B)} \Sigma F_z$$

$$F_{sng} = \frac{X_B}{(X_A + X_B)} \Sigma F_z$$

Tire/Wheel Dynamics. With the completion of the aerodynamics, engine dynamics, and vertical strut dynamics, the equations of motion of the aircraft are readily solved, if one assumes a constant value for the coefficient of friction between the tire and runway. Unfortunately this coefficient of friction is dependent on many factors including runway surface condition, wheel speed and aircraft speed. For a given tire and runway condition, however, a characteristic nonlinear relationship between the degree of wheel slip and coefficient of friction will always hold (Ref 17:1). This relationship is known as a μ vs. σ curve, where μ is the coefficient of friction and σ is the ratio of $(\dot{X} - V_w)$ to $\dot{X}$. Recall that $\dot{X}$ is the true airspeed or ground speed in this no-wind case and V_w is the wheel speed or $V_{w_s} + R_r\omega$, where V_{w_s} is the wheel speed component due to fore-aft strut oscillation, where R_r is the tire rolling radius, and ω is the wheel angular velocity. To determine the wheel slip ratio, σ, it is necessary to find the wheel speed, V_w, since $\dot{X}$ has already been determined for

the aerodynamics model. If the fore-aft strut oscillation speed, V_{w_s}, is determined by the horizontal strut dynamics model and the tire rolling radius, R_r, is assumed to be a constant, then the wheel angular velocity, ω, is the only unknown. To determine ω it is helpful to recall the formula

$$\Sigma(\text{torques}) = I_w\dot{\omega}$$

where I_w is the mass moment of inertia about the rolling axis of the wheel. For a constant mass, constant geometry wheel, I_w is a constant. To determine ω it is only necessary to know the torques acting on the wheel. For a braked aircraft tire, assuming the normal forces act through the center of the wheel, the only torques are those caused by the ground on the tire and the brakes on the wheel. Summing moments about the center of mass of the wheel, one obtains

$$I_w\dot{\omega} = (\text{Ground Torque}) - (\text{Brake Torque})$$

If the brake torque is determined in the brake dynamics model, the only unknown is the ground torque. Working with a single main gear wheel, the torque can be represented by

$$(\text{Ground Torque}) = 1/2(\mu F_{z_{mg}})R_r$$

where $1/2(\mu F_{z_{mg}})$ is the load on one main gear strut/tire.

Note, that in a round-about way, it takes μ to be able to calculate μ. On the analog computer, an initial value of wheel speed will provide an initial value for μ, therefore, the loop is self perpetuating once begun. To scale this for the computer, once again, requires an estimate of the maximum values for the variables as summarized in Table II.

Table II

Variable	Maximum Value	Computer Variable
$\dot{\omega}$	10^4 rad/sec^2	$[\dot{\omega}/10^4]$
ω	10^4 rad/sec	$[\omega/10^4]$
$\mu F_{z_{mg}}$	10^5 lbs	$[\mu F_{z_{mg}}/10^5]$
BT	25,000 ft-lbs	[BT/25000]
V_w	10^4 ft/sec	$[V_w/10^4]$

Substituting for the constants, the equation of motion for the wheel is

$$(2.71)[\dot{\omega}/10^4]10^4 = (0.5)[\mu F_{z_{mg}}/10^5]10^5(1.16) - [BT/25000]25000$$

Dividing through by the coefficients of the left side and simplifying, one arrives at

$$[\dot{\omega}/10^4] = 2.140[\mu F_{z_{mg}}/10^5] - 0.9225\ [BT/25,000]$$

By integrating $\dot{\omega}$, ω is known. With ω, the wheel slip ratio is known. To obtain σ it is necessary to scale $(x - V_w)$.

Recalling that $\dot{X}$ had been originally scaled to 280 ft./sec. to be compatible with $[V_W/10^4]$, it may now be rescaled to a maximum value of 10,000 by multiplying by 0.0280. Therefore, one arrives at

$$[\sigma/1] = (0.0280[\dot{X}/10000] - [V_W/10000]) \div 0.0280[\dot{X}/10000]$$

For the particular tire on the F-4E the μ vs. σ relationship is plotted at several velocities and several runway surface conditions from dry to flooded (Ref 17). The general form of this curve is shown in Fig. 7.

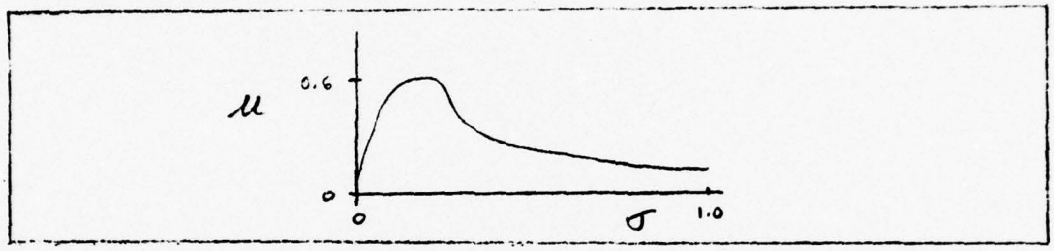

Fig. 7. Coefficient of Braking Friction vs. Wheel Slip Ratio

By programming a Variable Diode Function Generator (VDFG) on the analog computer, the μ vs. σ relationship can be represented by a ten straight line segment approximation. To correct this curve for a velocity other than the one it is plotted against, one may assume a linear relationship of $\Delta\mu$ to $\Delta\dot{X}$ about a central velocity. For example, the central velocity selected for this problem was 75 knots or approximately mid-way between the maximum touchdown velocity and a stop. The VDFG was programmed with μ vs. σ at 75 knots. To determine the $\Delta\mu$ vs. $\Delta\dot{X}$ relationship, the maximum values of μ at 0 knots and 150 knots

were compared against the maximum value of μ at 75 knots. A median value of Δμ over the two 75 knot spans was selected and also programmed. The resulting equation was

$$[\Delta\mu/1] = (0.1849 - 8.684[V_w/10^4]) \times [\mu/1]$$

Combining the μ and Δμ produces a coefficient of friction as a function of runway surface condition, wheel speed, and aircraft speed.

Brake Dynamics. The brake dynamics model must be designed to develop the brake torque required by the tire/wheel dynamics model. To do this several aspects of the brake hydraulic system must be considered. Assuming that the aircraft brake hydraulic pump delivers a constant pressure source of hydraulic fluid, brake torque is developed dependent on antiskid system inputs, pressure lag, the pressure to torque relationship, brake fade, and torque peaking. The antiskid system inputs will be developed in the antiskid dynamics model and are assumed to be known at this point. The pressure lag characteristic of the F-4E system is modeled as a first order lag transfer function with a 0.1 second time constant as is done in McDonnell's Motion Base Simulator (Ref 3?41). The Laplace transform for this lag can be written as 10/(s+10) which is readily programmed on the analog computer. The pressure to torque relationship for the F-4E brake as plotted in Air Force Aeronautical System Division/ENFL

TM-73-1 takes the form as shown in Fig. 8.

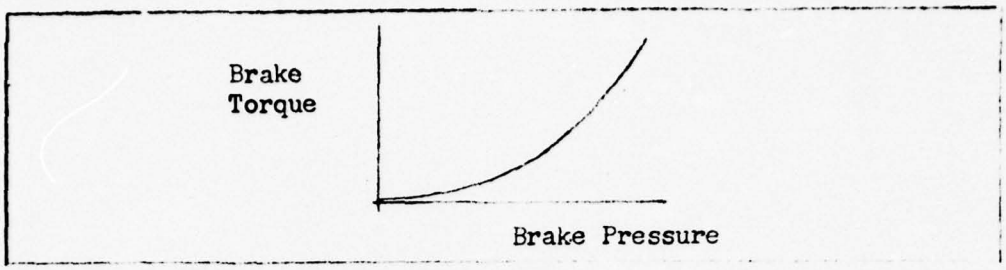

Fig. 8. Brake Pressure Vs. Brake Torque

By programming a Variable Diode Function Generator this relationship between brake torque and brake pressure can be stored in the analog computer. To model the brake fade phenomena, the technique used in Boeing's Brake Control Simulator was used (Ref 15:129). By conservation of energy

$$E_b = W_b = \int BT \, d\theta = \int BT\omega \, dt$$

where E_b is the energy absorbed by the brake heat sink (assuming no energy losses to convection, radiation, conduction, etc.), W_b is the work done by the brake, θ is the angular displacement of the wheel, ω is the wheel angular velocity, and t is time. The conversion from energy to brake temperature is required so that fade initiation can begin once a threshhold temperature is reached. This is done by dividing the energy absorbed by the brake by the mass of the brake heat sink and the specific heat of the heat sink material. Thus, the equation becomes

$$Btemp = \frac{1}{M_b C_{p_b}} \int (BT)(\omega)\,dt + Btemp\ (0)$$

Boeing in their brake control simulator suggested a brake fade initiation threshhold of 1000° F above ambient. Using this value as a switch, above which brake torque fades, then a formula for ΔBT as a function of temperature would describe the fade phenomena. For this model a value of $\Delta BT_F = -0.5BT/100°$ F was used.

The torque peaking effect or the tendency of brakes to increase brake torque at an increasing rate as a stop is approached, was patterned after the Boeing Brake Control Simulator model. Boeing's analysis of brake torque histories showed a pattern as depicted in Fig 9.

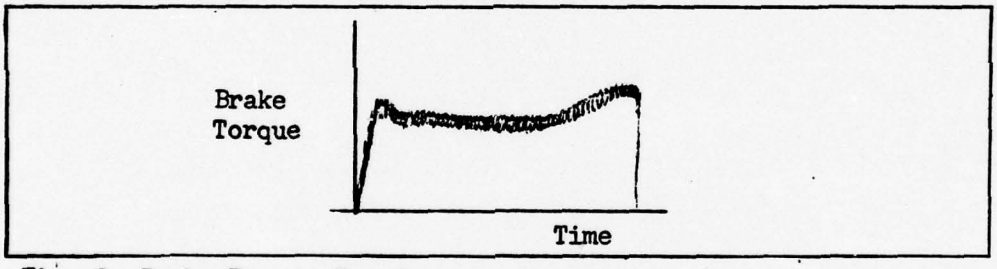

Fig. 9. Brake Torque Vs. Time

The curve shows a quasi-steady-state level of torque with a sharp increase at the end of the ground roll. The characteristic value of this torque peak at the end of the ground roll was found to be, on the average, 25% of the quasi-steady-state torque value. Using this value and a wheel speed of 90 ft./sec. as a threshhold, the average initiation value for F-4E type brakes, a formula for torque peaking is arrived at

$$\Delta BT_{TP} = (0.0463 - 5.140[V_w/10^4]) \times [BT/25000]$$

By combining the antiskid command, pressure lag, pressure to torque relationship, brake fade, and torque peaking, the brake dynamics model is complete.

Antiskid Dynamics. The Hytrol Mark II antiskid system used on the F-4E, basically, measures the wheel speed, differentiates it with respect to time, and compares this value of wheel deceleration against reference values to determine when and how much hydraulic pressure to damp (Ref 14:55). A deceleration below approximately 20 ft/sec^2, will result in full system pressure being delivered. Above 20 ft/sec^2 and below 140 ft/sec^2, a fraction of the brake pressure proportioned to $(\dot{V}_W - 20)/(140-20)$ will be dumped. $\dot{V}_W$ in this case is the wheel deceleration. Above 140 ft/sec^2 full brake pressure is dumped. Modeling this on the analog computer, however, requires a value for $\dot{V}_W$ to be able to calculate $\dot{V}_W$. To do this a feedback loop must be created. To accomplish

$$\frac{(\dot{V}_W - 20)}{(140 - 20)} = \frac{\dot{V}_W - 20}{120}$$

$\dot{V}_W$ must be scaled and a division operation performed. The scaling causes the rumerator value of this expression to be on the order of 10^{-4}, a value of marginal accuracy on the analog computer. When division is performed, the inaccuracy is multiplied and when this value is processed through the feedback loop, further distortion occurs. Hence, the wheel deceleration is lost in the background noise of the computer.

Instead of the exact reproduction of the antiskid system, a facsimile was tried where the results of a real system were modeled. McDonnell, on their Motion Base Simulator, derived a formula for the on-off action of the pressure dump valve based on a square wave. The on portion of the square wave was a fraction of the total period of the wave and dependent on the wheel speed. The total period, in turn, was a second function of the wheel speed (Ref 3:41).

$$(\text{On Time}) = (1 - 0.001075\ V_W)\ (\text{Period})$$

$$(\text{Period}) = (1.2 - 0.005\ V_W)$$

To model this on the analog computer would require an expanded memory capability or a restartable time reference to keep track of the elapsed time of each period in the square wave. Neither of these were feasible without resorting to a digital-analog hybrid system. In an attempt to keep the system model totally analog, a third procedure was attempted where, once again, the results of the real system were modeled. In this approach the wheel speed was measured against the aircraft speed, and controlled to remain in the region $\dot{X} \geq V_W \geq (\dot{X} - 60)$. The 60 ft./sec. value was arrived at by observing traces of wheel speed vs. time for real aircraft landings, wherein the wheel speed cycled between the aircraft velocity and this value. When the aircraft reached a speed 25 ft./sec. the antiskid system was by-passed and full brake pressure was delivered; otherwise a stop would have been approached asymptotically.

To keep the wheel speed within the physical range of $0 \leq V_w \leq \dot{X}$, comparator circuits had to be installed that set $V_w = 0$ or $V_w = \dot{X}$ depending on the actual calculated value of ω.

Fore-Aft Strut Dynamics. The phenomena that caused a tire to develop a coefficient of braking friction is the occurence of a velocity differential between the tire and contacting surface. Since the relative velocity of the tire sensed by the runway is at issue, all components of wheel velocity must be considered. By limiting the landing aircraft problem to three degrees of freedom, the lateral or side to side motion of the tire is eliminated, thus, leaving only rotational and translational components. The rotational component of wheel speed was addressed by the tire/wheel dynamics model; the translational motion remains.

If all the structures between the wheel and aircraft center of gravity were rigid, the wheel translational velocity would be identical to the ground velocity and no speed differential would exist. Since the landing gear is not rigid, its equation of motion must be considered to determine this component.

By taking the landing gear strut to be a cantilever beam, it is known that any load in the form of a force or a torque will result in a linear and an angular displacement due to the elastic effects. However, in the case of a cantilever beam where the deflections are small, such as a landing gear strut, a reasonable assumption can be made to uncouple the linear displacement from the angular. For the F-4E, the fore-aft spring constant is 304,800 lbs./ft. at static equilibrium strut

extension. If the maximum strut load is 50,000 lbs. and the maximum tire coefficient of friction is 0.7, the maximum braking force is 35,000 lbs. Such a force would cause a deflection of 1.38 inches. When considered over the length of the strut, 3.91 feet, this results in an angular deflection of 1.68 degrees, a negligible amount. Therefore, a mass spring damper analogy can be made where the mass of the unsprung strut and wheel is concentrated in the wheel and the strut serves as a spring-damper combination for linear movement in the fore-aft direction as depicted in Fig. 10.

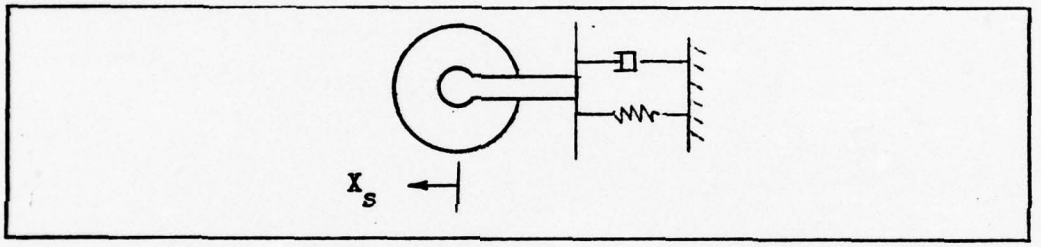

Fig. 10. Fore-Aft Strut Analogy

If the damping coefficient for the F-4E is 200 lb.-sec./ft., the equation of motion becomes

$$M_s\ddot{X}_s = -200\dot{X}_s - 304{,}800X_s - 0.5\mu F_{z_{mg}}$$

Substituting scaled variables and dividing through by the coefficients of the left, the equation takes the form

$$[\ddot{X}_s/50000] = -0.6275[\dot{X}_s/2000] - 9.562[X_s/20]$$

$$-0.0784[\mu F_{z_{mg}}/10^5]$$

Since a positive strut velocity exacerbates the velocity differential between tire and runway, the $\dot{X}_s$ is actually subtracted from the wheel velocity to produce the relative velocity of the tire to runway.

Total System Integration. The completion of the subsystem models now allows the three equations of motion and the static load distribution equation to be solved in the form of the aircraft dynamics model. Starting with the summation of forces in the x-direction as depicted in Fig. 4, one obtains

$$\Sigma F_x = M\ddot{X} = T\cos\Phi_T - D - \mu F_{z_{mg}} - \mu_r F_{z_{ng}} - D_{dc}$$

where M is the mass of the aircraft, T is the thrust, Φ_T is the thrust inclination angle, D is the aircraft drag, μ is the braking coefficient of friction, $F_{z_{mg}}$ is the total main gear load, μ_r is the rolling coefficient of friction, $F_{z_{ng}}$ is the total nose gear load, and D_{dc} is the drag of the drag chute.

If $\ddot{X}$ is scaled to have a maximum value of 40 ft./sec./sec. and μ_r is equal to a constant, 0.025, then the scaled equation takes the form

$$M[\ddot{X}/40]40 = [T/1](0.9958) - [D/1] - [\mu F_{z_{mg}}/10^5]$$
$$- 0.025[F_{z_{ng}}/10^5] - [D_{dc}/1]$$

Substituting for [T/l], [D/l], and [D_{dc}/l] with the values developed previously and dividing by the coefficients of the left side, the equation takes the form

$$[\ddot{X}/40] = \frac{23.4014}{M} - \frac{26.2571}{M}[\dot{X}/280] - \frac{144.5106}{M}[\dot{X}/280]^2$$
$$- \frac{2500}{M}[\mu F_{z_{mg}}/10^5] - \frac{62.5000}{M}[F_{z_{ng}}/10^5]$$
$$- \frac{231.5875}{M}[\dot{X}/280]^2$$

If X has a maximum value of 8000 ft., the equations for $\dot{X}$ and X are

$$[\dot{X}/280] \approx 0.1429 \int [\ddot{X}/140]\, dt + \dot{X}(0)$$

$$[X/8000] \approx 0.0350 \int [\dot{X}/280]\, dt + X(0)$$

The equation representing the summation of forces in the z-direction is actually two separate equations due to the distinction between quasi-static and dynamic gear loads. For the quasi-static gear loads, the equation can be stated as

$$F_{s_{mg}} + F_{s_{ng}} = mg - L - T\sin\Phi_T$$

where $F_{s_{mg}}$ and $F_{s_{ng}}$ are the main and nose gear static loads, respectively, and mg is the weight of the aircraft.

Scaling $F_{s_{mg}} + F_{s_{ng}}$ to a max value of 100,000 lbs. and substituting scaled equations for L and T, one arrives at

$$[(F_{s_{mg}} + F_{s_{ng}})/10^5] = 3.2174 \times 10^{-4}(M) - 0.1344[\dot{X}/280]^2 - 0.0009 + 0.00010[\dot{X}/280]$$

By specifying the center of gravity location the proportion of the total gear load going to the nose gear is determined by the ratio $X_B \div (X_A + X_B)$ where X_B is the horizontal distance from the center of gravity to the nose gear and X_A is the horizontal distance from the main gear to the center of gravity. For a $0.33\bar{c}$ center of gravity this ratio is equal to 0.1396 implying that the ratio of main gear load to total static load is 0.8604. Therefore the static load distribution equation becomes

$$[(F_{s_{mg}} + F_{s_{ng}})/10^5] = 0.1396[(F_{s_{mg}} + F_{s_{ng}})/10^5] + 0.8604\ [(F_{s_{mg}} + F_{s_{ng}})/10^5]$$

$$[F_{s_{mg}}/10^5] = 0.8604[(F_{s_{mg}} + F_{s_{ng}})/10^5]$$

$$[F_{s_{ng}}/50{,}000] = 0.1396[(F_{s_{mg}} + F_{s_{ng}})/10^5]$$

For the dynamic gear loads the equation of motion can be stated as

$$M\ddot{Z} = F_{d_{mg}} + F_{d_{ng}}$$

If $\ddot{Z}$ has a maximum value of 200 ft./sec.^{2}, the scaled values for $F_{d_{mg}}$ and $F_{d_{ng}}$ are substituted, and the equation is divided by the coefficients of the left side, the equation takes the form

$$[\ddot{Z}/200] = -\frac{500}{M}[F_{d_{mg}}/10^5] - \frac{250}{M}[F_{d_{ng}}/50{,}000]$$

Note that the negative signs allow a positive force to compress the strut.

If $\dot{Z}$ and Z have maximum values of 100 ft./sec. and 10 ft., respectively, then equations for $[\dot{Z}/100]$ and [Z/10] can be written as

$$[\dot{Z}/100] = 2\int[\ddot{Z}/200]\,dt + \dot{Z}(0)$$

$$[Z/10] = 10\int[\dot{Z}/100]\,dt + Z(0)$$

Summing moments about the center of gravity of the aircraft as depicted in Fig 4, the pitching moment equation becomes

$$\Sigma M_{cg} = I_{yy}\ddot{\theta} = M_p + D_{dc}Z_{dc} + F_{z_{ng}}X_B - \mu_r F_{z_{ng}}Z_{ng}$$

$$- F_{z_{mg}}X_A - \mu F_{z_{mg}}Z_{mg}$$

where I_{yy} is the aircraft mass moment of inertia about

the y-axis, $\ddot{\theta}$ is the angular acceleration, M_p is the pitching moment caused by the untrimmed flight controls, Z_{dc} is the vertical distance from the drag chute attachment point to the aircraft center of gravity, $F_{z_{ng}}$ and $F_{z_{mg}}$ are the summation of static and dynamic gear loads on the nose gear and main gear, respectively, and Z_{ng} and Z_{mg} are identical constants representing the vertical distance from the runway to the aircraft center of gravity.

By substituting scaled equivalents for terms developed in the subsystem models, by scaling $\ddot{\theta}$ to a maximum value of 25 rad./sec./sec., and by substituting values for the moment arms, the equation can be expressed as

$$I_{yy}[\ddot{\theta}/25]25 = 16641.691[\dot{X}/280]^2 + 31403.26[\dot{X}/280]^2 + 1,001,250[F_{z_{ng}}/50,000] - 7887.5[F_{z_{ng}}/50,000] - 325,000[F_{z_{mg}}/10^5] - 631,000[\mu F_{z_{mg}}/10^5]$$

Dividing through by the coefficients of the left and combining the two nose gear terms, the equation takes on its final form

$$[\ddot{\theta}/25] = \frac{665.668}{I_{yy}}[\dot{X}/280]^2 + \frac{1256.130}{I_{yy}}[\dot{X}/280]^2 + \frac{39734.5}{I_{yy}}[F_{z_{ng}}/50,000] - \frac{13000}{I_{yy}}[F_{z_{mg}}/10^5] - \frac{25240}{I_{yy}}[\mu F_{z_{mg}}/10^5]$$

If $\dot{\theta}$ and θ have maximum values of 2.5 rad./sec. and 0.25 rad., respectively, then the equations for $[\dot{\theta}/2.5]$ and $[\theta/0.25]$ are

$$[\dot{\theta}/2.5] = 10 \int [\ddot{\theta}/25]\, dt + \dot{\theta}(0)$$

$$[\theta/0.25] = 10 \int [\dot{\theta}/2.5]\, dt + \theta(0)$$

The analog computer wiring diagram for the total system integration to this point is depicted in Fig. 11. The variables are all scaled to their respective maximum values. Triangles represent summers, and triangles with rectangles on the left side represent integrators. The sign of a variable is reversed when passing through the summers and integrators to account for apparent reversed signs. The oblong circles represent attenuators through which the variables are scaled and proportioned according to their appropriate coefficients. The computer program in this figure would be sufficient to calculate main gear loads if a constant coefficient of friction between the tire and runway were assumed.

By referring to wiring flow charts, the process of producing a coefficient of friction based on wheel speed, aircraft velocity, and runway surface condition is more easily grasped. In Fig. 12, page 44, the top row of summers and integrator produces the wheel speed given the ground torque and brake torque. The second row, consisting of comparators and relays, keeps the wheel speed within

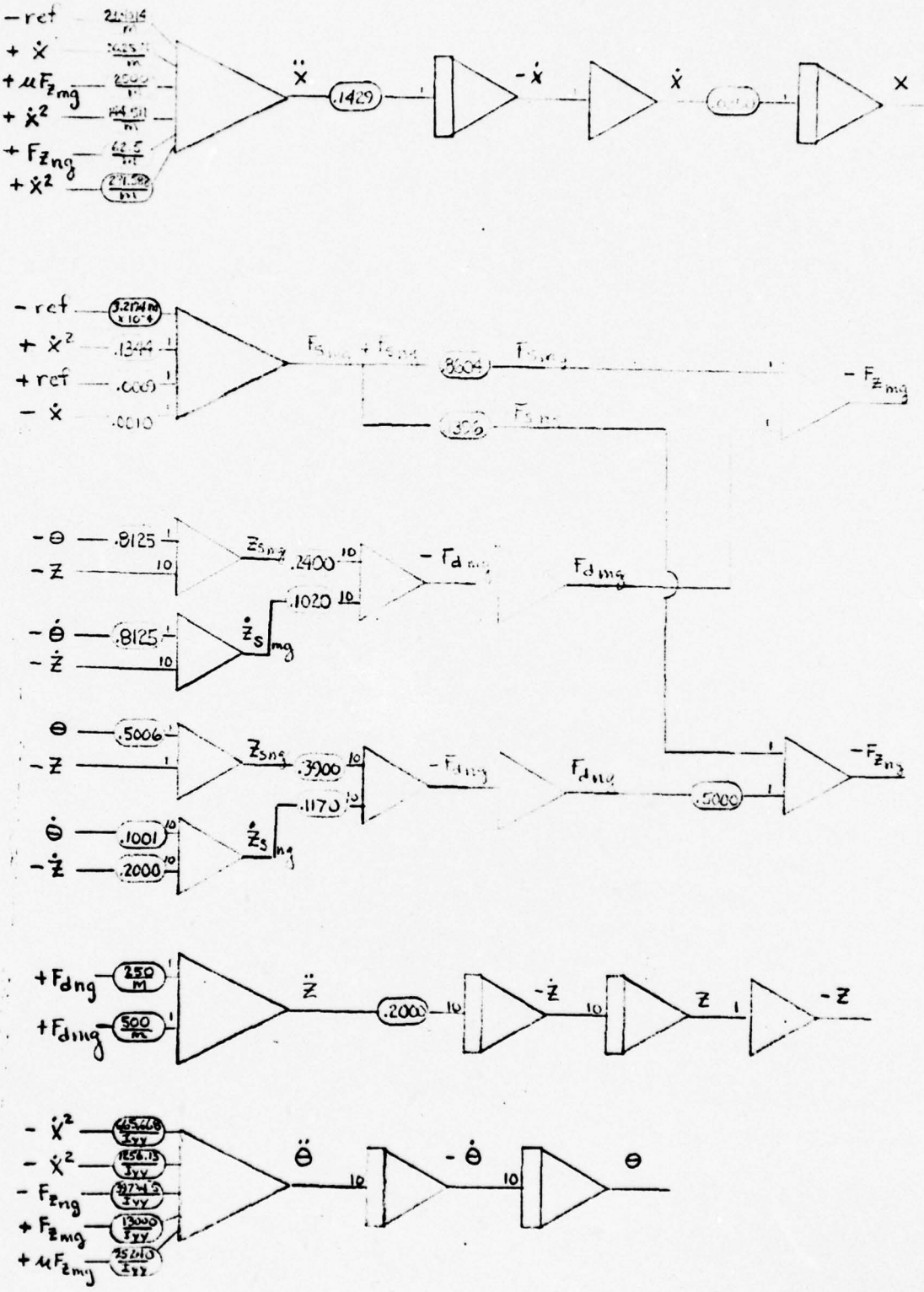

Fig. 11. First Level System Integration

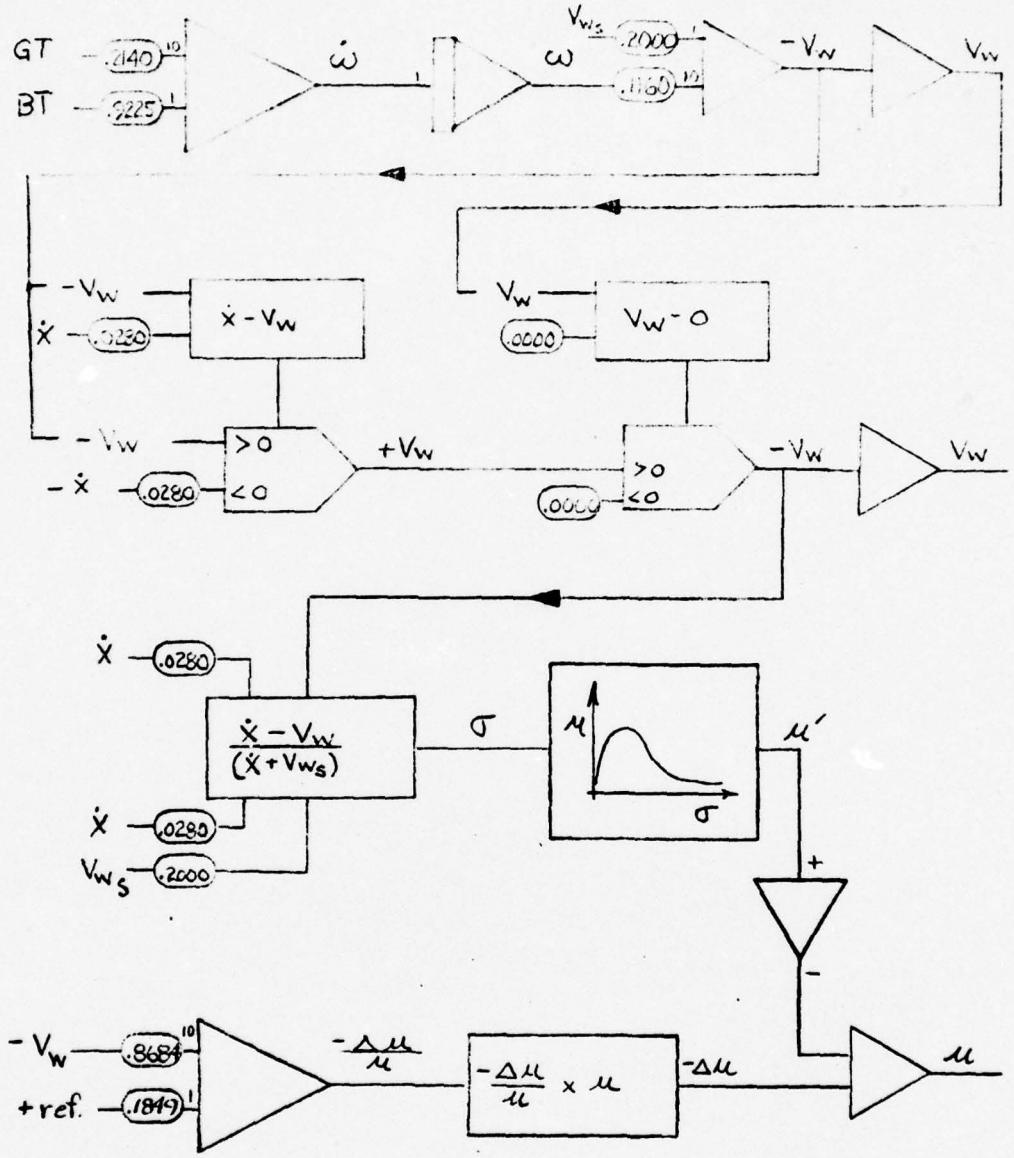

Fig. 12. Tire/Wheel Dynamics Schematic

the range $0 \leq V_w \leq \dot{X}$ so that the wheel slip velocity is only in one direction. The reason for this becomes evident in the third row where the wheel slip velocity is divided by the sum of the aircraft velocity and the fore-aft strut component to the wheel velocity to produce σ, the wheel slip ratio. The sign of σ must always be positive to conform to the physical realities. Continuing in the third row, the Variable Diode Function Generator produces μ' based on the median velocity of 75 knots. In the fourth row, μ is modified for any wheel velocity other than 75 knots. The values of the coefficients in the fourth row correspond to dry runway conditions.

In Fig. 13, the brake dynamics model is depicted. The top row, consisting of a Variable Diode Function Generator, provides the brake torque component produced by brake pressure. The second row, relying on a summer, a comparator, a relay, and a multiplication circuit, produces the brake torque component resulting from operating in the torque peaking velocity range. The third row, consisting of a multiplication circuit, an integrator, a summer, and a comparator/relay combination, produces the brake torque component due to brake fading. The sum of the three brake torque components results in the brake torque.

In Fig 14 page 47, the antiskid and fore-aft strut dynamics models are depicted. The antiskid model uses a series of two comparators and relays to test the wheel

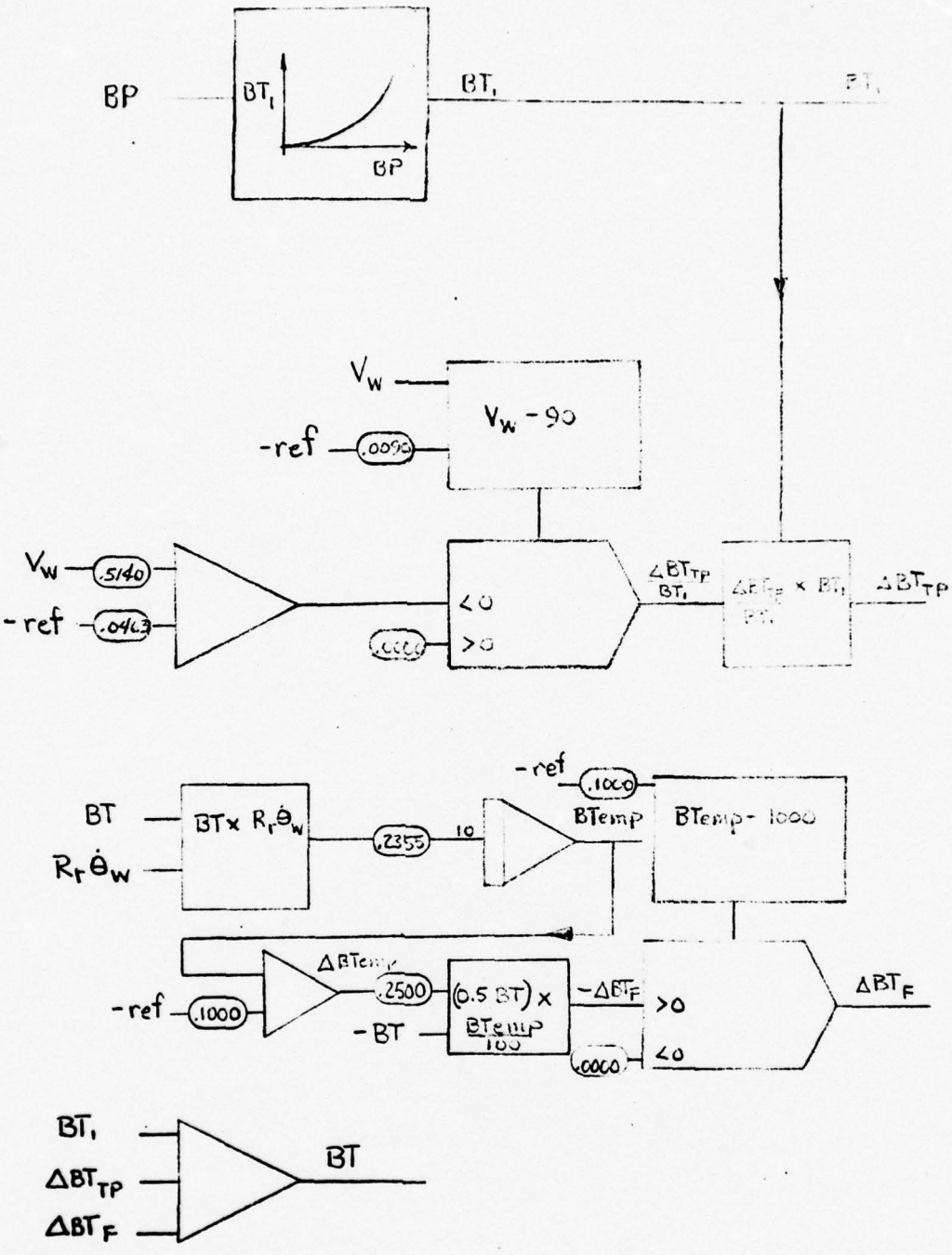

Fig. 13. Brake Dynamics Schematic

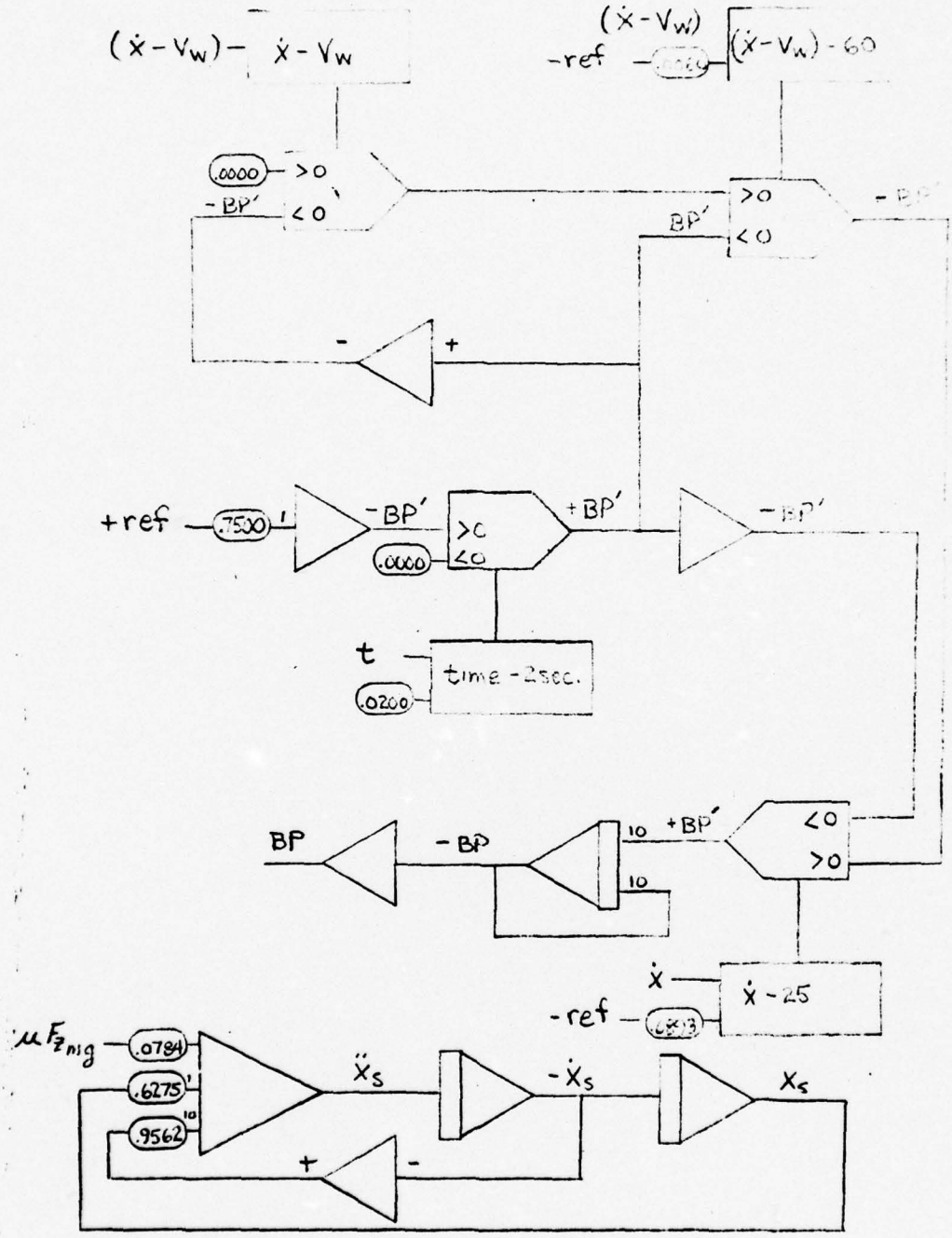

Fig. 14. Antiskid and Fore-Aft Strut Dynamics Schematic

slip speed for compliance with the range $0 \leq (\dot{X} - V_W) \leq 60$ ft./sec. If so, full brake pressure is delivered to the brakes. If not, zero brake pressure is delivered to the brakes. A test is then made on the aircraft velocity, $\dot{X}$, using the third comparator and relay to check if the aircraft velocity is in the range $0 \leq \dot{X} \leq 25$ ft./sec. If so, full brake pressure is delivered to the brakes. In the second row, the touchdown protection feature of the antiskid system is modeled. By comparing the time elapsed against a two-second reference value, a two-second delay on brake application is provided. Furthermore, this delay allows the wheel to spin-up to a near-aircraft velocity before braking commences. In the third row, the brake pressure, BP', is modified by the $10 \div (S + 10)$ transfer function to provide a first order lag. In the fourth row, the fore-aft strut dynamics are modeled to provide $\dot{X}_S$, where $\dot{X}_S$ equals V_{W_S}, the wheel speed component due to strut oscillation. Physical constants pertinent to the F-4E are listed in Appendix A. Source data necessary to complete the model is listed in Appendix B.

Data Acquisition

To test the aircraft dynamics model, initial conditions were placed on the $-\dot{X}$ integrator corresponding to the touchdown velocity, on the $-\dot{Z}$ integrator corresponding to the sink rate and on the ω integrator corresponding to a value that would cause the wheel speed to be near

the aircraft velocity two seconds after touchdown. All other integrators had initial conditions of zero. Inherent in this procedure is the assumption that the wheel speed will, indeed, spin-up in the allotted time. For all but flooded and icy runways this is a good assumption (Ref 14:218). It is important to note that this procedure is, not only, a necessary boundary condition on the mathematics for the model to simulate a real landing, but it is a requirement for the actual Mark II antiskid system to ensure proper operation (Ref 14:7). For a given gross weight the touchdown speed is determined by the flight manual (Ref 13:B18). The sink rate is arbitrarily determined to provide the maximum main gear strut deflection without entering into a bounce condition, where the main gear would lose contact with the runway.

Test runs were made for wet and dry runway μ vs. σ data (Ref 17). For each runway condition, test runs were made at gross weights of 30,000 lbs., 35,000 lbs., 40,000 lbs., and 45,000 lbs. At each gross weight, the mass moment of inertia of the aircraft was adjusted accordingly. Actual values for the test run variables are listed in Table III.

Data Analysis

To determine the validity of the model, the gear loadings should conform to actual test results of gear loadings. In the absence of these, however, it is

Table III

Independent Variables for Each Data Run

	Gross Weight (lbs)			
	30,000	35,000	40,000	45,000
I_{yy} (ft-lb-sec^2)	$1.074X10^5$	$1.086X10^5$	$1.098X10^5$	$1.110X10^5$
$\dot{X}_o$ (knots)	127	137	147	155
$\dot{Z}_o$ (ft/sec)	5.40	5.50	5.80	5.94
$\dot{\theta}_o$ (rad/sec)	200	270	370	380
M (slugs)	932.43	1087.83	1243.24	1398.64

necessary to validate the test results circumstantially.

Assuming that the basis of the model is sufficient to cover all the phenomena occuring in a landing, it was shown that, primarily, the aerodynamics, engine dynamics and vertical strut dynamics produce the gear load, while the tire/wheel dynamics, brake dynamics, antiskid dynamics, and fore-aft strut dynamics are required to determine the stopping distance. If the coefficient of friction, μ, is accurate, the gear loads should be accurate within the scope of the assumptions since the aerodynamics, engine dynamics, and landing gear spring constants and damping coefficients are well documented.

To determine if the coefficient of friction, μ, is accurate consider the latter four subsystems. In the case of the tire/wheel dynamics model, the actual μ vs. σ data is well documented. To determine if σ, the wheel slip ratio, is accurate one must know if the aircraft

velocity, fore-aft strut velocity, and wheel velocity are accurate. Aircraft velocity will be accurate if μ, once again, is accurate, because the aerodynamics, engine dynamics, and strut dynamics can be modeled with a high degree of certainty. Since fore-aft strut spring constants and damping coefficients are well documented, the fore-aft strut velocity should be accurate. Wheel speed accuracy can then be traced to braking action accuracy. Since the brake torque vs. brake pressure relationship is well documented, the accuracy of μ can be traced back to the accuracy of the antiskid system. To determine if the model approximates real aircraft antiskid operation, traces of wheel speed vs. time and stopping distance will be enlightening. If the simulation wheel speed wave form approaches the actual wheel speed wave form and the stopping distances are accurate, then the model should be accurate.

III. Results and Conclusions

System checkout revealed that fore-aft strut dynamics contributions to the wheel velocity occured only at the instant of touchdown and were damped out within the first two seconds thereafter. Considering the fact that the brake system is locked-out by the touchdown protection circuit until two seconds after touchdown, the effect of the fore-aft strut model was deemed negligible and bypassed. Also, system checkout revealed that at no time did the brake fade phenomena occur. Considering that the brake energy absorbed is characteristically 30% to 50% of that for a rejected take-off, for which the brakes are designed, this result is quite reasonable.

Comparison of the plots for both wet and dry runway runs, contained in Appendix B, shows a marked difference in the effect of a more slippery surface on the initial deceleration at touchdown and on the stopping distances. For the eight combinations of gross weight and runway surface condition, the stopping distances are assembled in Table IV and compared to flight test stopping distance as extracted from the flight manual (Ref 13:B8-2).

In general, the model brakes to a stop in a shorter distance than the aircraft. The maximum stopping distance differences are 6.25% on dry runways for the 40,000 lbs. aircraft and 6.10% on wet runways for the 45,000 lbs. aircraft.

Table IV
Stopping Distance of Model and Aircraft (ft.)

Gross Weight	Model		Aircraft	
	Dry	Wet	Dry	Wet
30,000	2300	4590	2400	4600
35,000	2640	5480	2800	5600
40,000	3000	6270	3200	6500
45,000	3390	6760	3500	7200

Figure 17, page 64, shows the decelerating effect of brakes and drag chute quite prominently at two and four seconds, respectively. When zero aircraft velocity occurs, instabilities result from the tire/wheel dynamics model attempting to divide by zero and cause erratic plotting pen movement. The plots of landing gear load and angular motion also demonstrate a lurching tendency as the stop is reached.

With the possible exception of the antiskid system, the subsystem models behave well. The aerodynamics, as indicated indirectly in plots of aircraft velocity and stopping distance, show the characteristic parabolic curve as the velocity decreases. Furthermore, the assumption of constant angle of attack on the runway appears well justified after considering the brief influence of the aircraft pitch angle in the θ vs. time plots. The engine dynamics, though not plotted, follow the predicted values. The vertical strut loads correspond to both the dynamic strut loads and the quasi-static strut loads as depicted in the main and nose gear load plots. In these it is important to

note the damping of the dynamic loads and the gentle increase in static loads as the lift decays. Plots of σ, μ, V_w, and $\dot{X}$ when compared show that μ is accurate for a given σ, and σ is accurate for the given aircraft velocity and wheel velocity. The acceleration of the wheel, based on ground torque and brake torque is responsive to changes in the coefficient of friction, μ, thus indicating that the tire/wheel dynamics model produces reasonable results. Observation of the brake pressure and brake torque plots indicate strong cyclic dependence on the antiskid system commands. A strong decrease in brake pressure output as the wheel velocity approaches zero velocity illustrates the high frequency of the antiskid response and its ability to control wheel velocity in this region.

It is important to note that due to scaling requirements and the gain factor required to plot wheel velocity, the noise level becomes a factor in tending to mask the wheel velocity wave form. Figure 15 indicates the nature of the real aircraft wheel velocity wave form for dry and wet runways.

For the wet runway model, the pronounced "scalloping" effect is not realized, although both the real aircraft wheel velocity and the model wheel velocity tend to ride 50-60 ft./sec. less than the aircraft velocity. The lack of the "scalloping" effect indicates that the model reacts much quicker than the real aircraft to wheel velocity

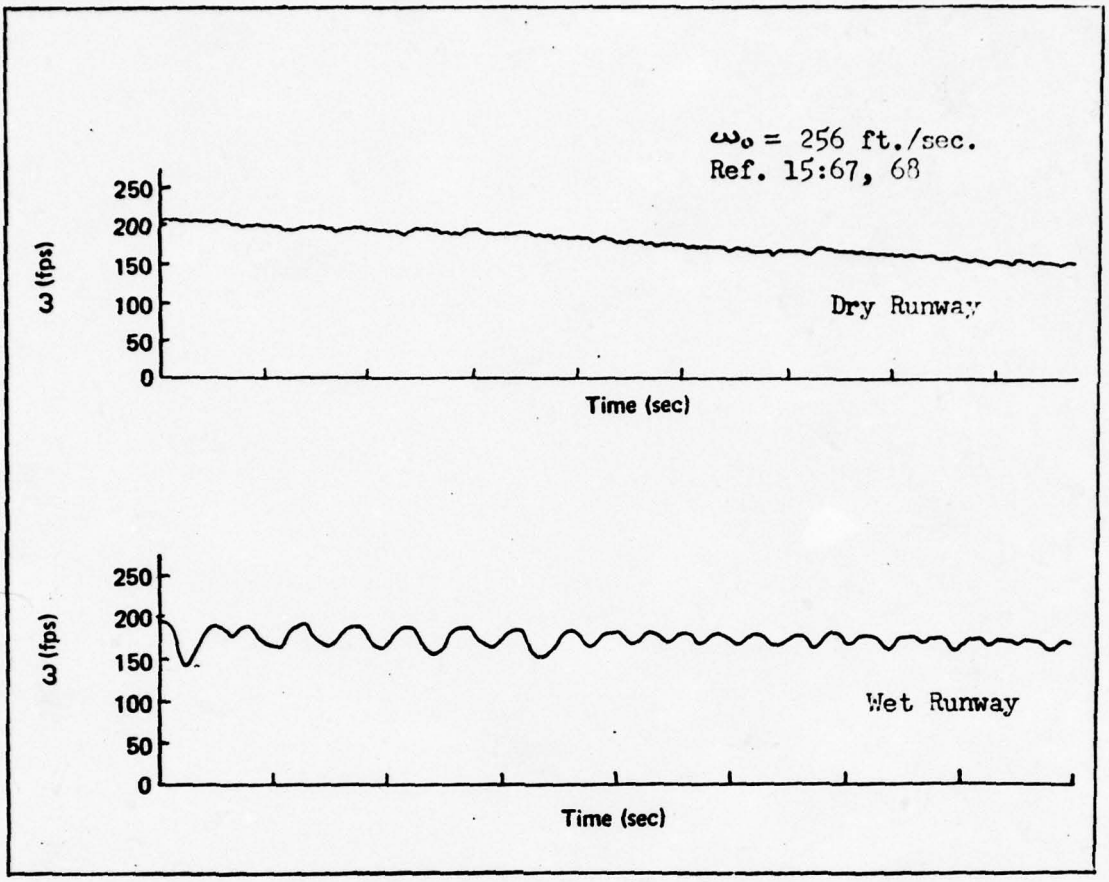

Fig. 15. Aircraft Wheel Speed vs. Time

deviations. This is to be expected when recalling that the first two attempts at modeling the antiskid system ran into difficulty when confronted with an inability of the analog computer to model a variable wave form with a specified minimum response time. Since the dry runway wheel velocity plots are comparable, a conclusion might be drawn to search for a better wet runway antiskid system, although stopping distances are generally better correlated than dry runway distances. An ideal substitute would be an actual antiskid system in the loop, although all that is really needed is an ability to command a specified "off" time during which full brake

pressure is dumped. An antiskid system of this nature would result in a more realistic wet runway wheel velocity plot and tend to lengthen the ground roll slightly.

Altogether the model gives reasonable stopping performance and system simulation. Assuming that the simulated stopping distances are within tolerance and the antiskid model is reasonably accurate, a schedule of load and velocity vs. distance may be constructed from cross plots of main gear load, velocity, and stopping distance vs. time. This alternative schedule is shown in Fig 16.

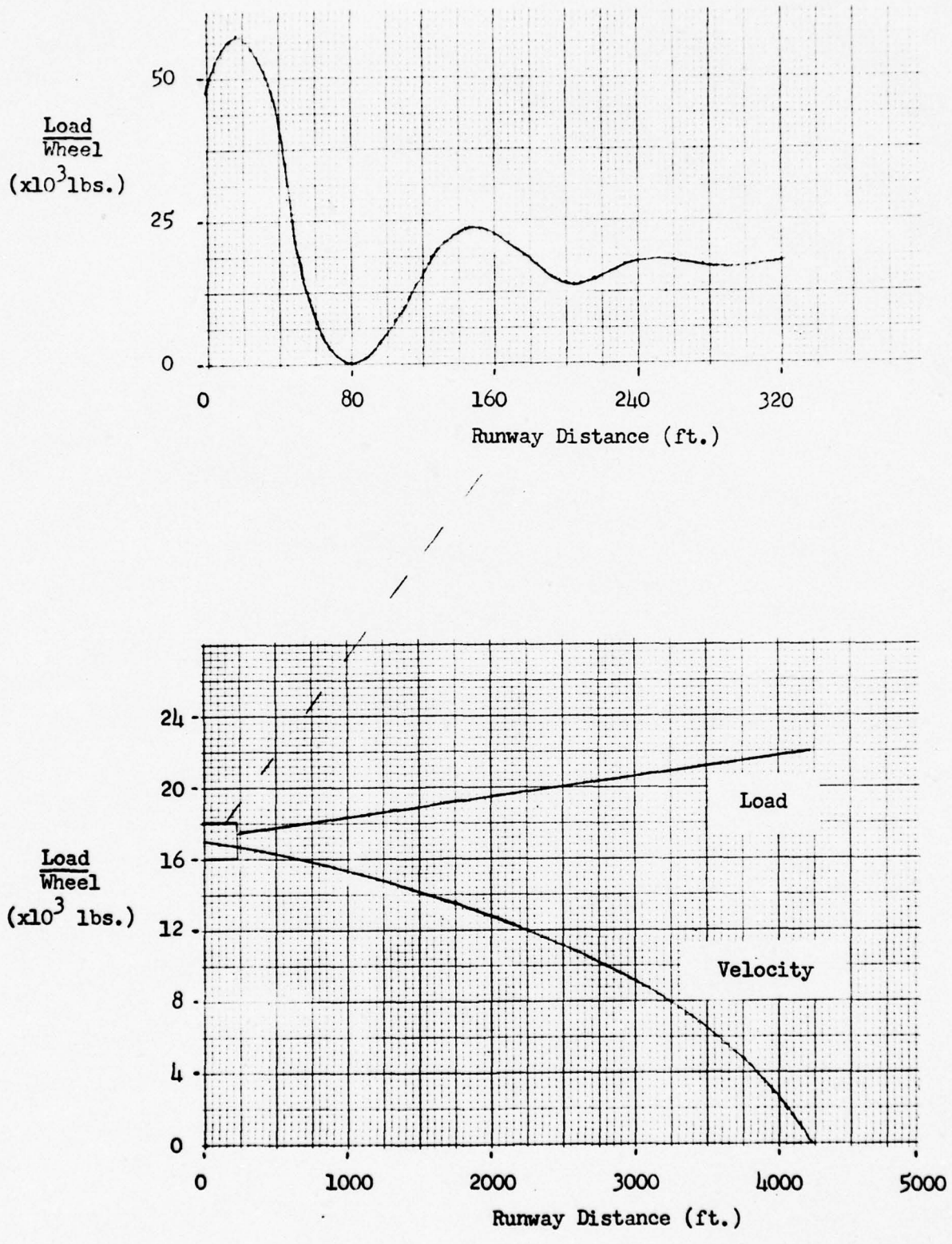

Fig. 16. Derived Main Gear Load/Velocity Schedule

IV. Recommendations

All indications are that an improved antiskid system will increase system accuracy considerably. The most likely method of simulation to achieve this is a hybrid analog-digital computer system. Such a system would eliminate the weakness of the analog system by providing precise control over the brake pressure-off time and increase the resemblance of the two wet runway wheel velocity vs. time plots.

Another recommendation is to place an actual braked tire/wheel with antiskid in the loop. By operating such a system on a dynamometer wheel wherein the exact load on the tire is controlled by the analog program, highly accurate performance should result. Furthermore, such a procedure would open up increased analog capacity to model the non-linear, dual-chamber nature of the F-4E main gear strut.

Finally, adoption of this system simulation procedure for tire and landing gear development is urged. Total analog simulation of the aircraft dynamics, despite drawbacks to the antiskid model, gives a reasonably accurate schedule of gear loading vs. velocity which, when compared to the current military specification, is considerably more realistic. Further improvements in the antiskid model by resorting to digital-analog models or by using actual antiskid systems in the circuitry, should provide highly realistic results.

Bibliography

1. Carleton, David L. Stability and Control Derivatives for the F-4E Aircraft. FTC-TD-69-9. Edwards AFB: Air Force Flight Test Center, September 1969.

2. Crane, R. C. and Gentry, J. R. F-4E Category II Performance Tests. FTC-SD-69-21. Edwards AFB: Air Force Flight Test Center, August 1969.

3. Expansion of Flight Simulator Capability for Study and Solution of Aircraft Directional Problems on Runways. MDC Report A3304. St. Louis: McDonnell Aircraft Company, March 1975.

4. Faulkner, Clem R. USAF Drawing 62J4031, Exhibit B, Specifications for MLG Tire Type VIII, Size 30X11.5-14.5. Wright-Patterson AFB: Aeronautical Systems Division, February 1962.

5. Greiner, H. and Hilbig, J. H. Method for Evaluating the Effectiveness and Weight of Aircraft Deceleration Devices. Chula Vista: Rohr Corporation, June 1968.

6. Hirzel, E. A. Antiskid and Modern Aircraft. SAE Publication 720868. San Diego: National Aerospace Engineering and Manufacturing Meeting, October 1972.

7. Horne, Walter B. Elements Affecting Runway Traction. SAE Publication 740496. Dallas: Air Transportation Meeting, May 1974.

8. Landing Gear Design Data. MDC Report 8581. St. Louis: McDonnell Aircraft Corporation, April 1962.

9. Miles, R. B. Model F-4E Performance Data. MDC Report A1158, Vol. 1. St. Louis: McDonnell Aircraft Corporation, July 1971.

10. Nichols, Donald E. Overall Braking for Jet Transports. ASME Publication 60-AV-2. Dallas: Aviation Conference, June 1959.

11. Sands, R. L., et al. Model F4 Aerodynamic Derivatives F-4E Addendum. MDC Report 9842, Addendum IV. St. Louis: McDonnell Aircraft Corporation, July 1967.

12. Straub, H. H., et al. Development of a Pneumatic-Fluidic Antiskid System. AFFDL-TR-74-117. Wright-Patterson AFB: Air Force Flight Dynamics Laboratory, October 1974.

13. T.O. 1F-4E-1, Flight Manual, USAF Series F-4E Aircraft, 1 Dec 76.

14. Tracy, William V., Jr. Wet Runway Aircraft Control Project (F4 Rain Tire Project). ASD-TR-74-37. Wright Patterson AFB: Deputy for Engineering, Aeronautical Systems Division, October 1974.

15. Wahi, M. K., et al. Combat Traction II, Phase II Vol I & II. ASD-TR-74-41. Wright-Patterson AFB: Deputy for Engineering, Aeronautical Systems Division, October 1974.

16. Woods, A. R. Model F-4E Propulsion and Aerodynamic Data. MDC Report A2447. St. Louis: McDonnell Aircraft Corporation, December 1973.

17. Yager, Thomas J. and Dreher, R. C. Traction Characteristics of a 30X11.5-14.5, Type VIII, Aircraft Tire on Dry, Wet, and Flooded Surfaces. NASA TM-X72805. Hampton: NASA Langley Research Center, February 1976.

Appendix A

Physical Constants

Contained herein are the specific values of terms that were assumed to be constant. Included are the physical constants and geometric measurements of the F-4E that are essential to solving the equations of motion.

Physical Constants

Roman Symbols

$\bar{c}$	16.04 ft
C_D	0.117
$C_{D_{BASIC}}$	0.140
$C_{D_{dc}}$	0.1875
C_L	0.272
$C_{L_{BASIC}}$	0.195
C_m	0.021
$C_{m_{BASIC}}$	0.025
C_{p_b}	0.11 BTU/lbm°F
g	32.174 ft/sec^2
I_w	2.71 ft-lb-sec^2
$K_{d_{mg}}$	5100 lb-sec/ft
$K_{d_{mgh}}$	200 lb-sec/ft
$K_{d_{ng}}$	1170 lb-sec/ft
$K_{s_{mg}}$	120,000 lb/ft
$K_{s_{mgh}}$	304,800 lb/ft
$K_{s_{ng}}$	19,500 lb/ft
M_b	3.85 slugs
M_s	12.75 slugs
R_r	1.16 ft
S	530 ft^2
X_A	3.25 ft
X_B	20.025 ft
Z_{dc}	3.39 ft
Z_{mg}	6.31 ft
Z_{ng}	6.31 ft

Greek Symbols

α	-1°
$\Delta C_{D_{ge}}$	-0.023
$\Delta C_{L_{ge}}$	0.077
$\Delta C_{M_{ge}}$	-0.004
μ_r	0.025
π	3.14159
ρ	0.002378 lb-sec/ft^2
Φ_T	5.25°

Appendix B

Modeled Aircraft Performance vs. Time

Contained herein are the test results of the system simulation in 5000 lb. increments of aircraft gross weight for dry and wet runway conditions. For each gross weight and runway condition there are six figures containing plots of the following variables versus time.

First figure: $\ddot{X}$; $\dot{X}$; X

Second figure: $\ddot{\theta}$; $\dot{\theta}$; θ

Third figure: $\ddot{Z}$; $\dot{Z}$; Z

Fourth figure: BP´; BP; BT

Fifth figure: σ; μ; V_w

Sixth figure: $F_{z_{mg}}$; $F_{z_{ng}}$; $\mu F_{z_{mg}}$

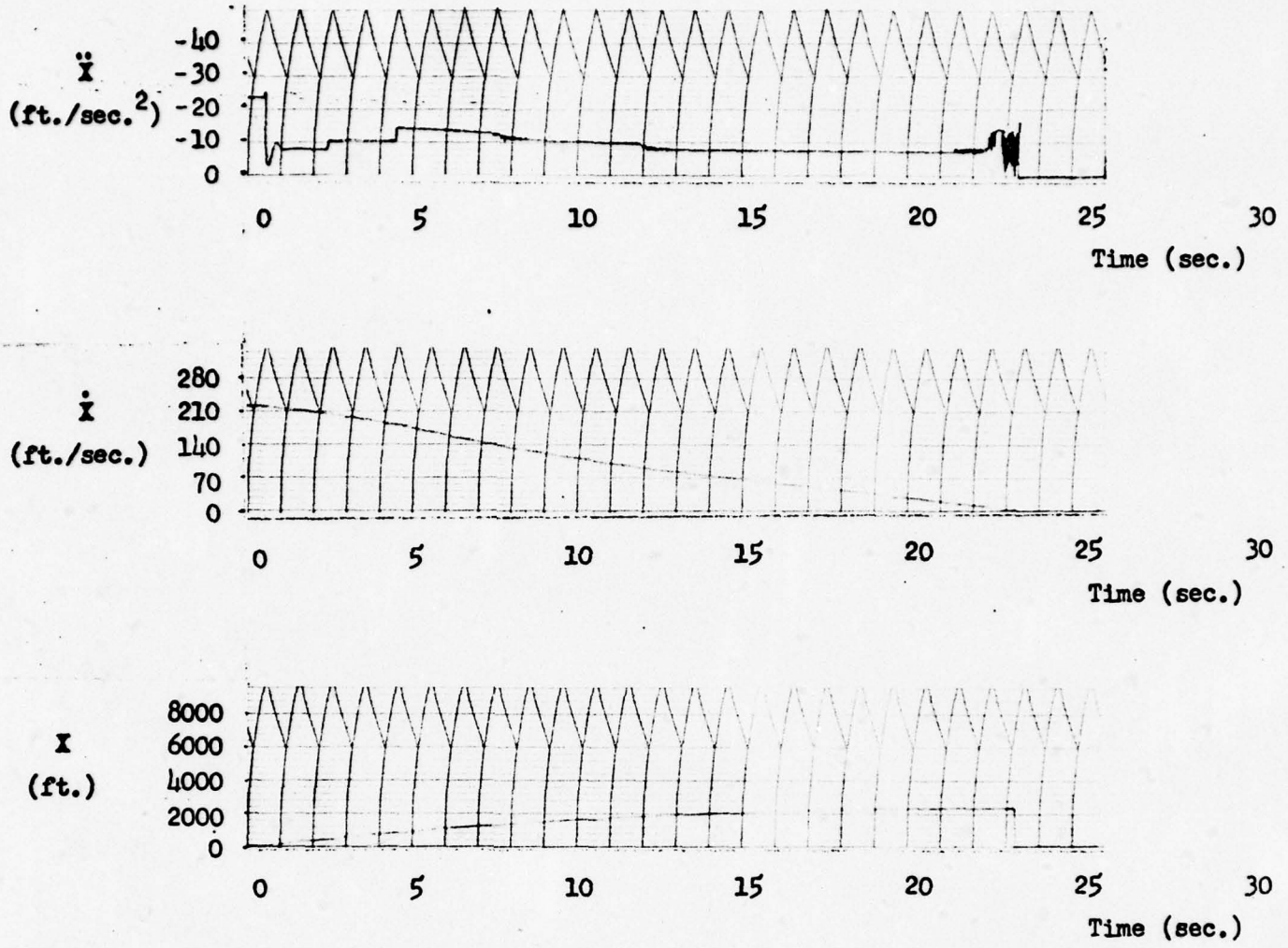

Fig. 17. $\ddot{X}$, $\dot{X}$, and X vs. Time for 30,000 lb. F-4E, Dry Runway

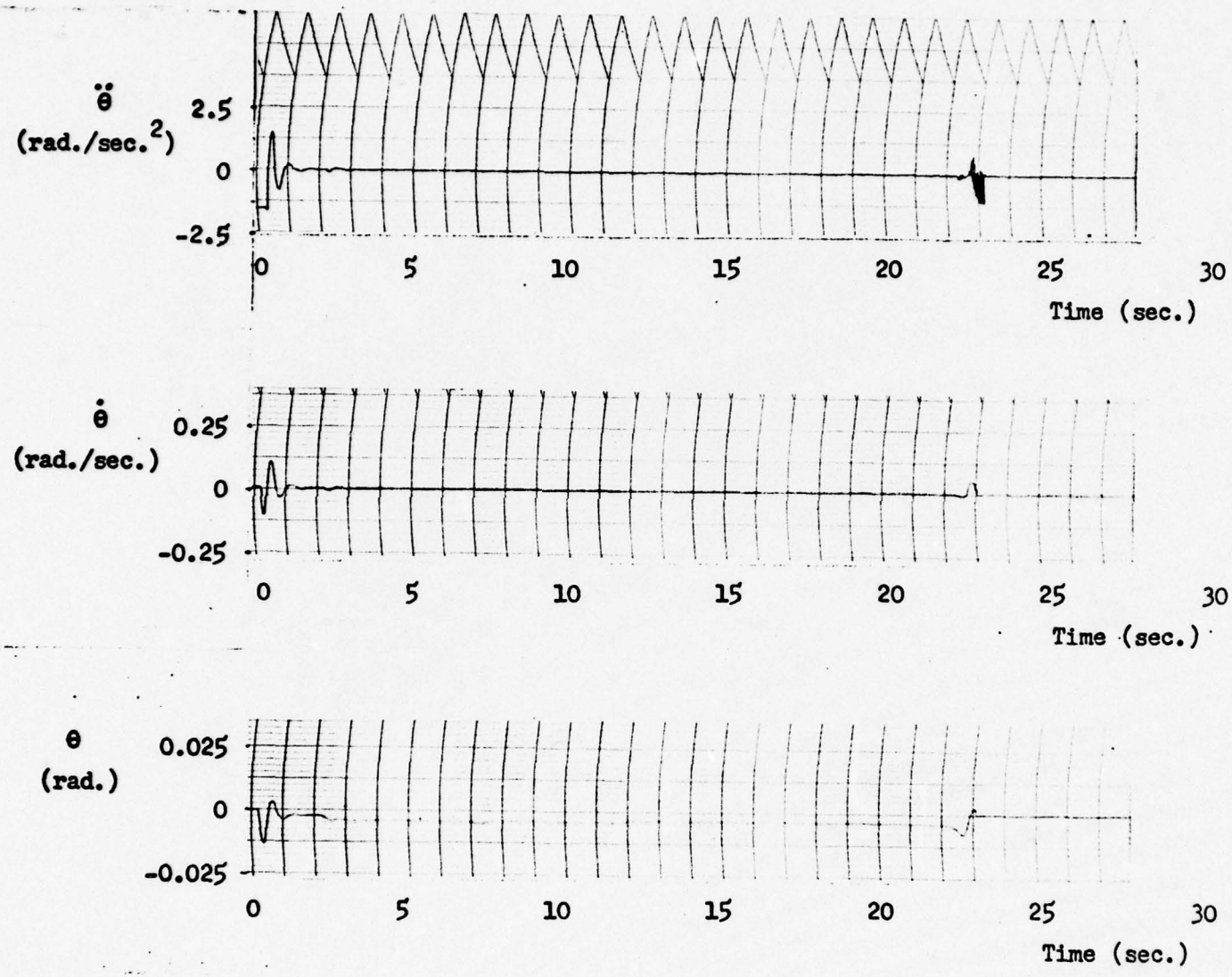

Fig. 18. $\ddot{\theta}$, $\dot{\theta}$, and θ vs. Time for 30,000 lb. F-4E, Dry Runway

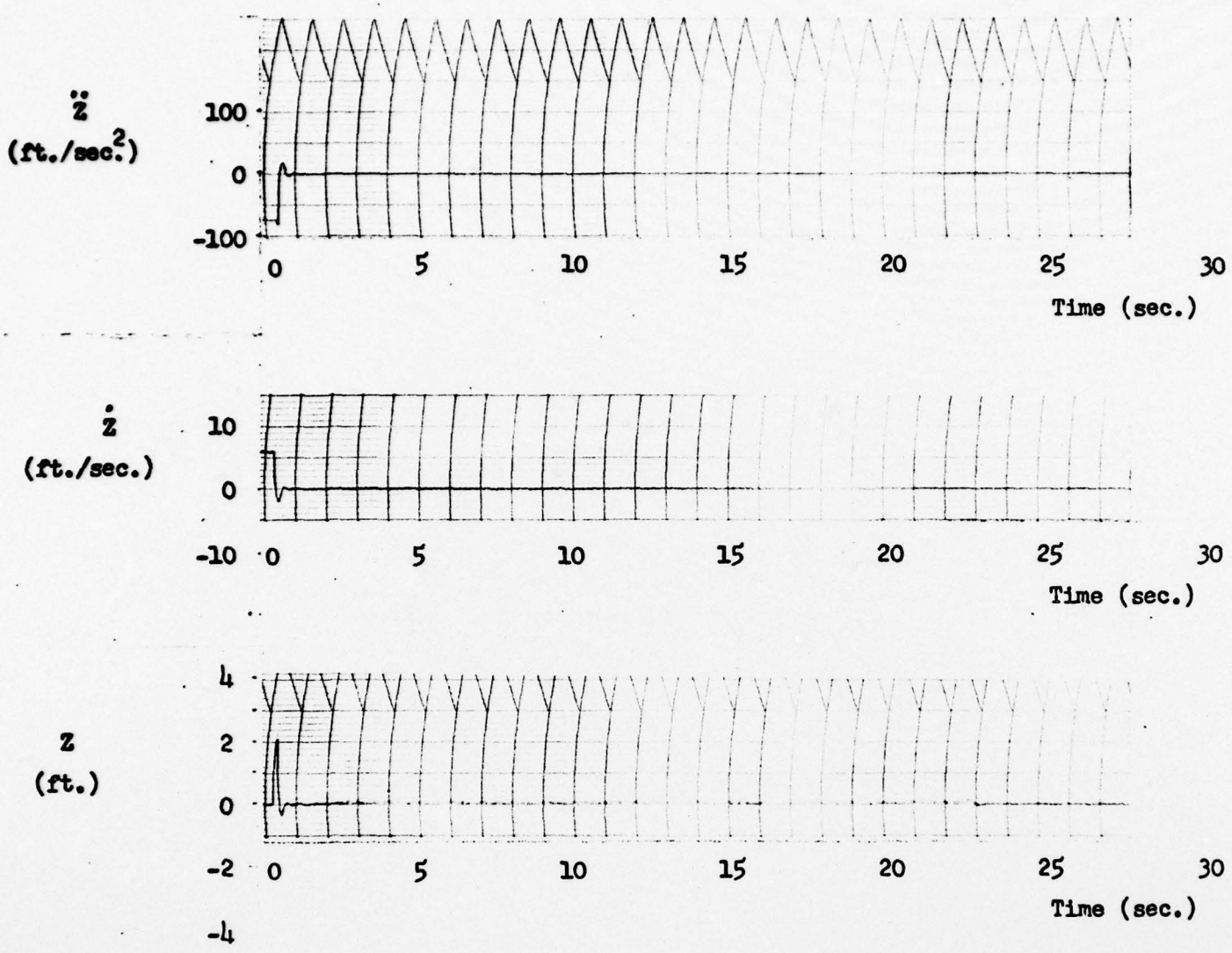

Fig. 19. $\ddot{z}$, $\dot{z}$, and Z vs Time for 30,000 lb. F-4E, Dry Runway

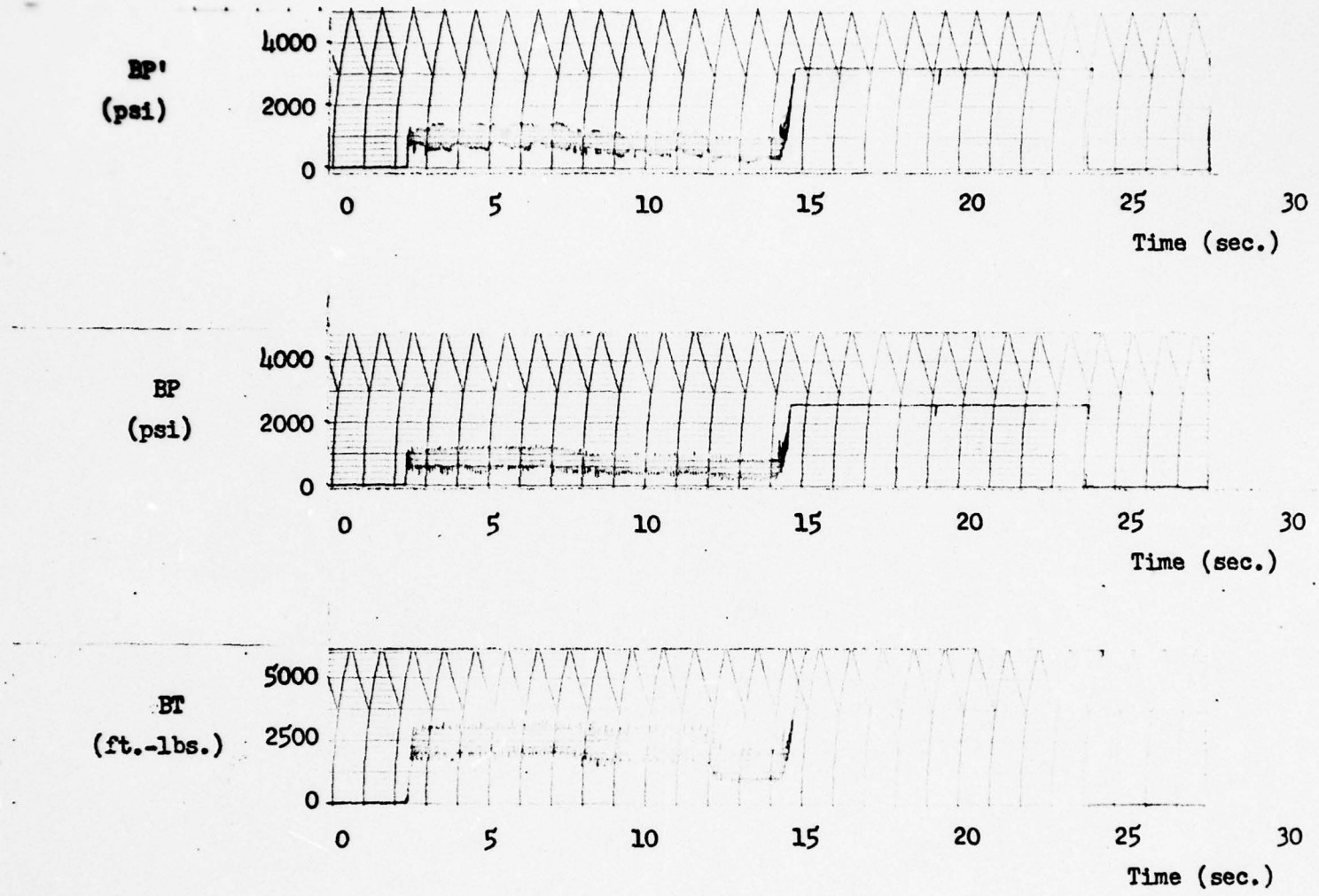

Fig. 20. BP', BP, and BT vs. Time for 30,000 lb. F-4E, Dry Runway

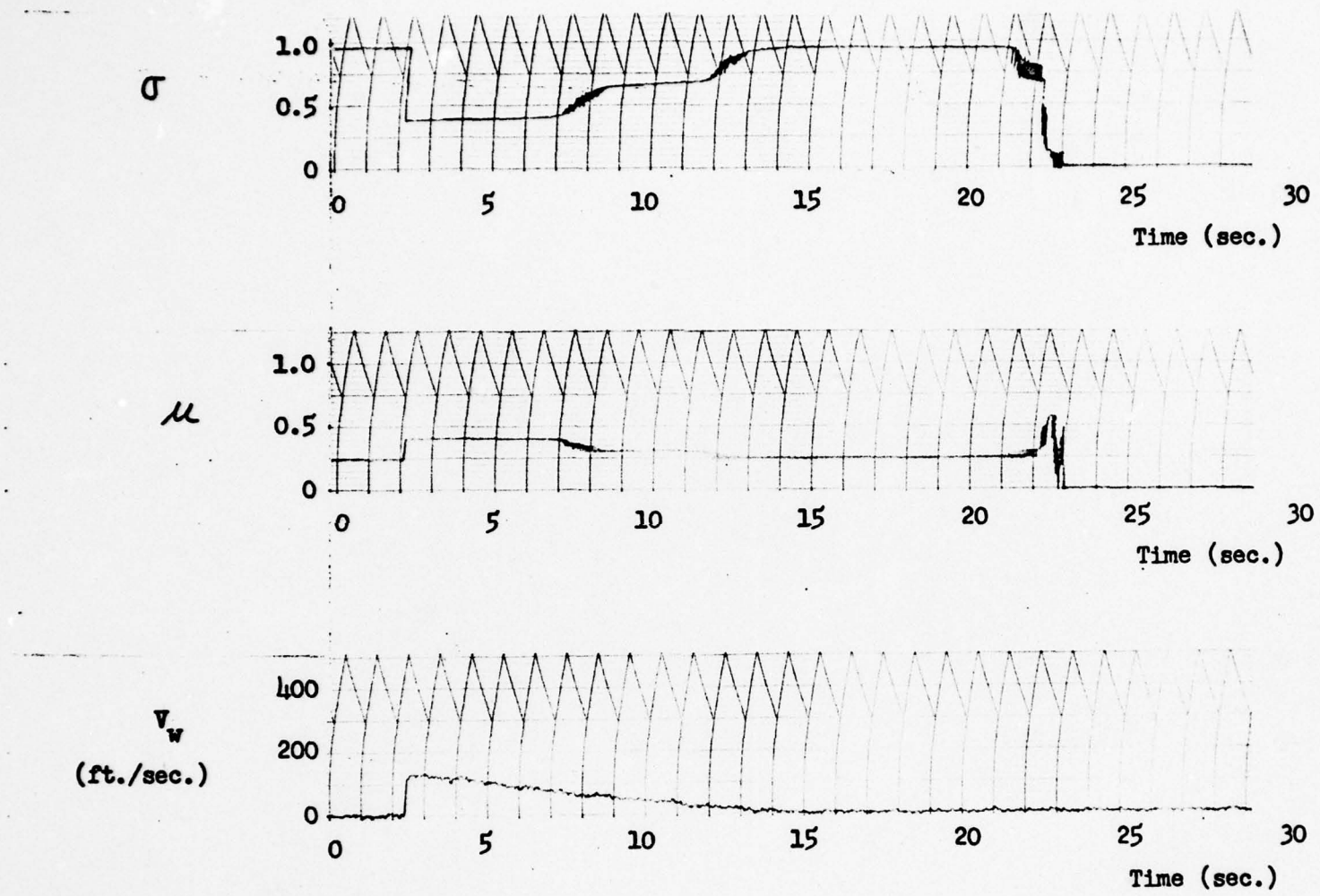

Fig. 21. σ, μ, and V_w vs. Time for 30,000 lb. F-4E, Dry Runway

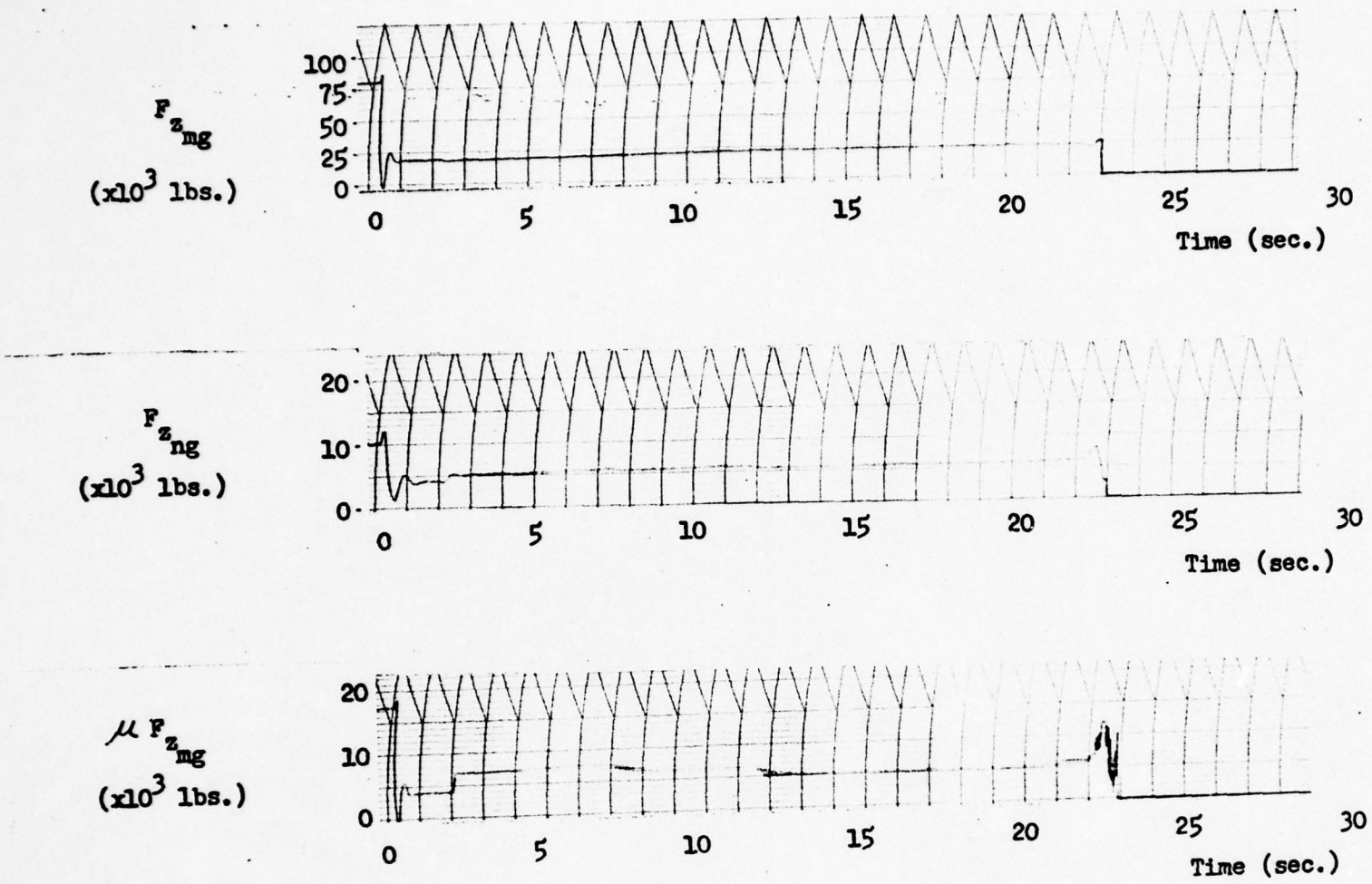

Fig. 22. $F_{z_{mg}}$, $F_{z_{ng}}$, and $\mu F_{z_{mg}}$ vs. Time for 30,000 lb. F-4E, Dry Runway

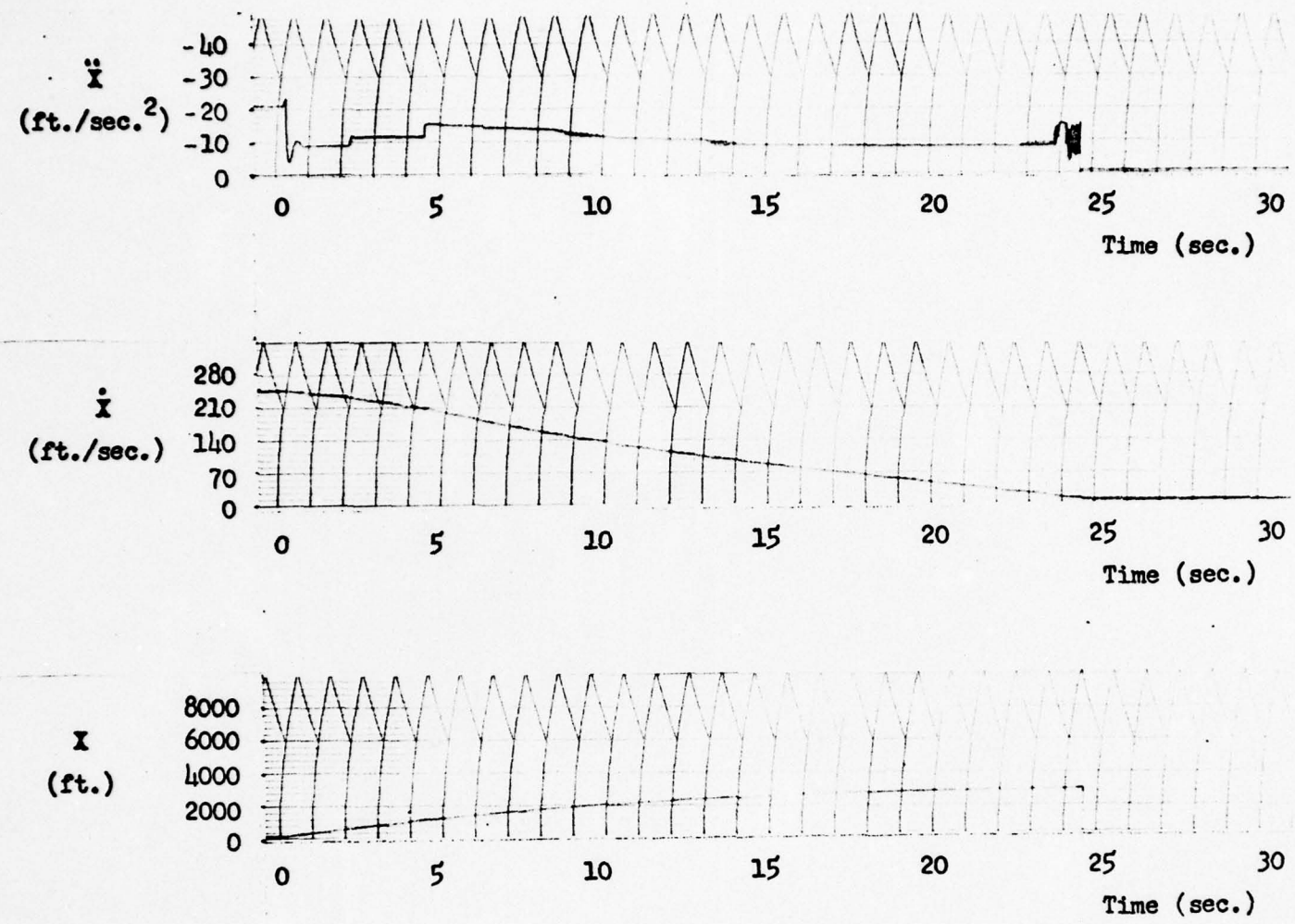

Fig. 23. $\ddot{X}$, $\dot{X}$, and X vs. Time for 35,000 lb. F-4E, Dry Runway

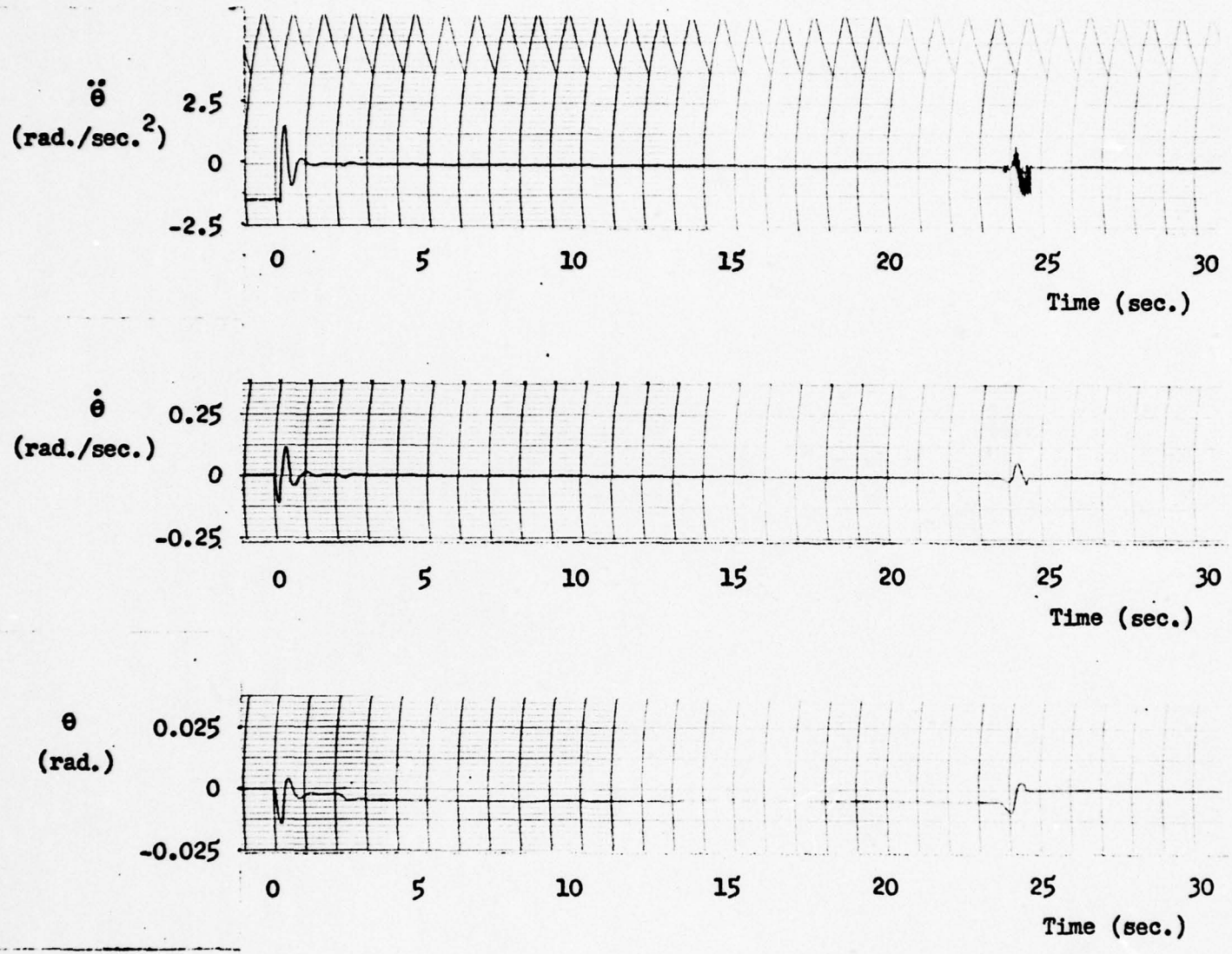

Fig. 24. $\ddot{\theta}$, $\dot{\theta}$, and θ vs. Time for 35,000 lb. F-4E, Dry Runway

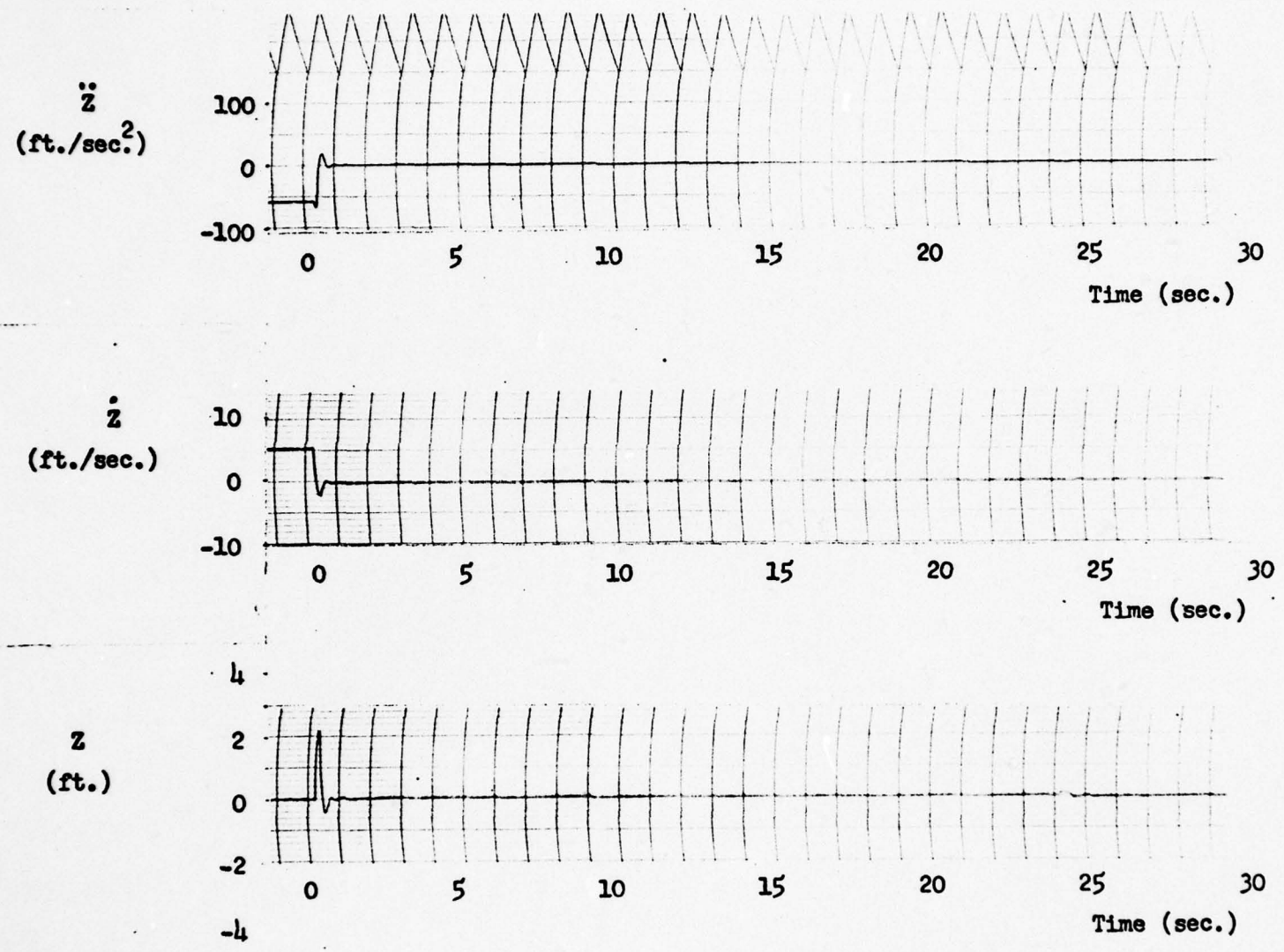

Fig. 25. $\ddot{z}$, $\dot{z}$, and Z vs. Time for 35,000 lb. F-4E, Dry Runway

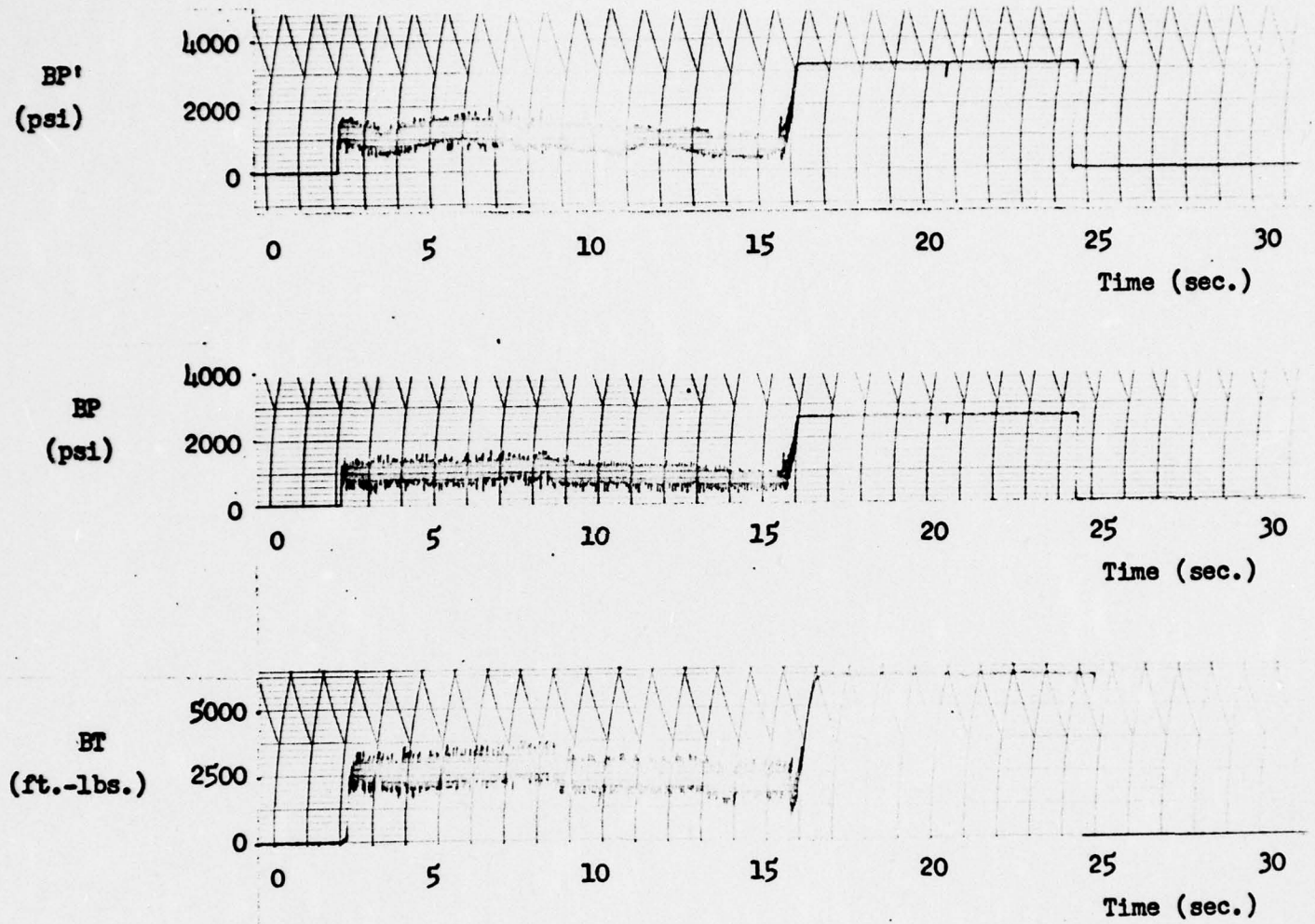

Fig. 26. BP', BP, and BT vs. Time for 35,000 lb. F-4E, Dry Runway

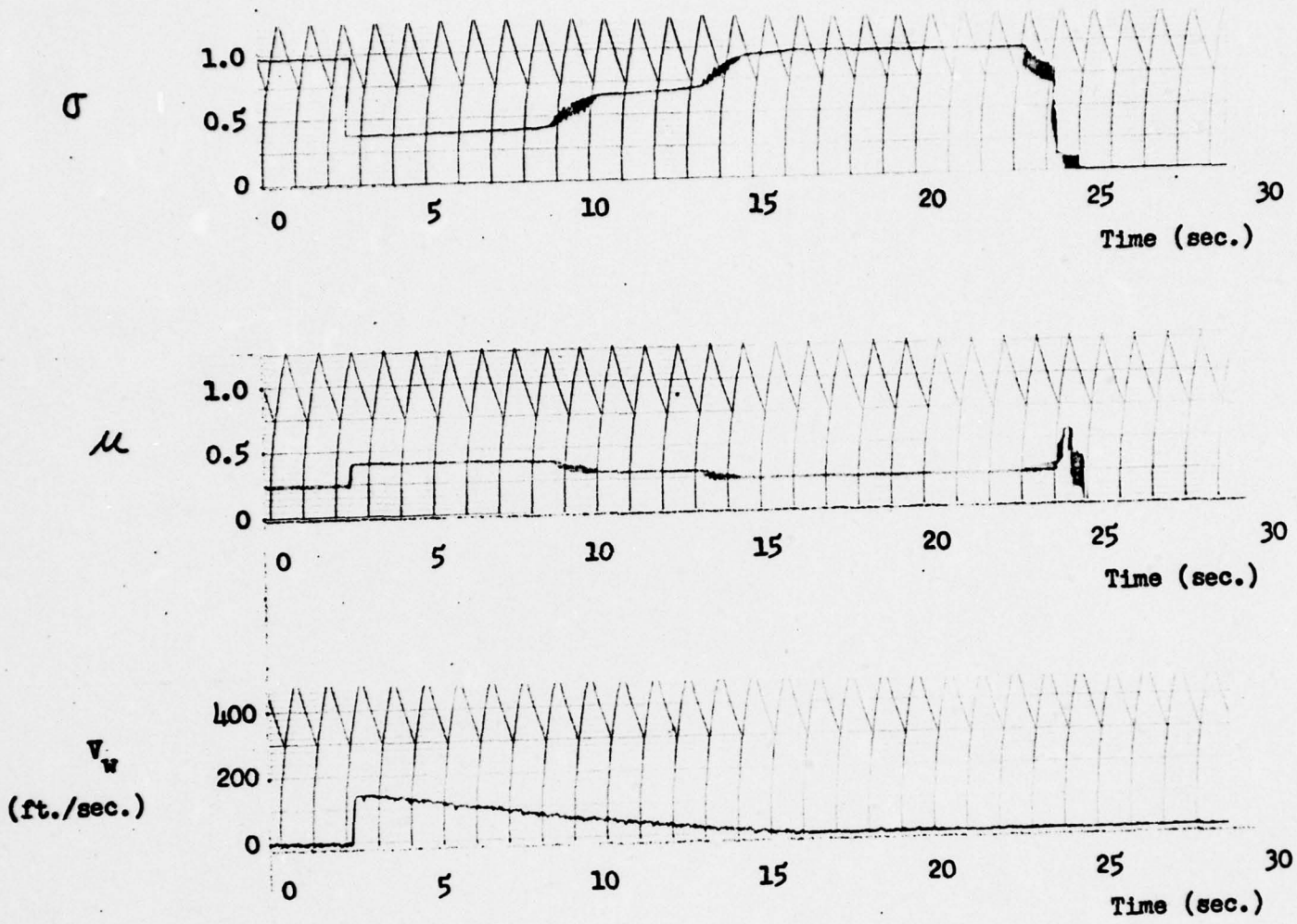

Fig. 27. σ, μ, and V_w vs. Time for 35,000 lb. F-4E, Dry Runway

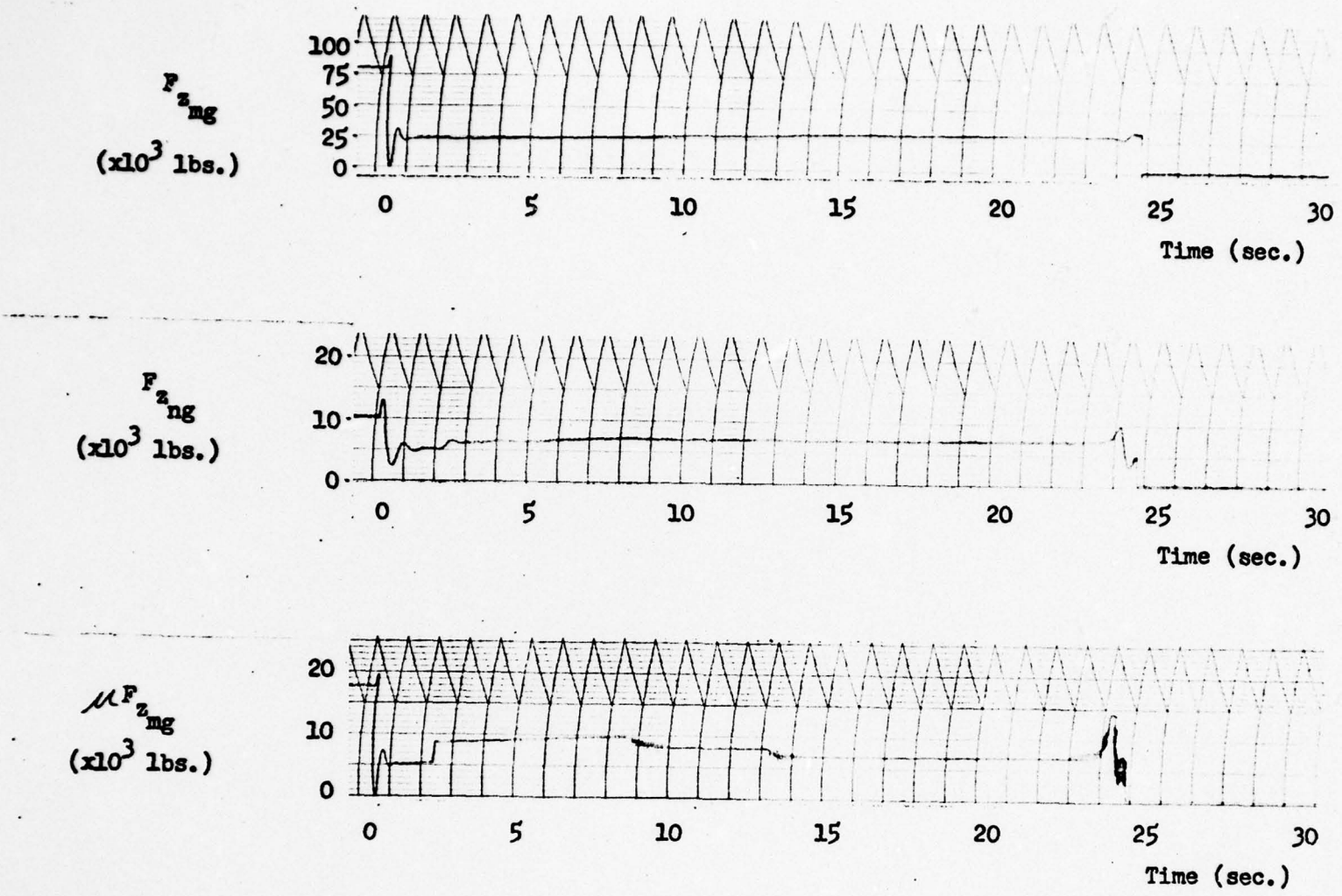

Fig. 28. $F_{z_{mg}}$, $F_{z_{ng}}$, and $\mu F_{z_{mg}}$ vs. Time for 35,000 lb. F-4E, Dry Runway

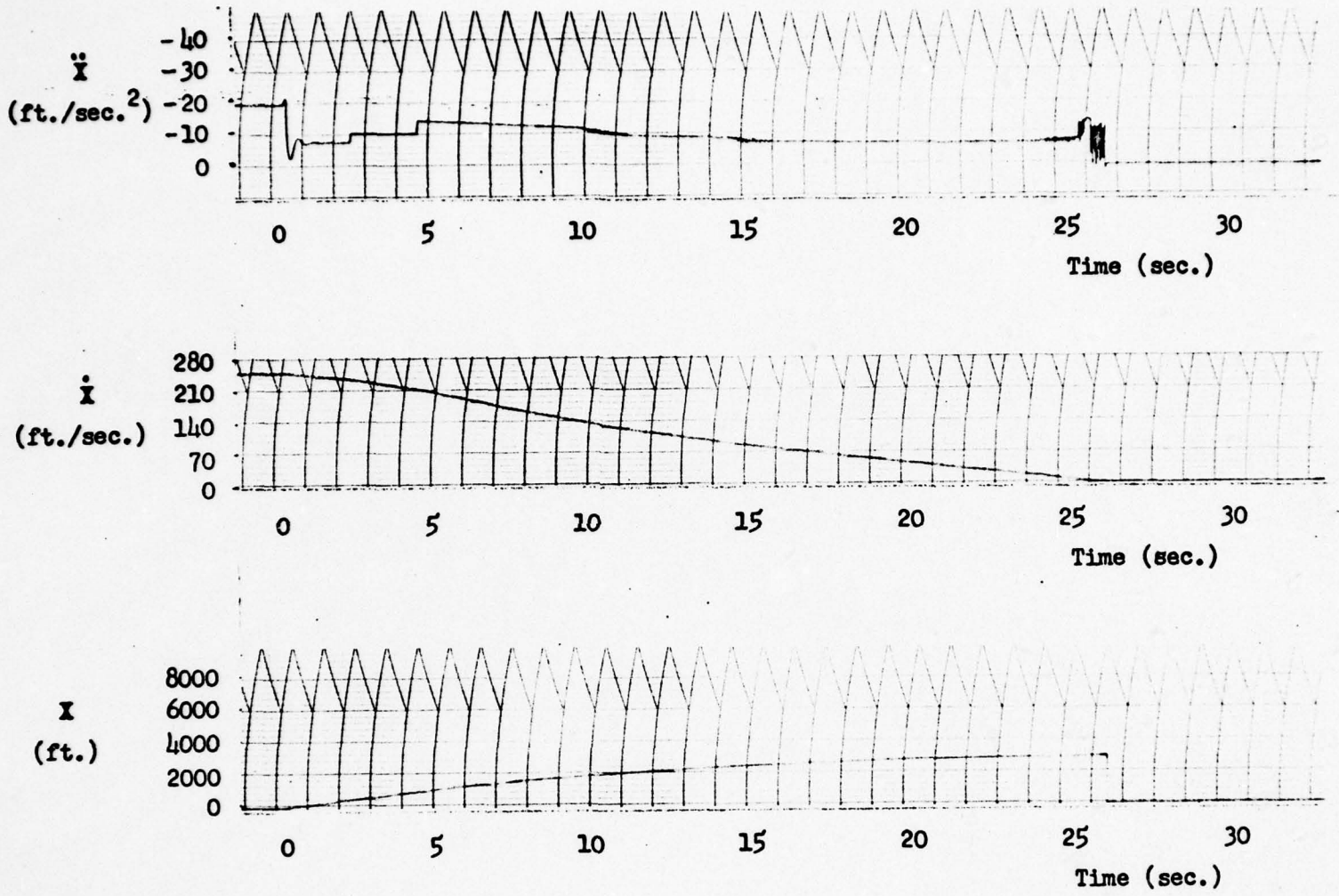

Fig. 29. $\ddot{X}$, $\dot{X}$, and X vs. Time for 40,000 lb. F-4E, Dry Runway

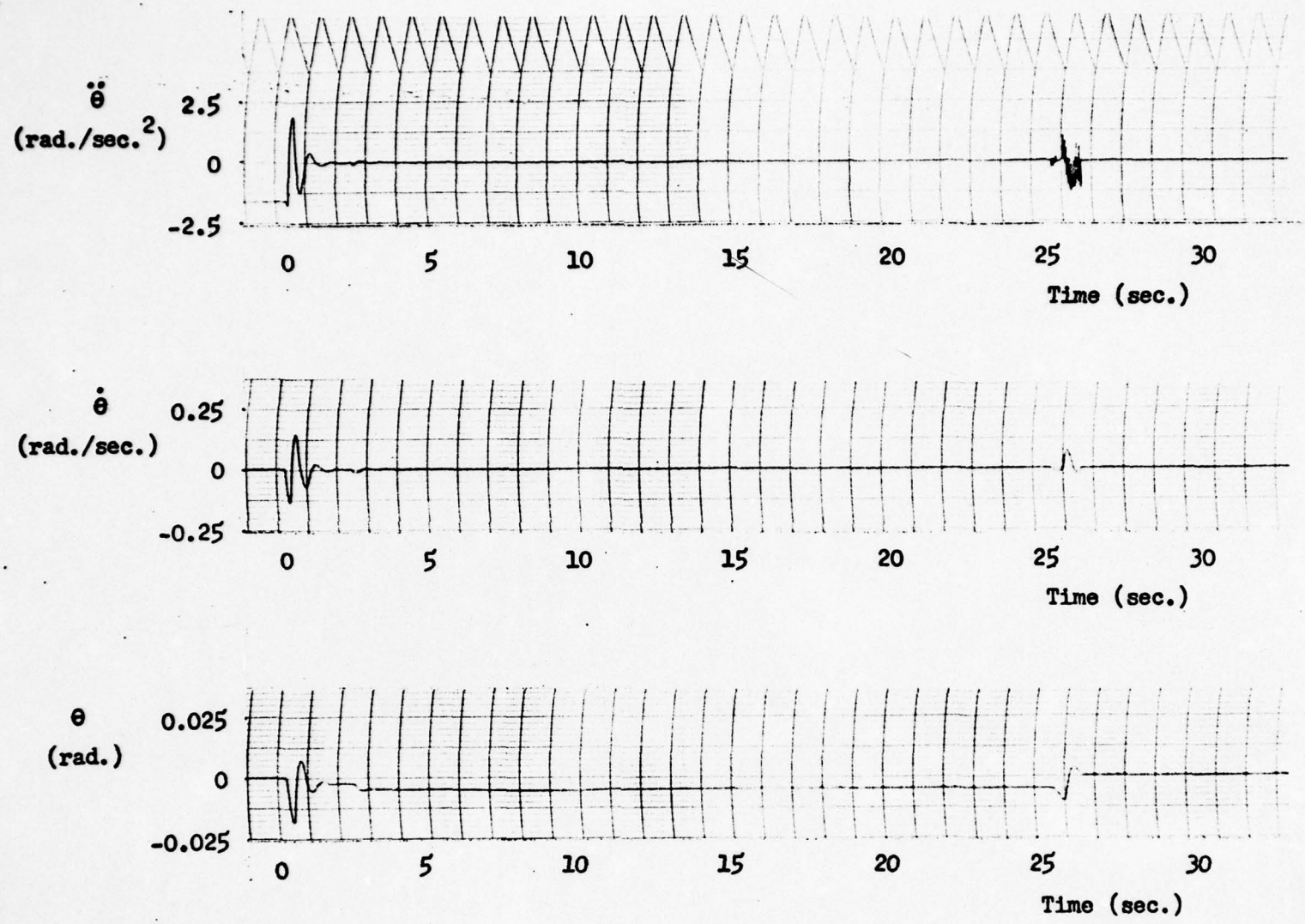

Fig. 30. $\ddot{\theta}$, $\dot{\theta}$, and θ vs. Time for 40,000 lb. F-4E, Dry Runway

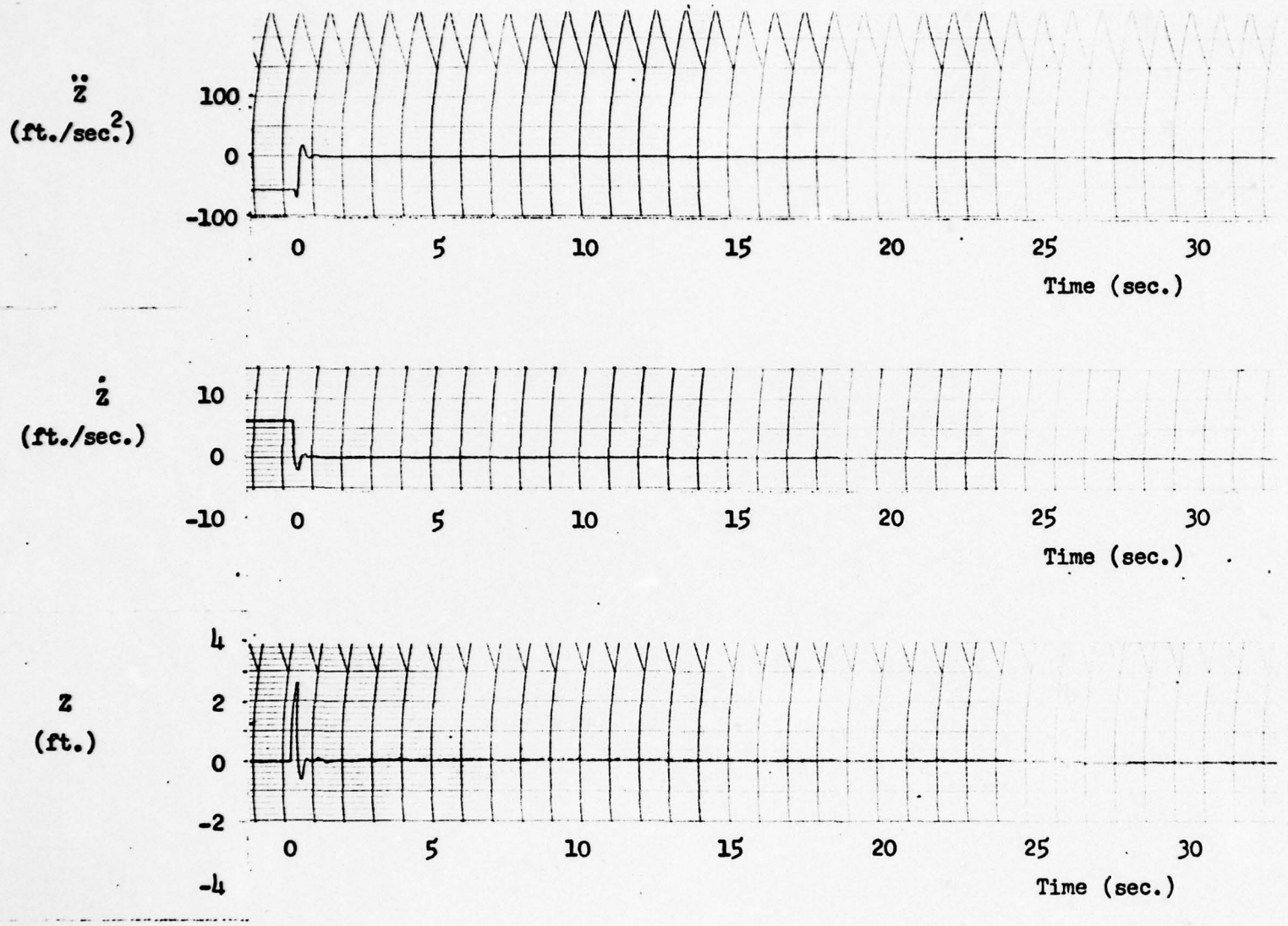

Fig. 31. $\ddot{z}$, $\dot{z}$, and z vs. Time for 40,000 lb. F-4E, Dry Runway

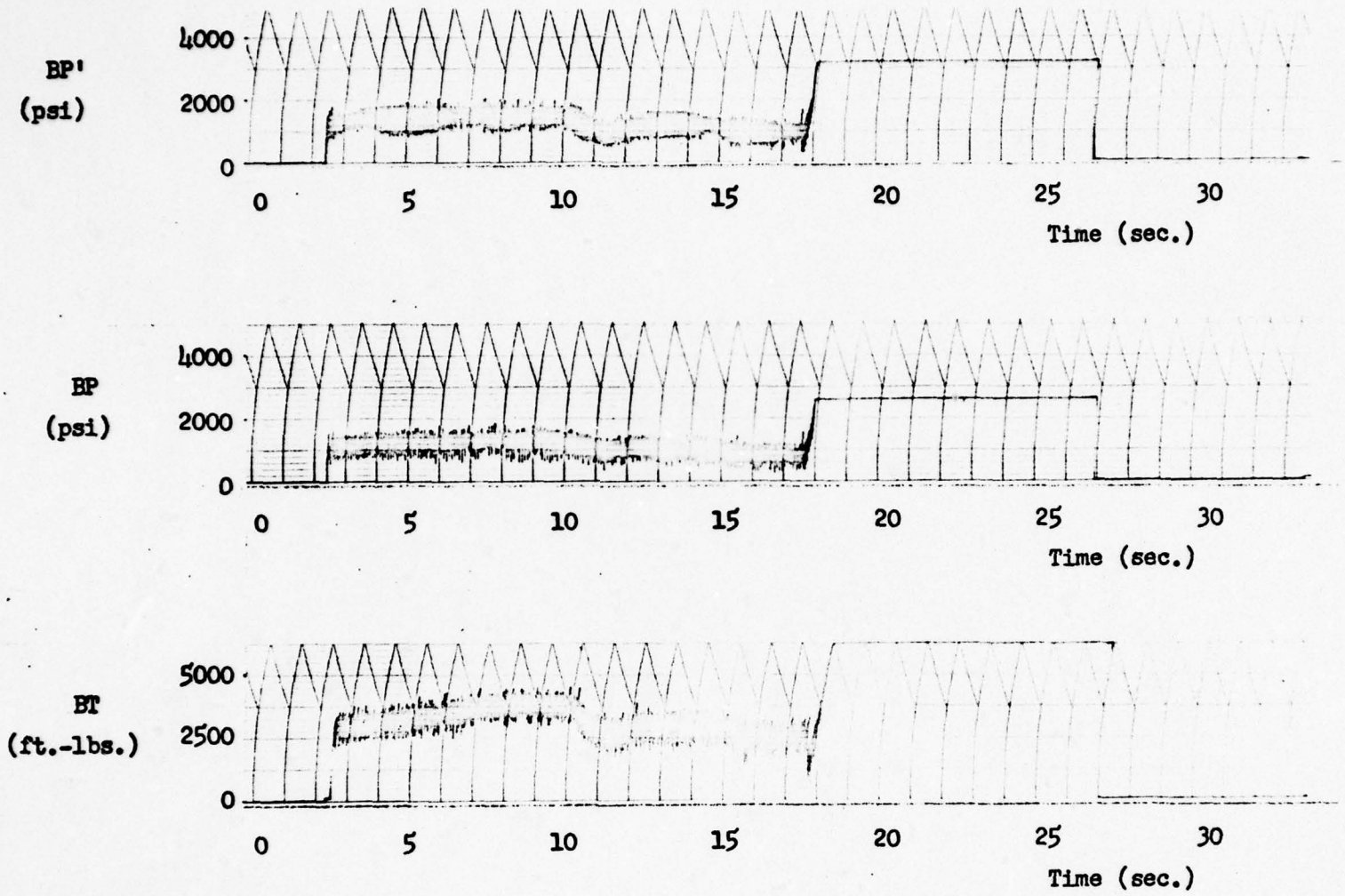

Fig. 32. BP', BP, and BT vs. Time for 40,000 lb. F-4E, Dry Runway

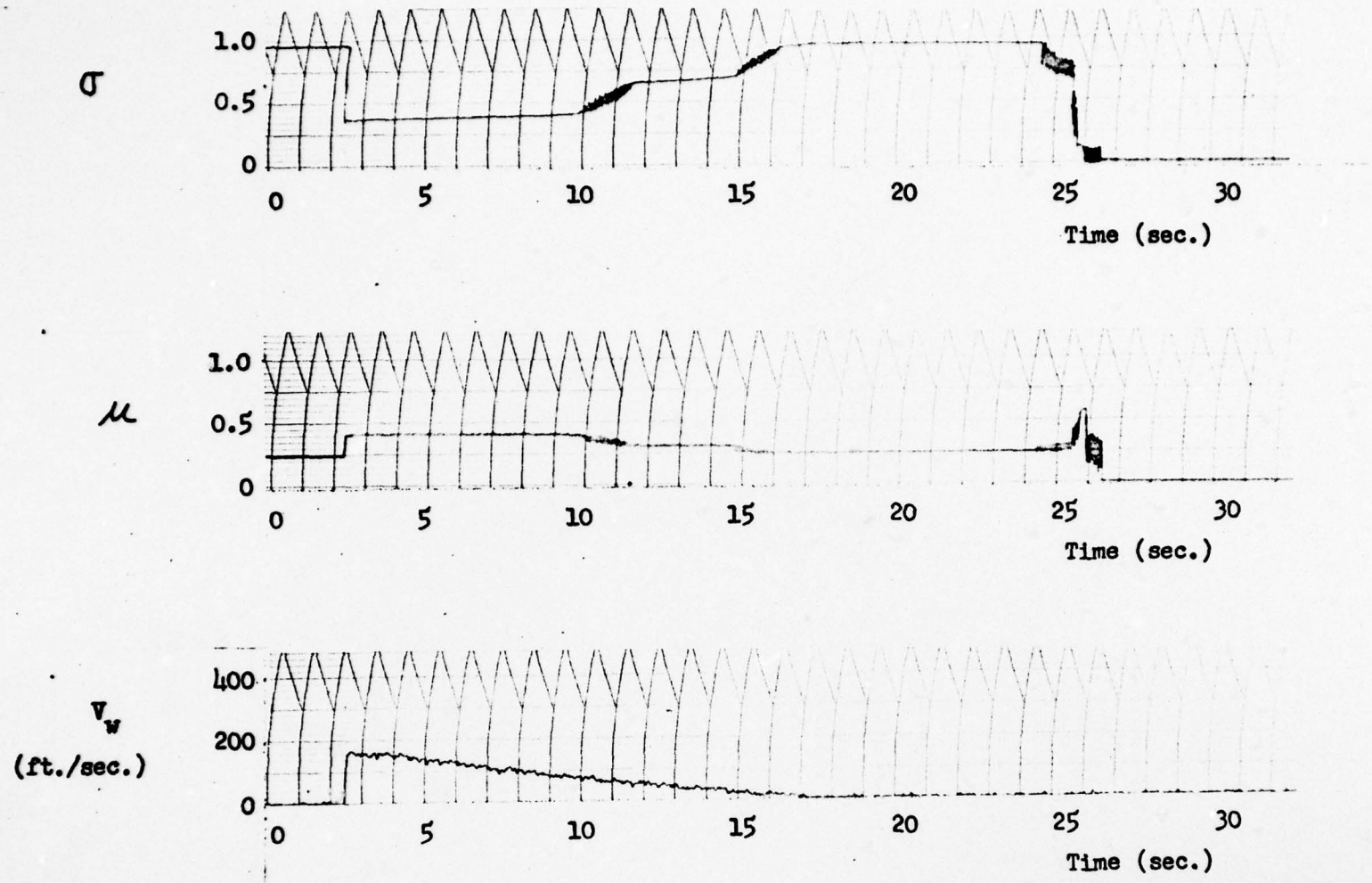

Fig. 33. σ , μ, V_w vs. Time for 40,000 lb. F-4E, Dry Runway

AD-A034 942 AIR FORCE INST OF TECH WRIGHT-PATTERSON AFB OHIO SCH--ETC F/G 1/2
SYSTEM SIMULATION IN AIRCRAFT LANDING GEAR AND TIRE DEVELOPMENT--ETC(U)
DEC 76 J A SKORUPA

UNCLASSIFIED GAE/MC/76D-7 NL

2 OF 2
ADA034942

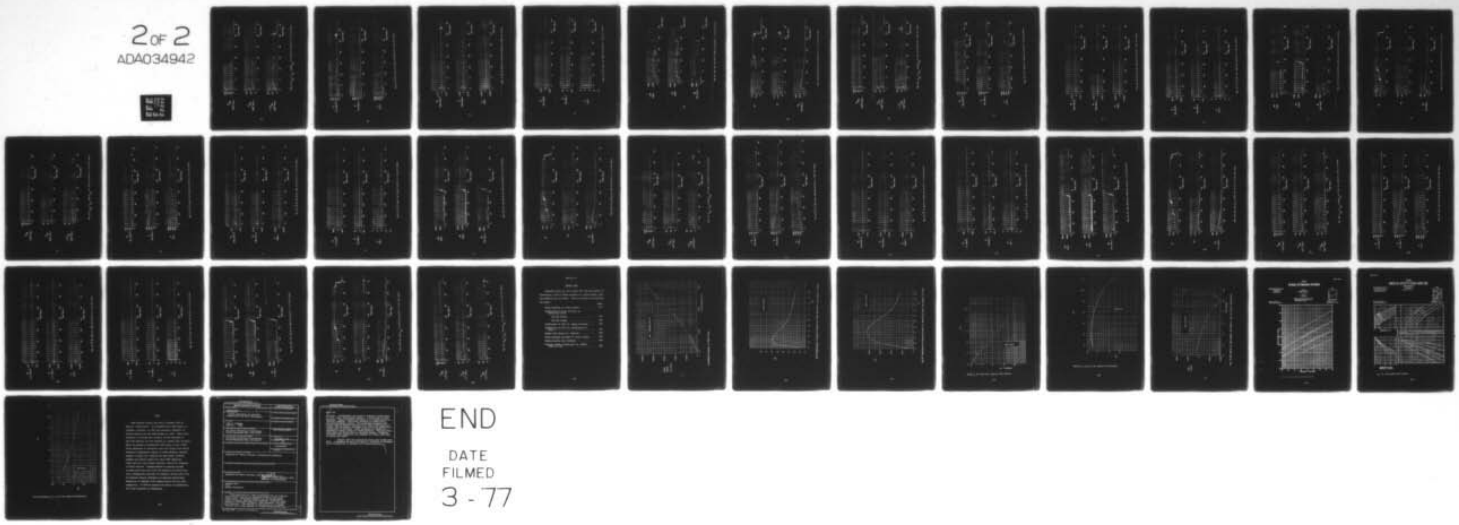

END

DATE
FILMED
3 - 77

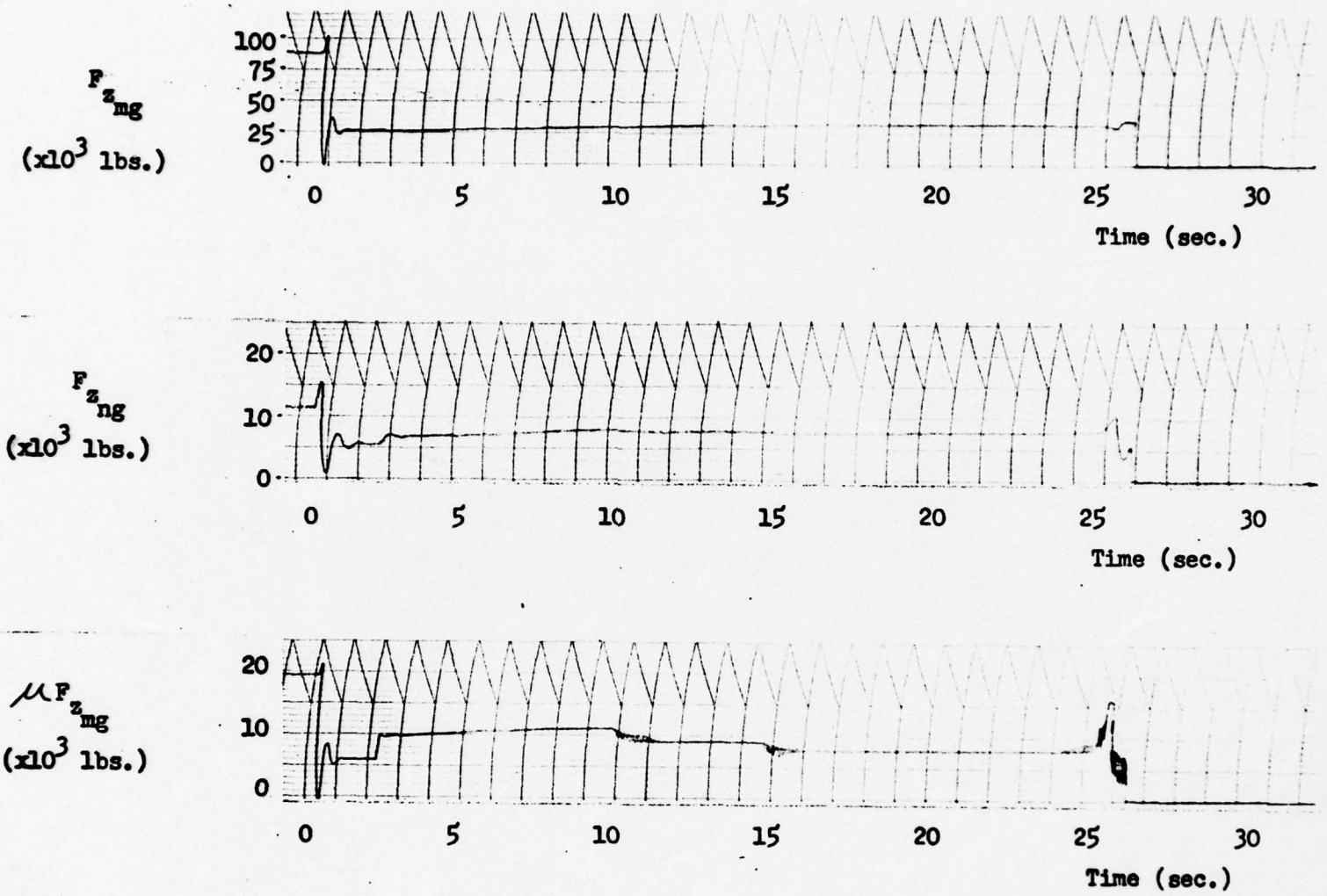

Fig. 34. $F_{z_{mg}}$, $F_{z_{ng}}$, and $\mu F_{z_{mg}}$ vs. Time for 40,000 lb. F-4E, Dry Runway

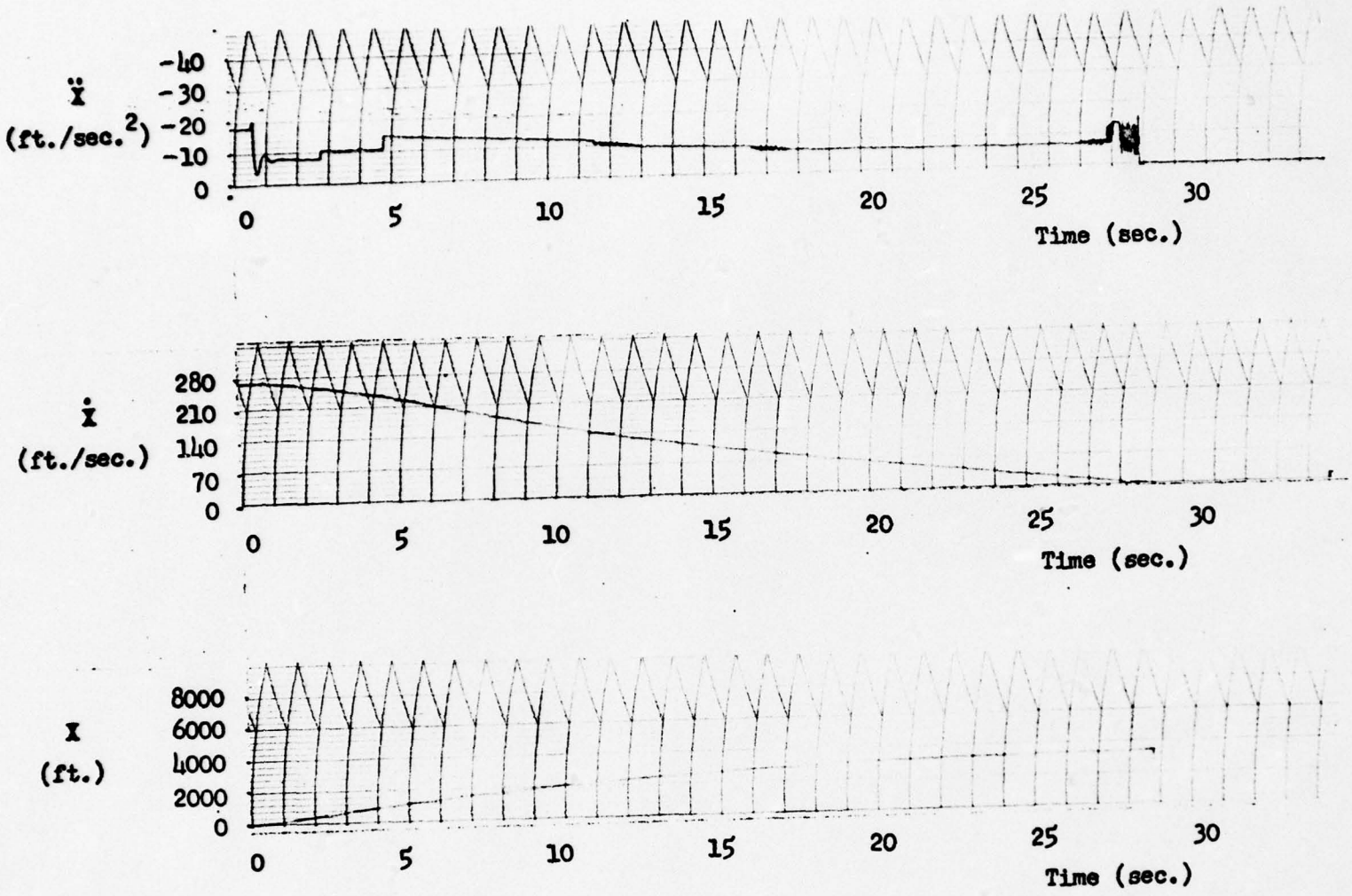

Fig. 35. $\ddot{X}$, $\dot{X}$, and X vs. Time for 45,000 lb. F-4E, Dry Runway

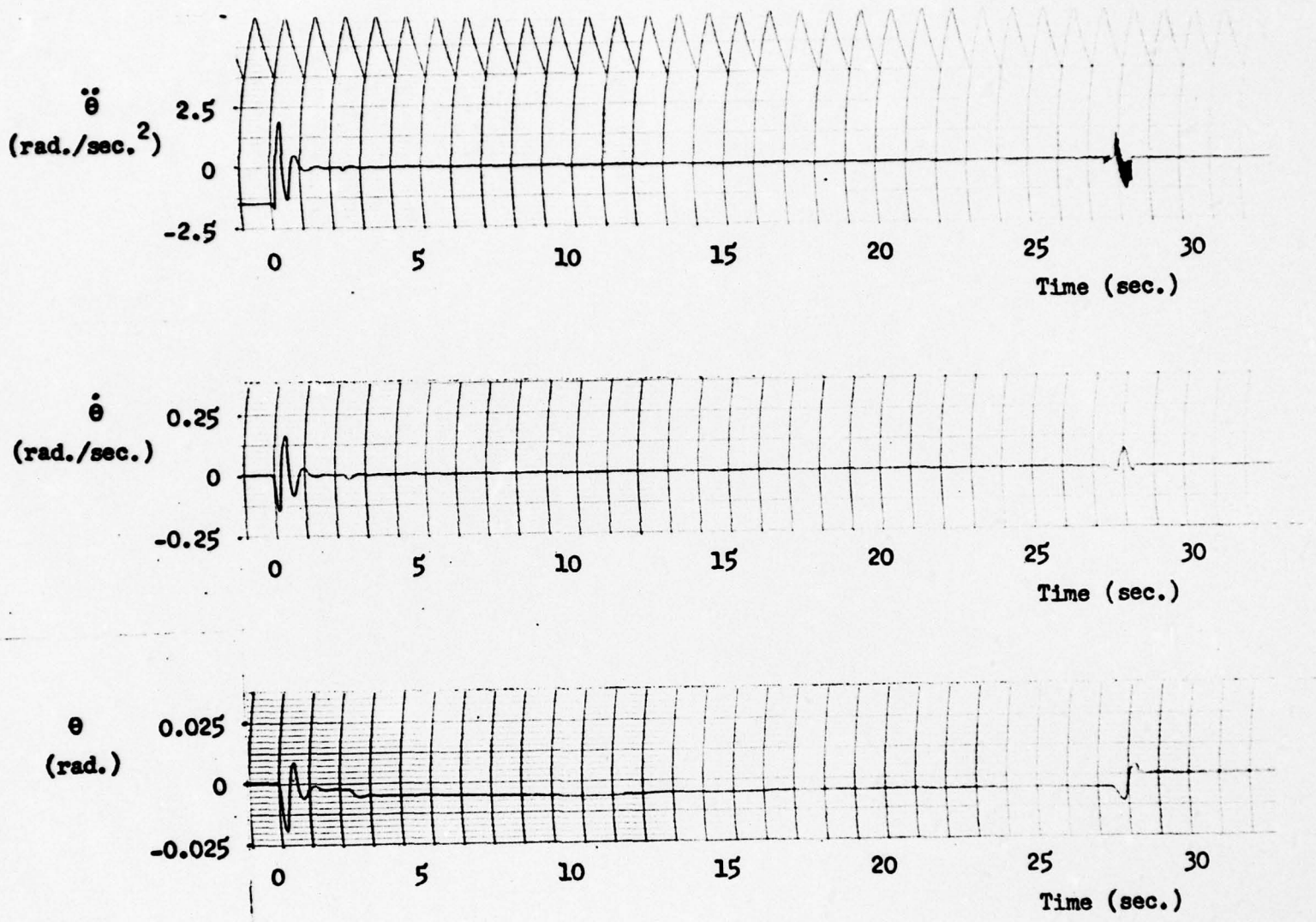

Fig. 36. $\ddot{\theta}$, $\dot{\theta}$, and θ vs. Time for 45,000 lb. F-4E, Dry Runway

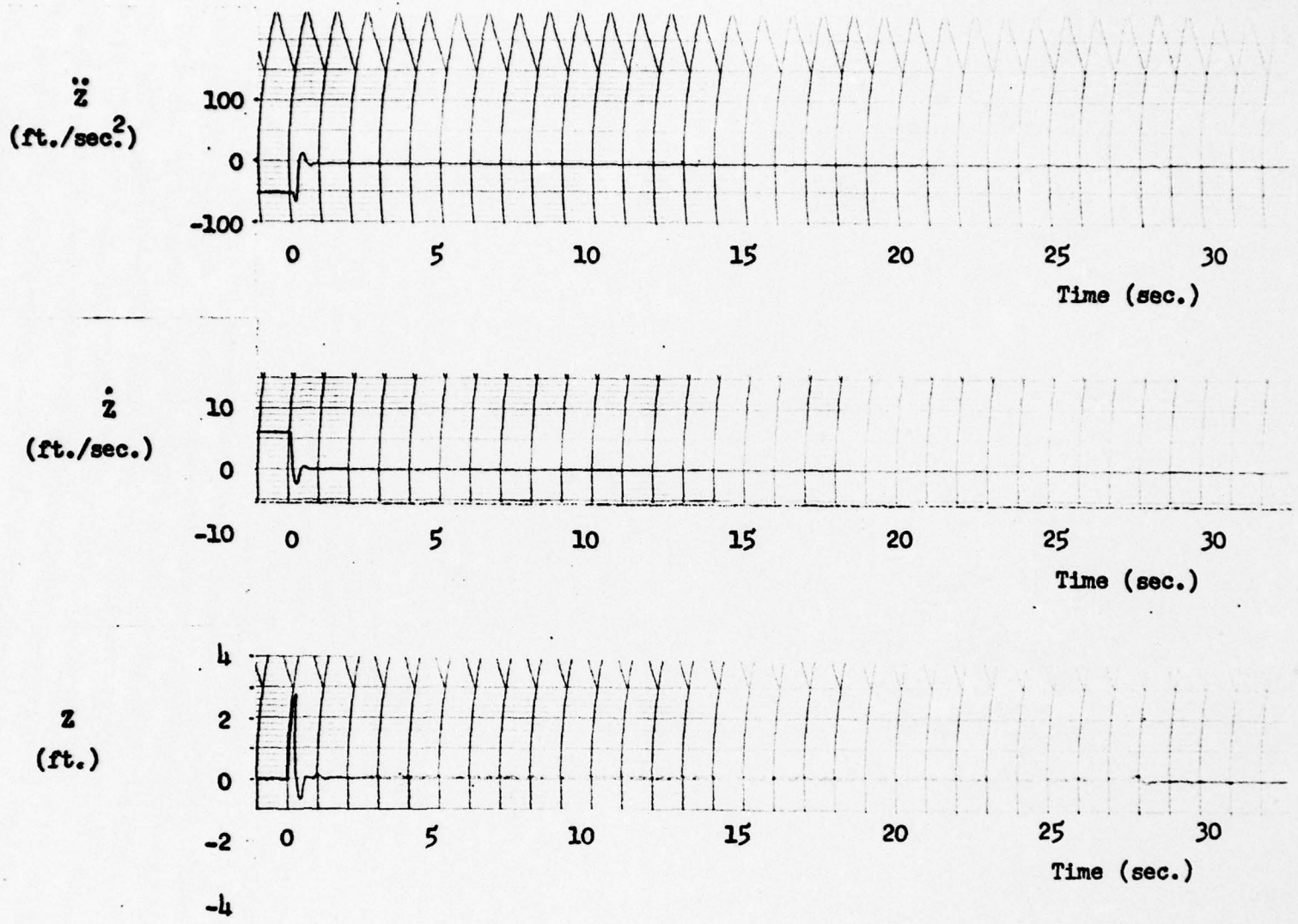

Fig. 37. $\ddot{z}$, $\dot{z}$, and z vs. Time for 45,000 lb. F-4E, Dry Runway

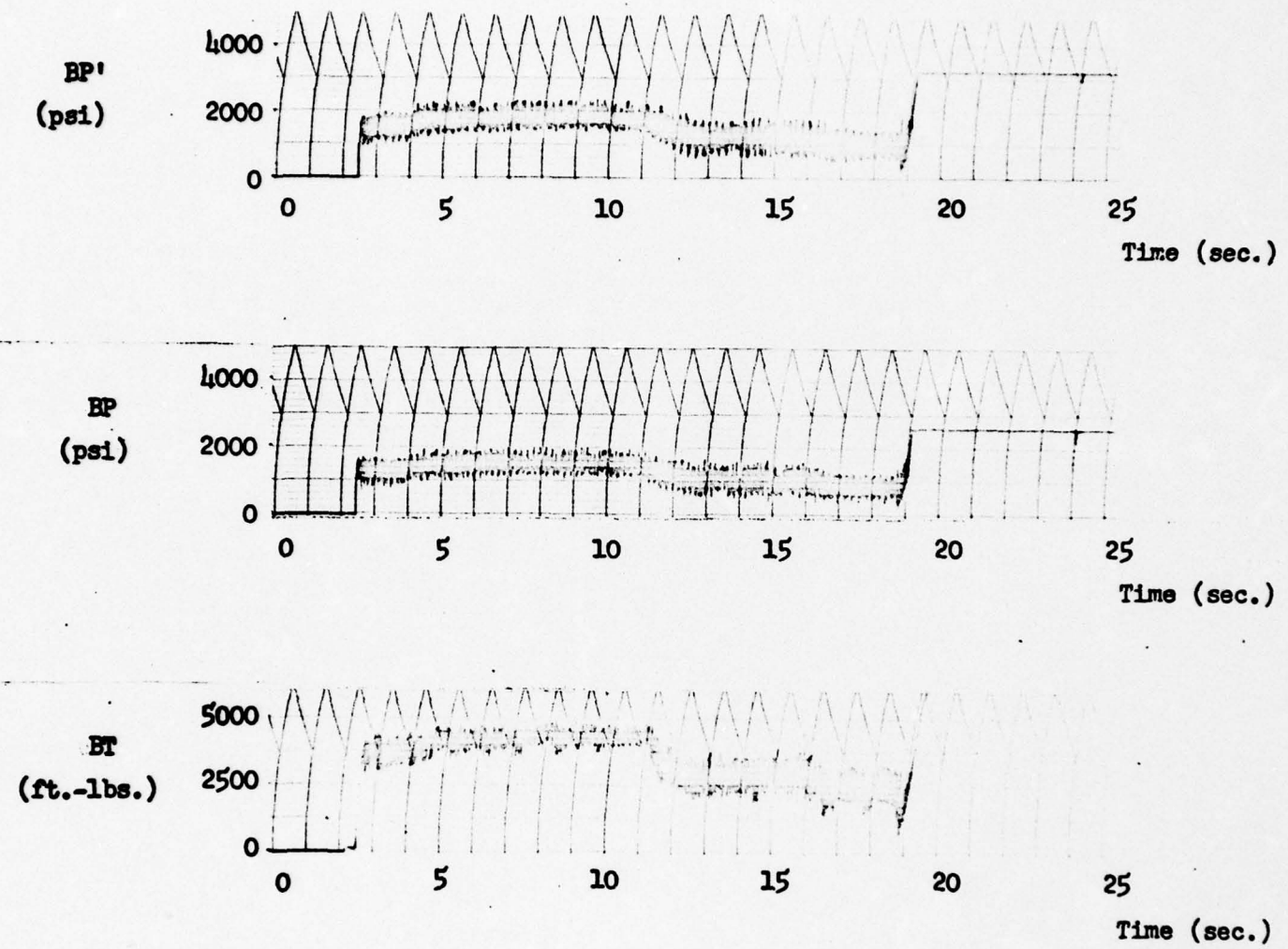

Fig. 38. BP', BP, and BT vs. Time for 45,000 lb. F-4E, Dry Runway

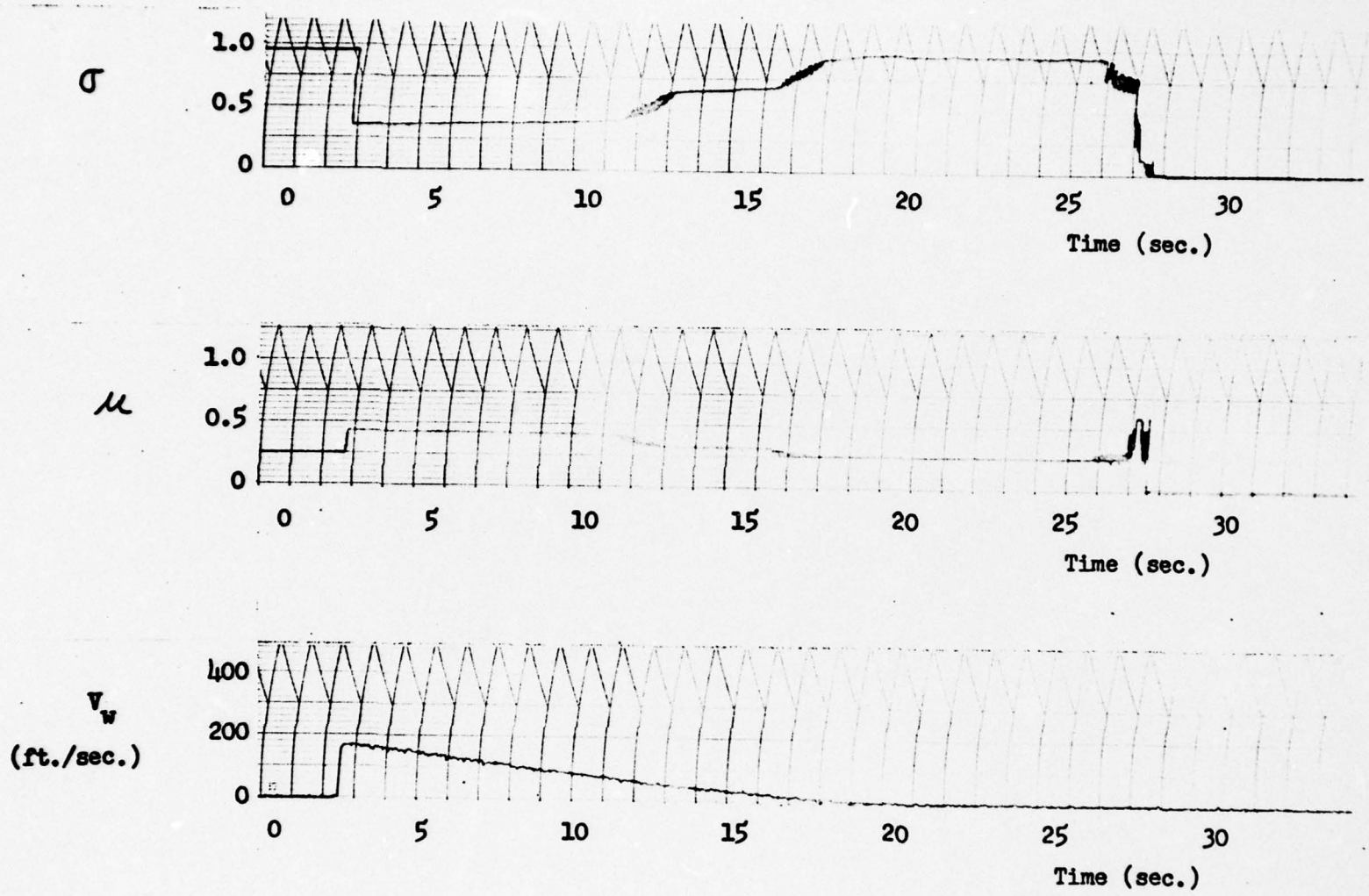

Fig. 39. σ, μ, and V_w vs. Time for 45,000 lb. F-4E, Dry Runway

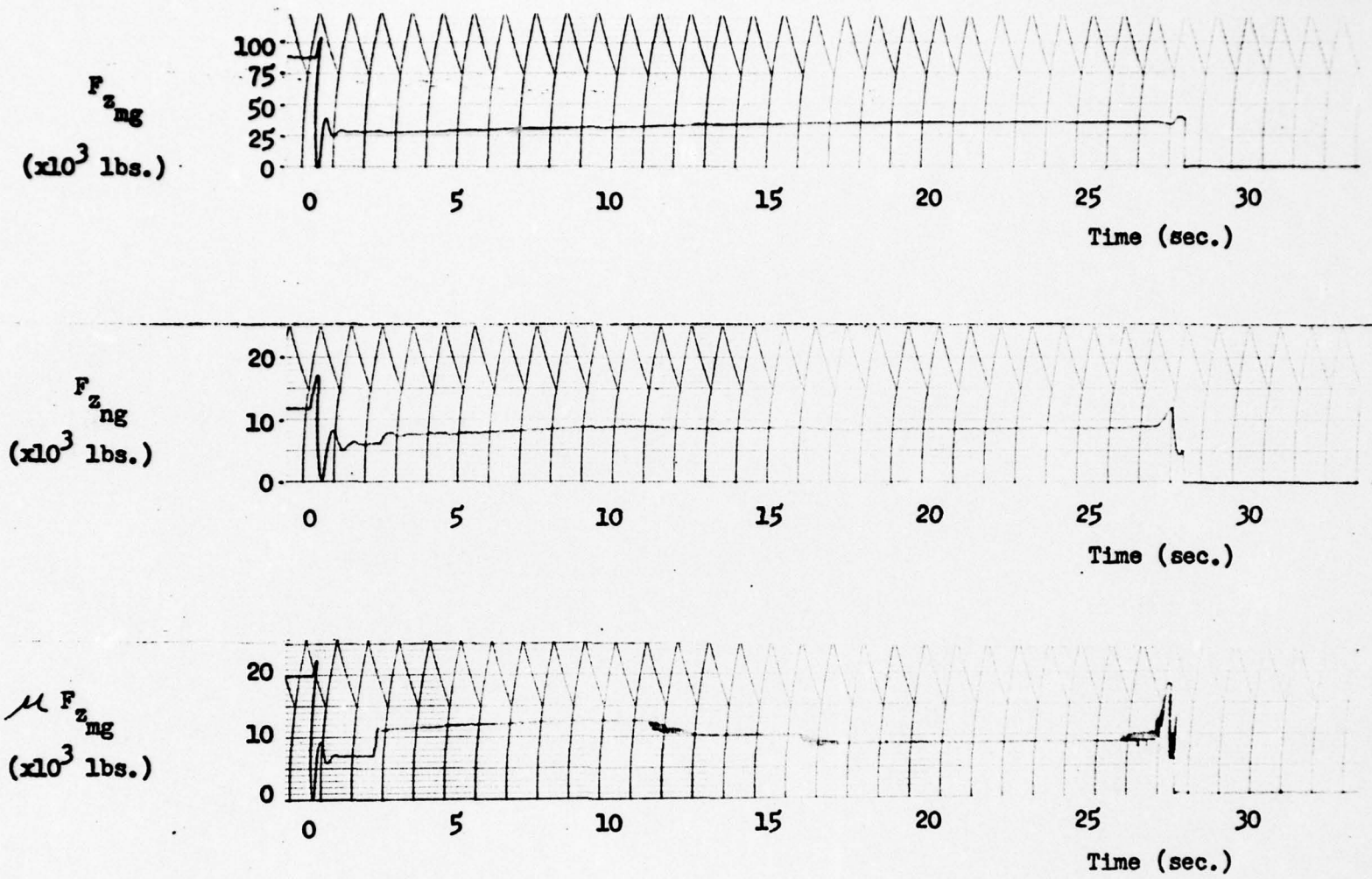

Fig. 40. $F_{z_{mg}}$, $F_{z_{ng}}$, and $\mu F_{z_{mg}}$ vs. Time for 45,000 lb. F-4E, Dry Runway

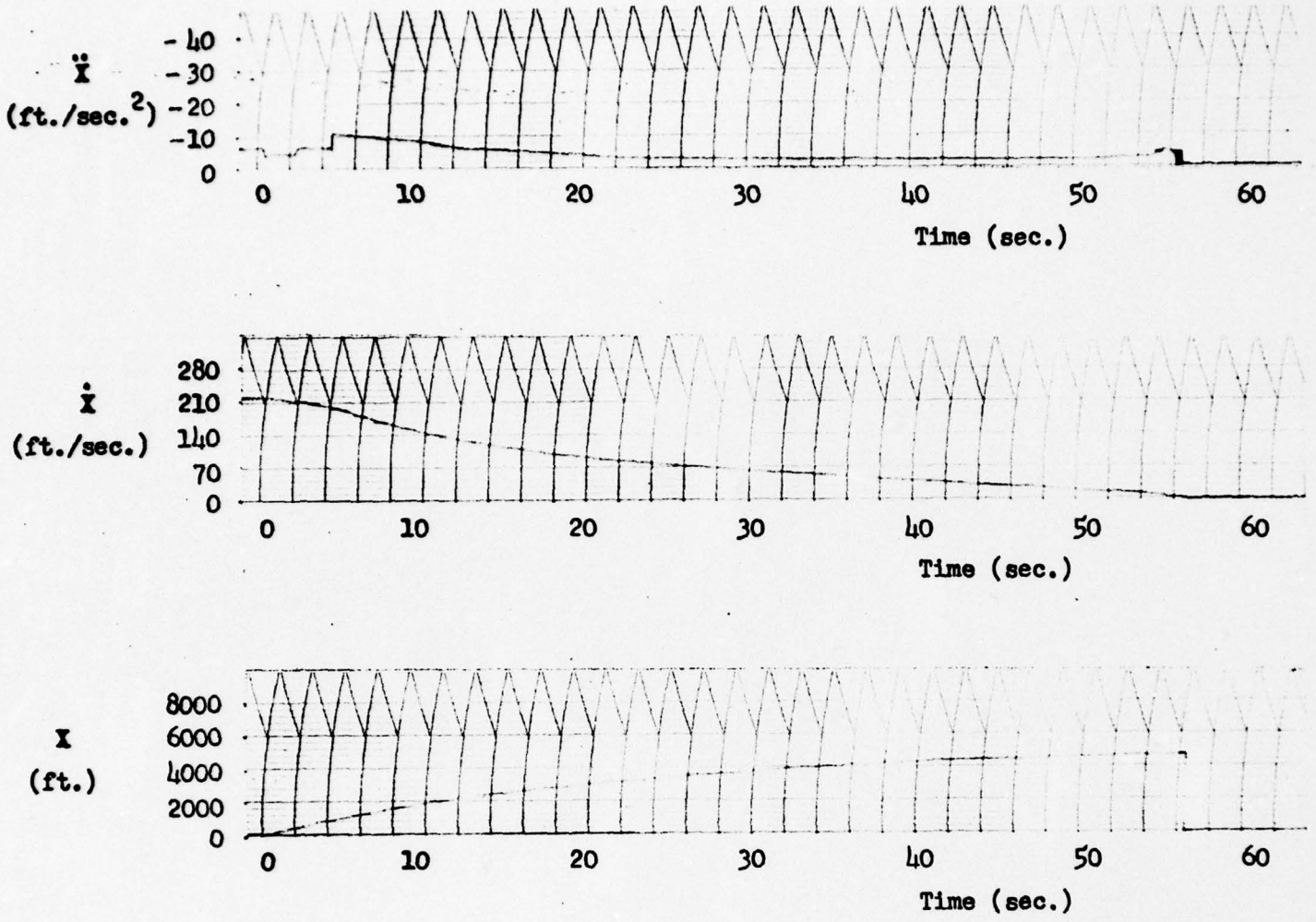

Fig. 41. $\ddot{X}$, $\dot{X}$, and X vs. Time for 30,000 lb. F-4E, Wet Runway

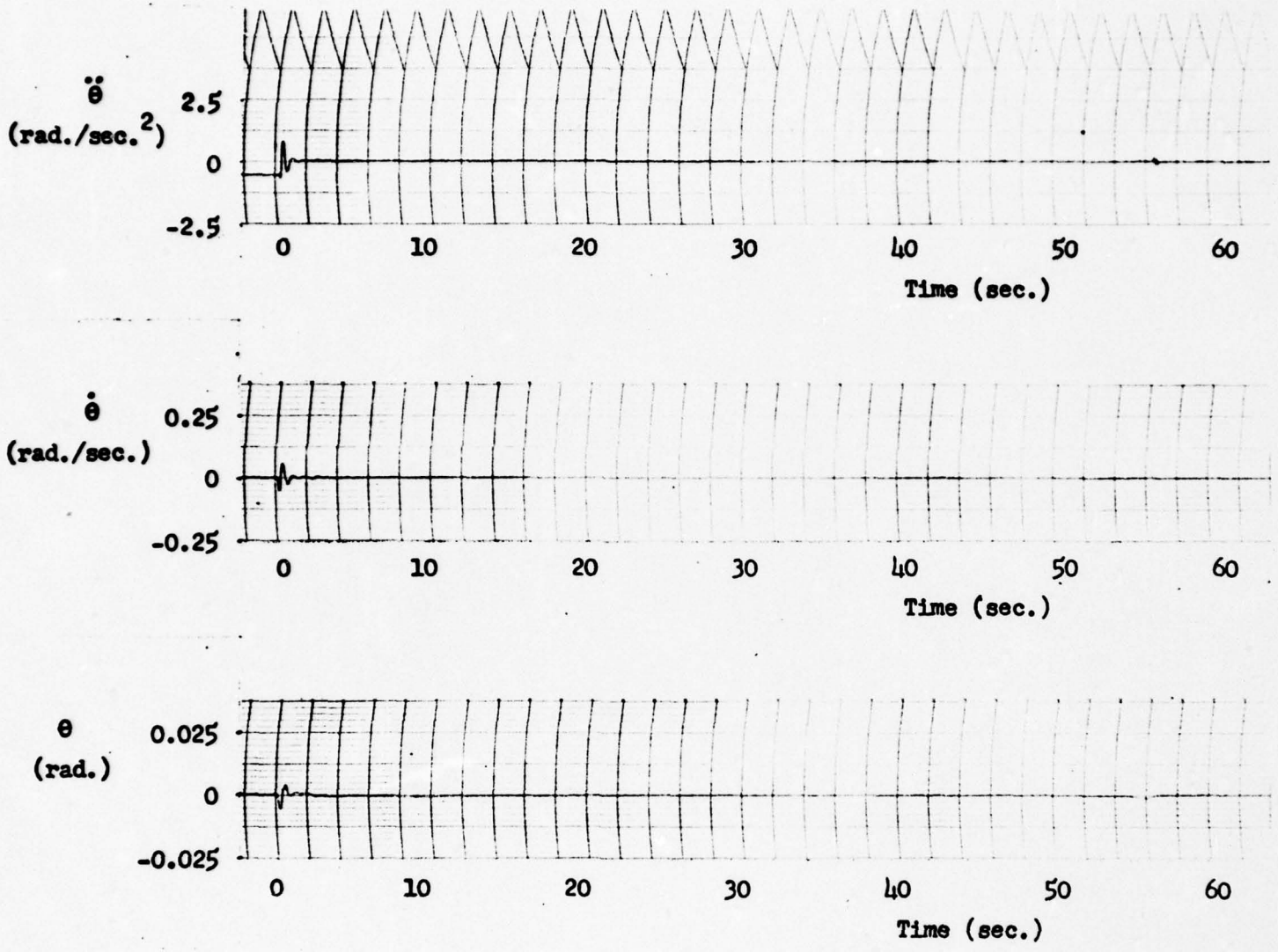

Fig. 42. $\ddot{\theta}$, $\dot{\theta}$, and θ vs. Time for 30,000 lb. F-4E, Wet Runway

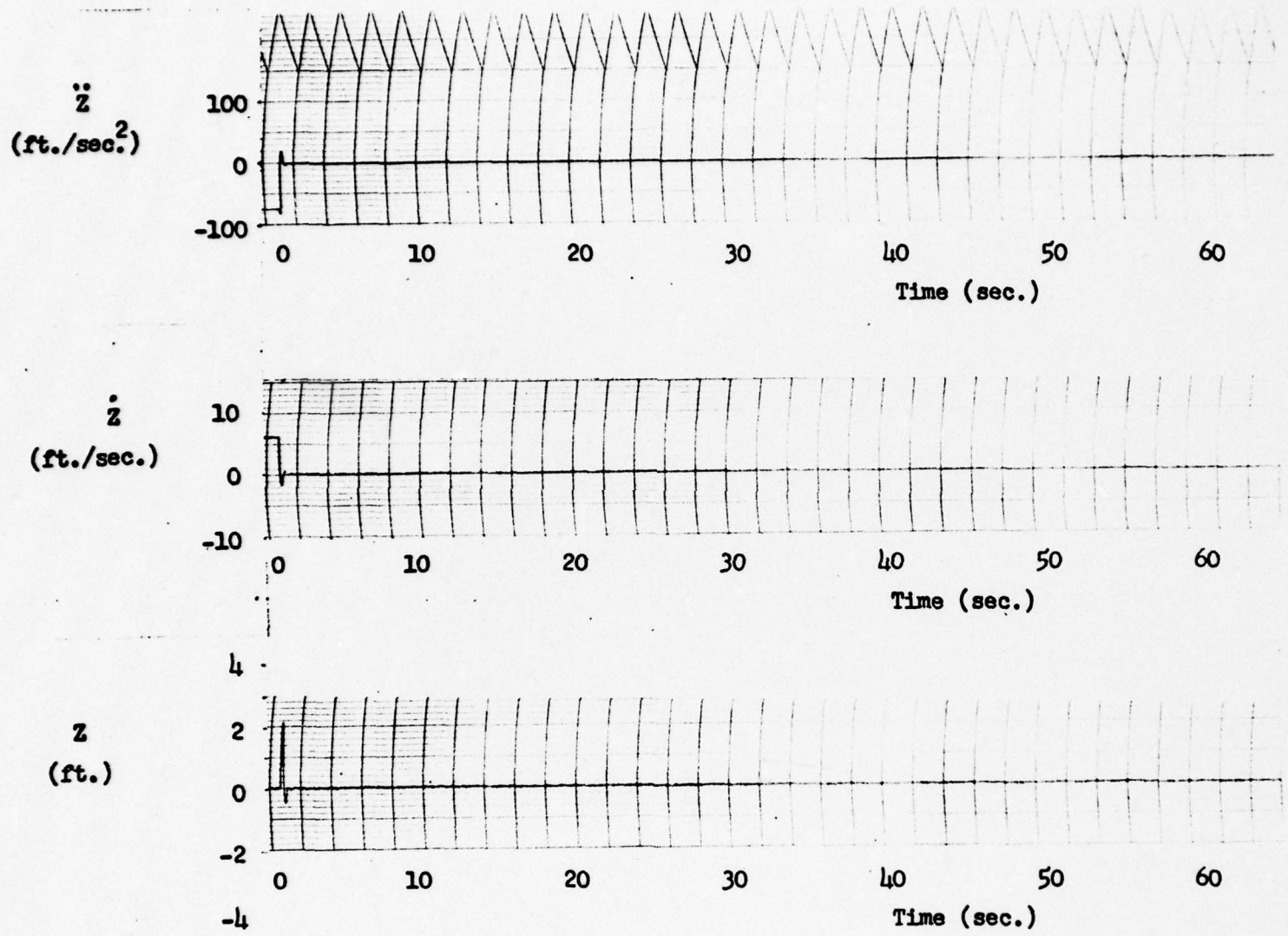

Fig. 43. $\ddot{z}$, $\dot{z}$, and z vs. Time for 30,000 lb. F-4E, Wet Runway

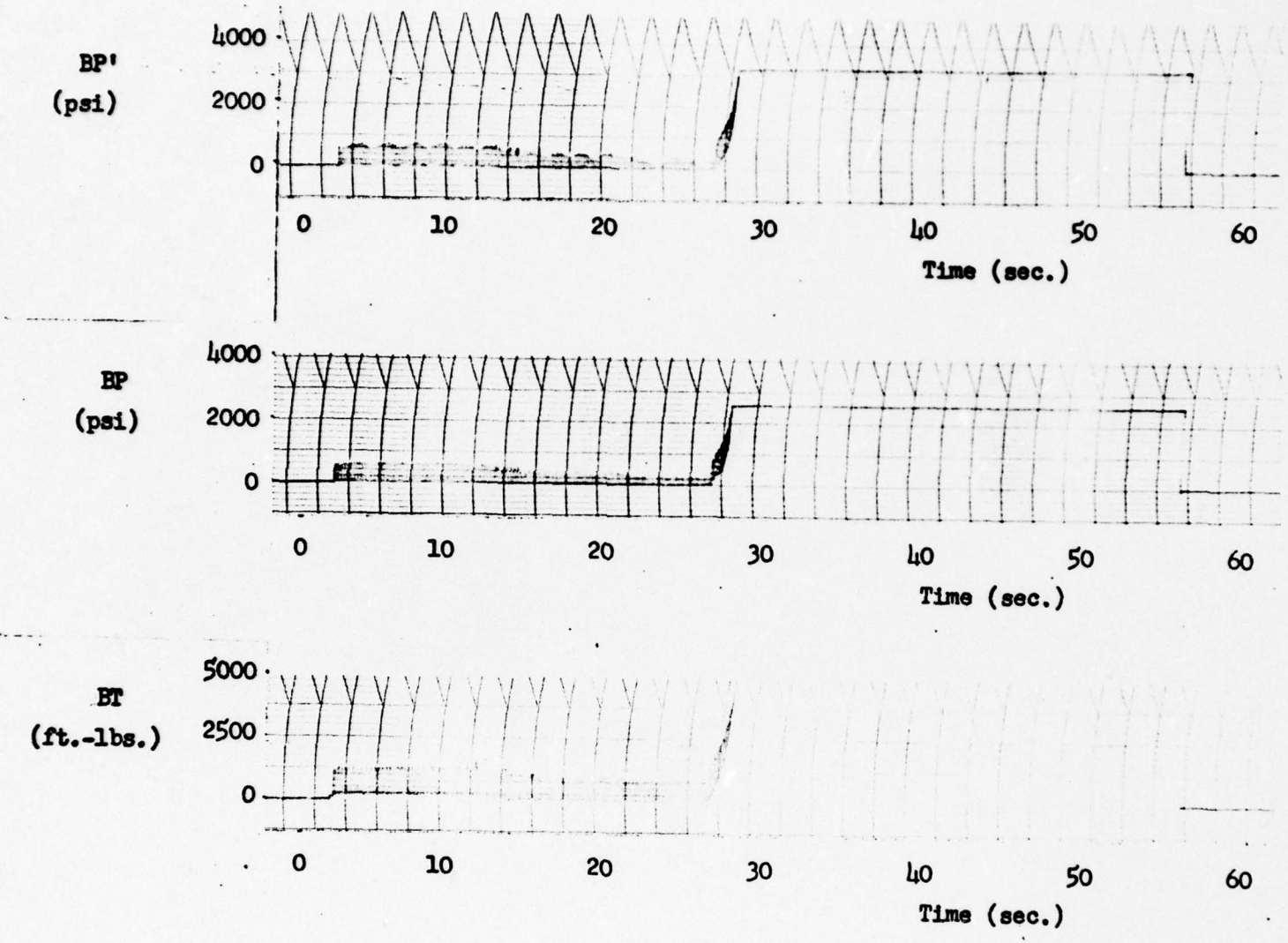

Fig. 44. BP', BP, and BT vs. Time for 30,000 lb. F-4E, Wet Runway

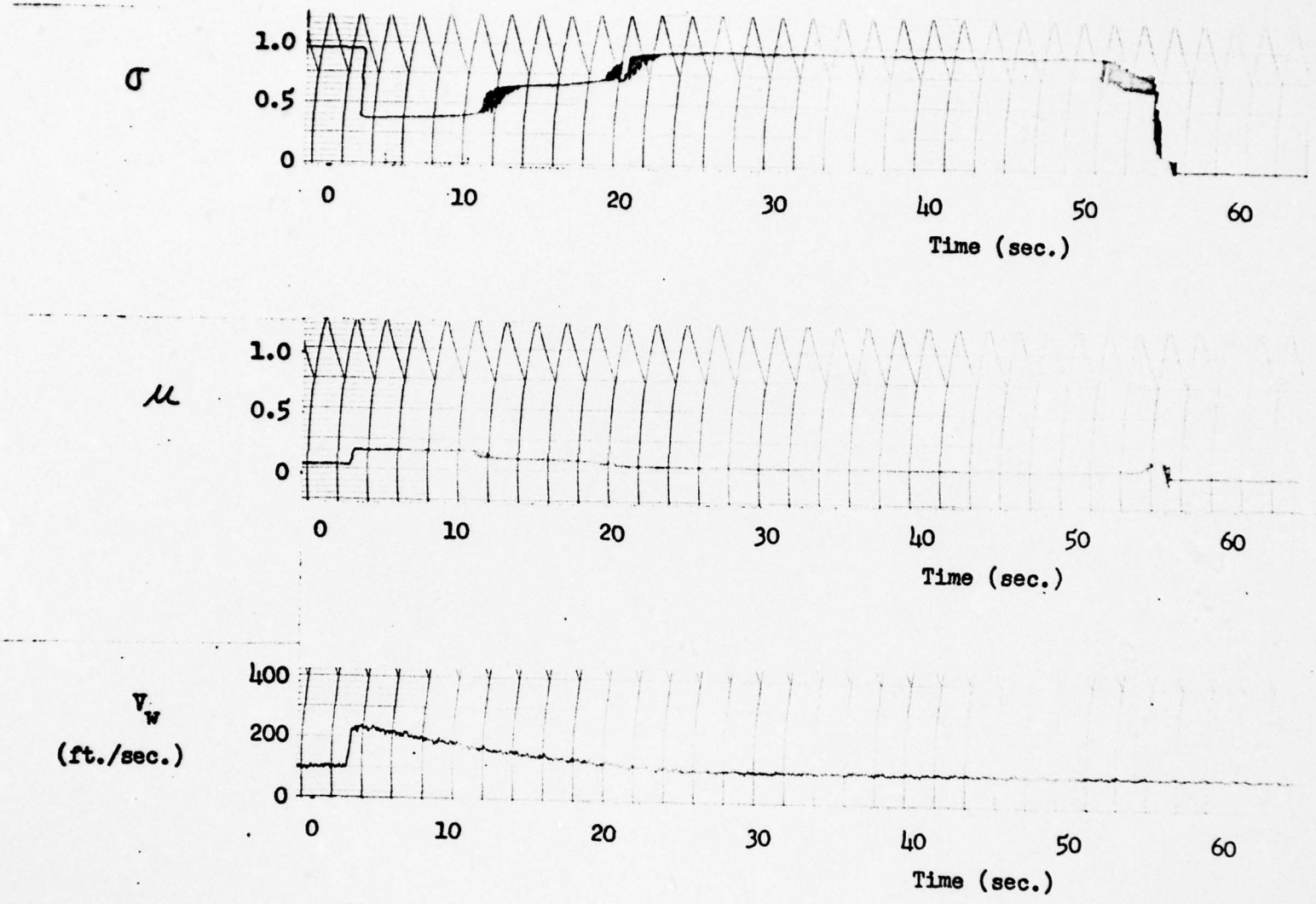

Fig. 45. σ, μ, and V_w vs. Time for 30,000 lb. F-4E, Wet Runway

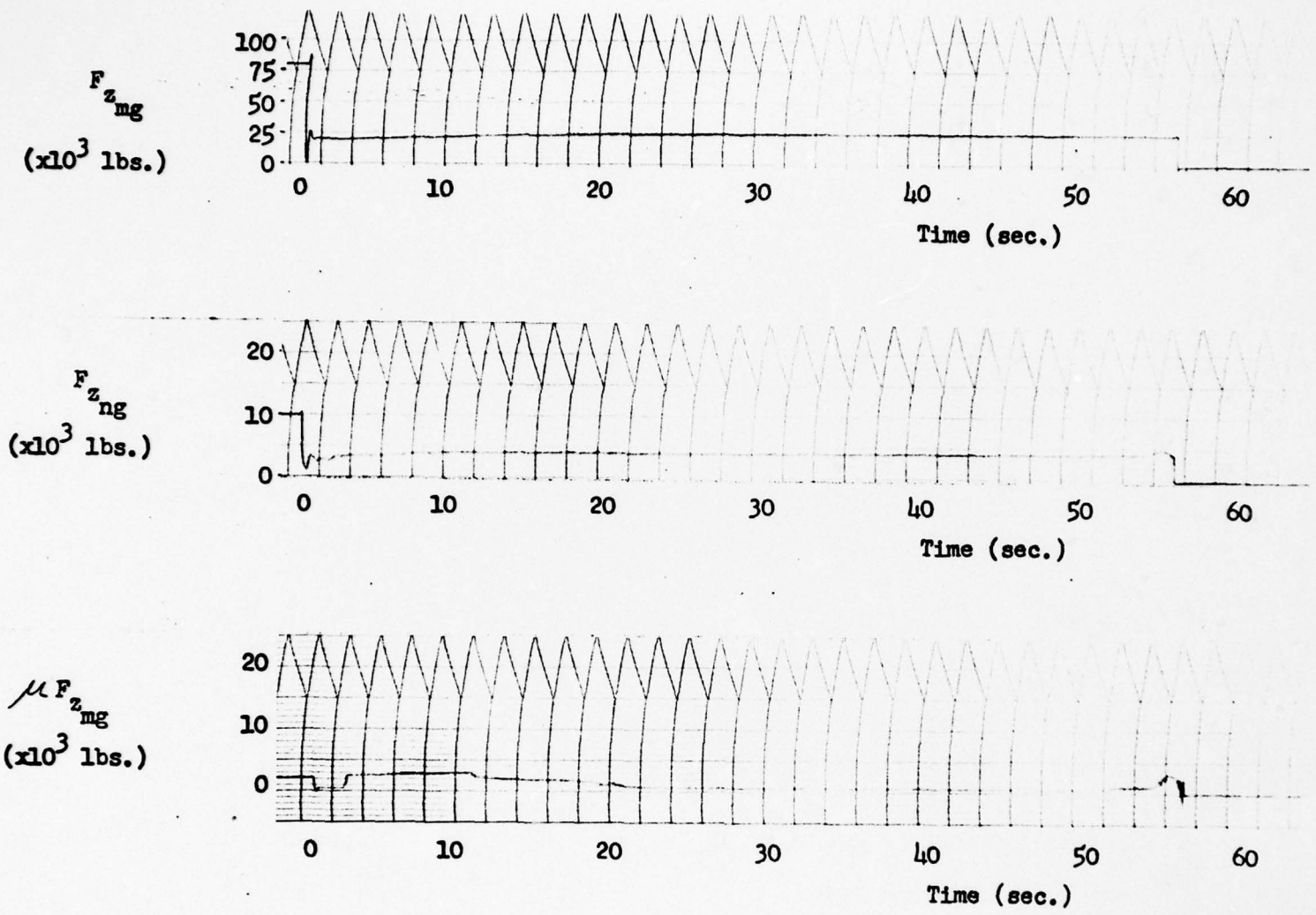

Fig. 46. $F_{z_{mg}}$, $F_{z_{ng}}$, and $\mu F_{z_{mg}}$ vs. Time for 30,000 lb. F-4E, Wet Runway

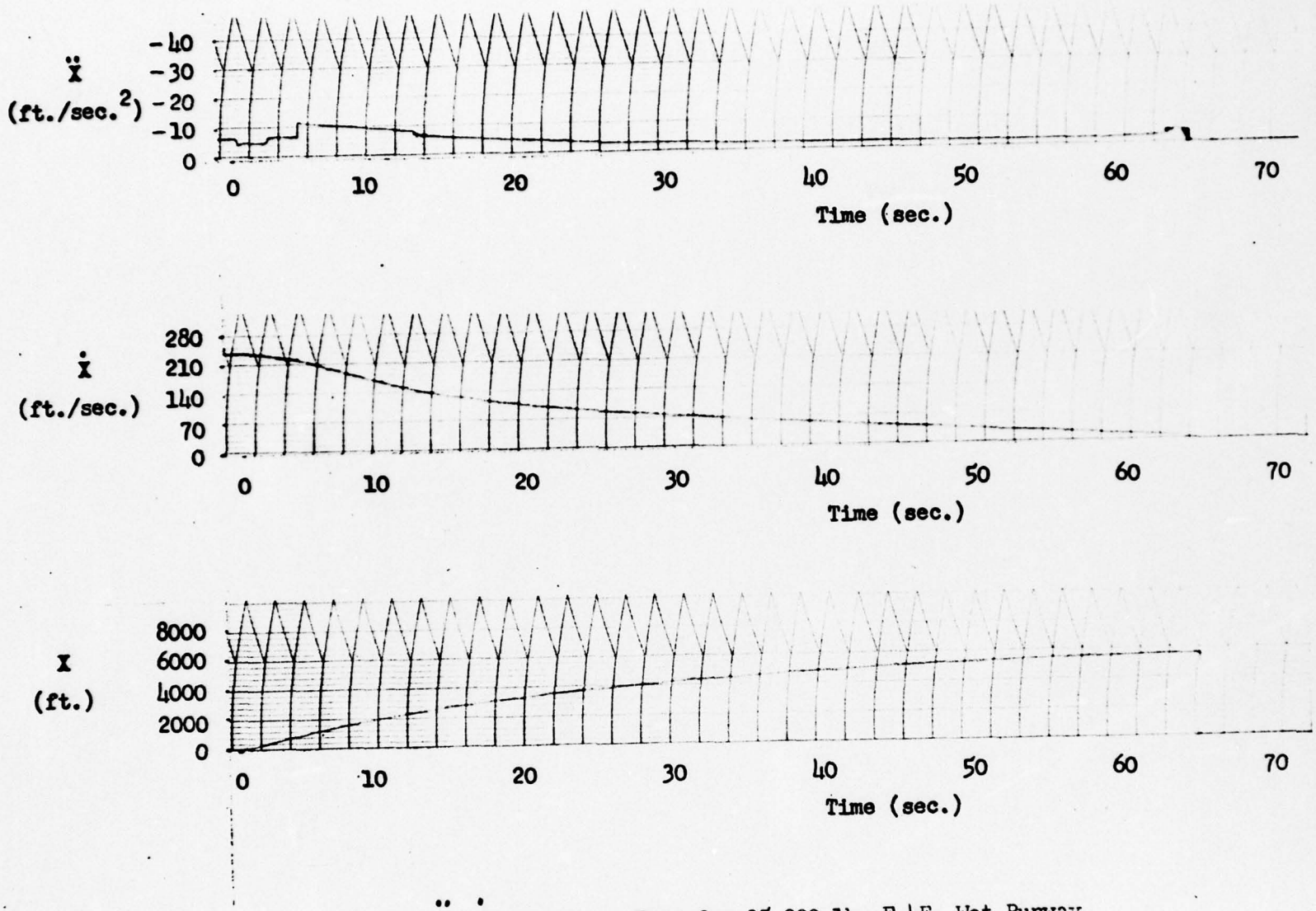

Fig. 47. $\ddot{X}$, $\dot{X}$, and X vs. Time for 35,000 lb. F-4E, Wet Runway

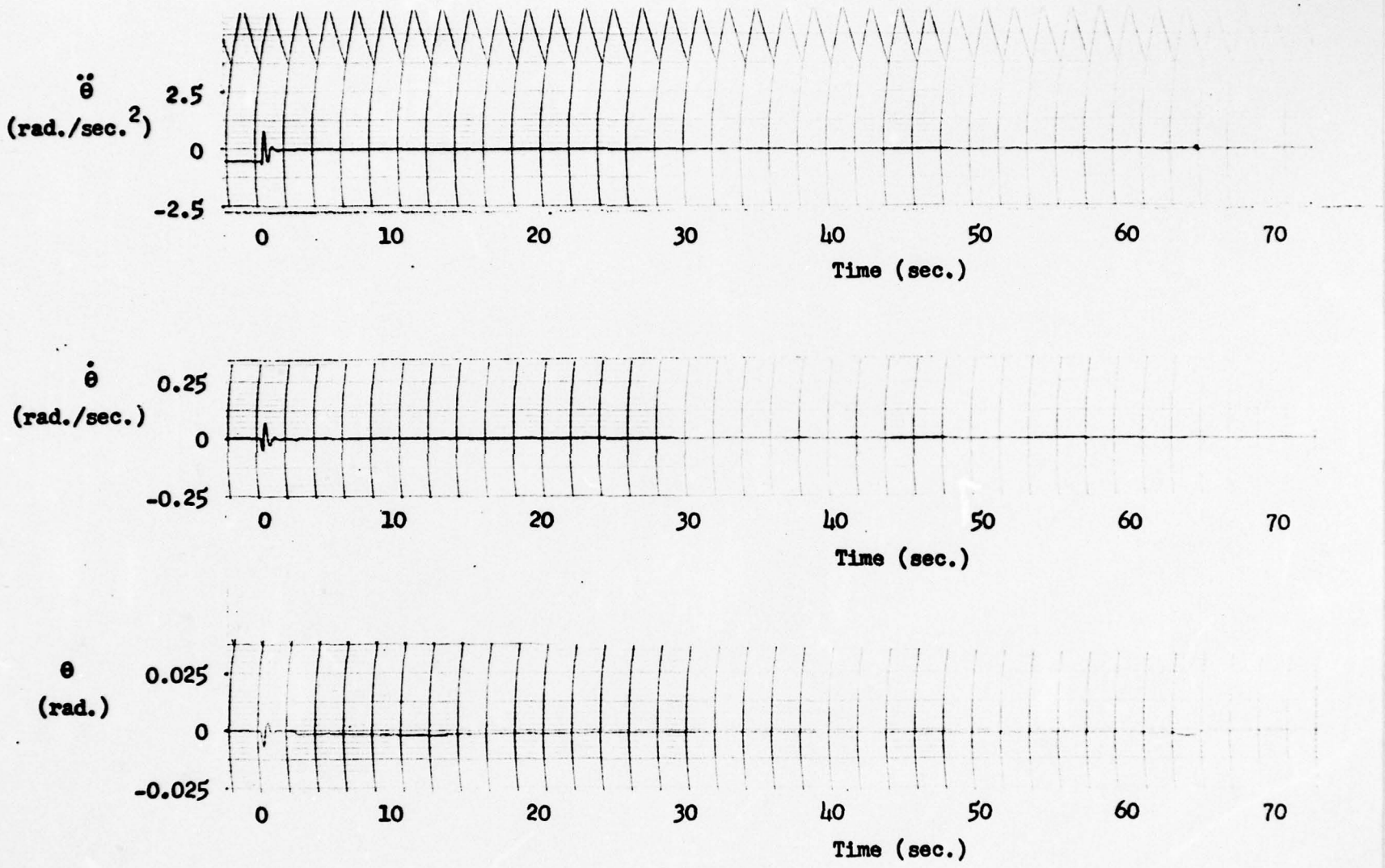

Fig. 48. $\ddot{\theta}$, $\dot{\theta}$, and θ vs. Time for 35,000 lb. F-4E, Wet Runway

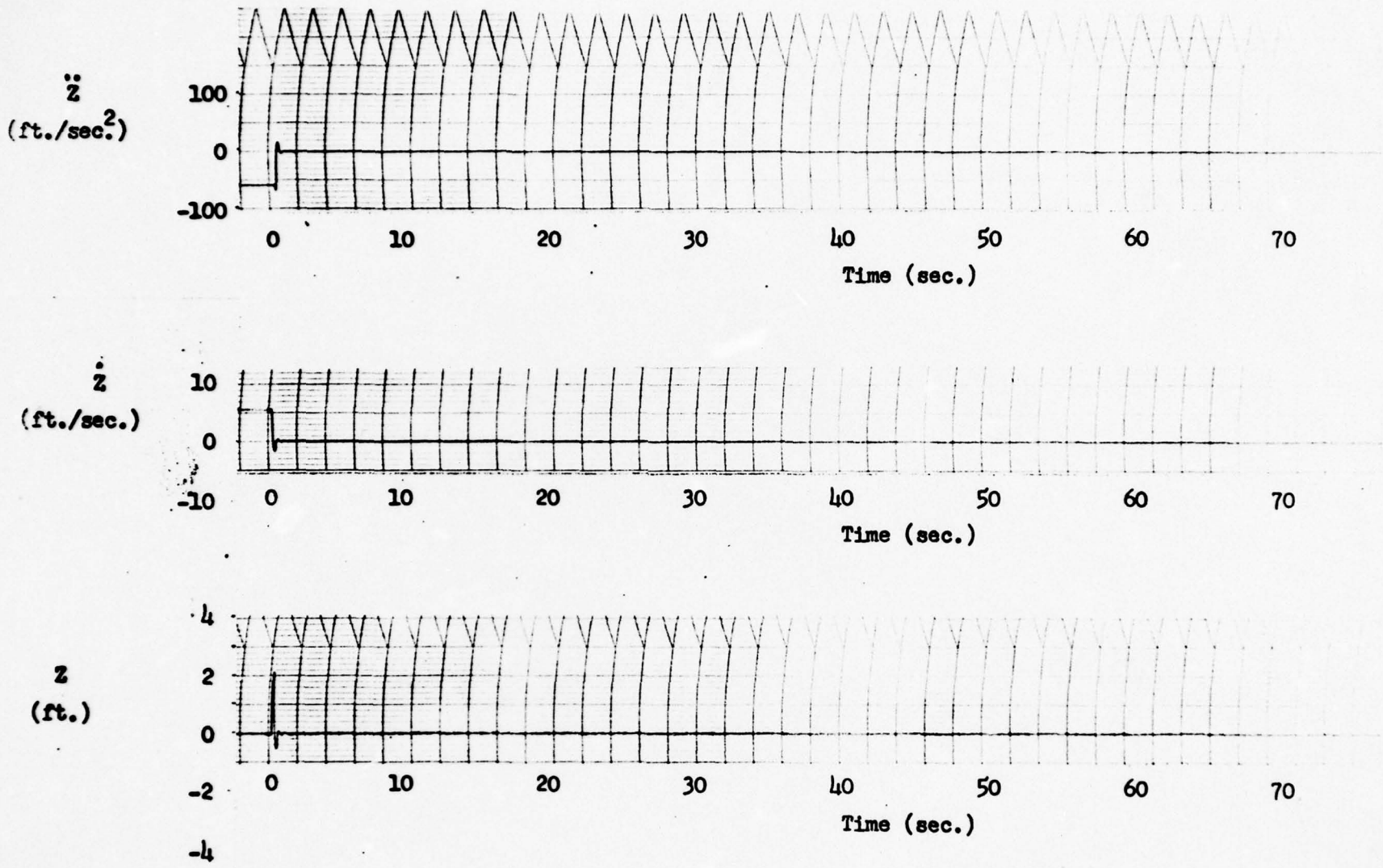

Fig. 49. $\ddot{z}$, $\dot{z}$, and z vs. Time for 35,000 lb. F-4E, Wet Runway

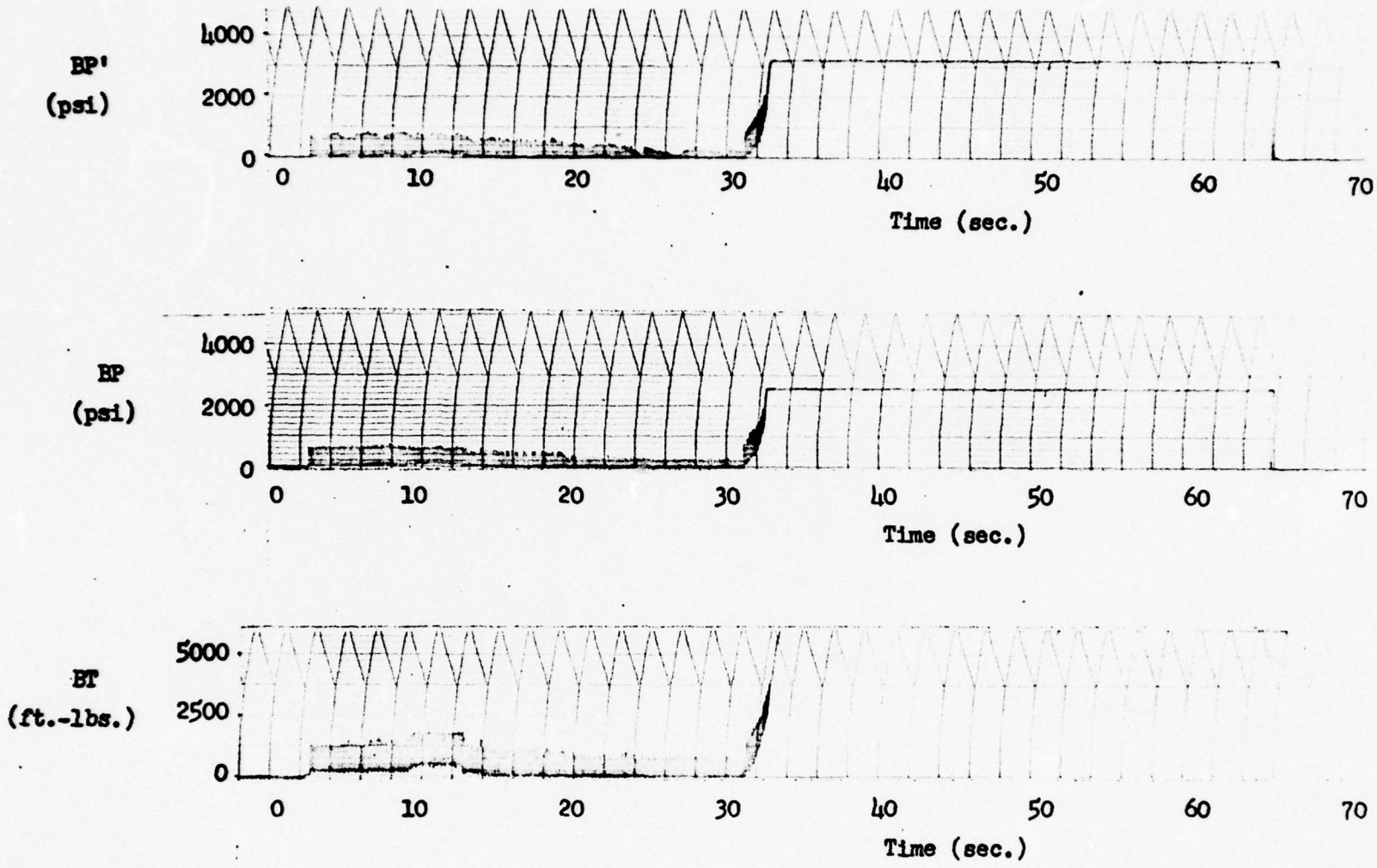

Fig. 50. BP', BP, and BT vs. Time for 35,000 lb. F-4E, Wet Runway

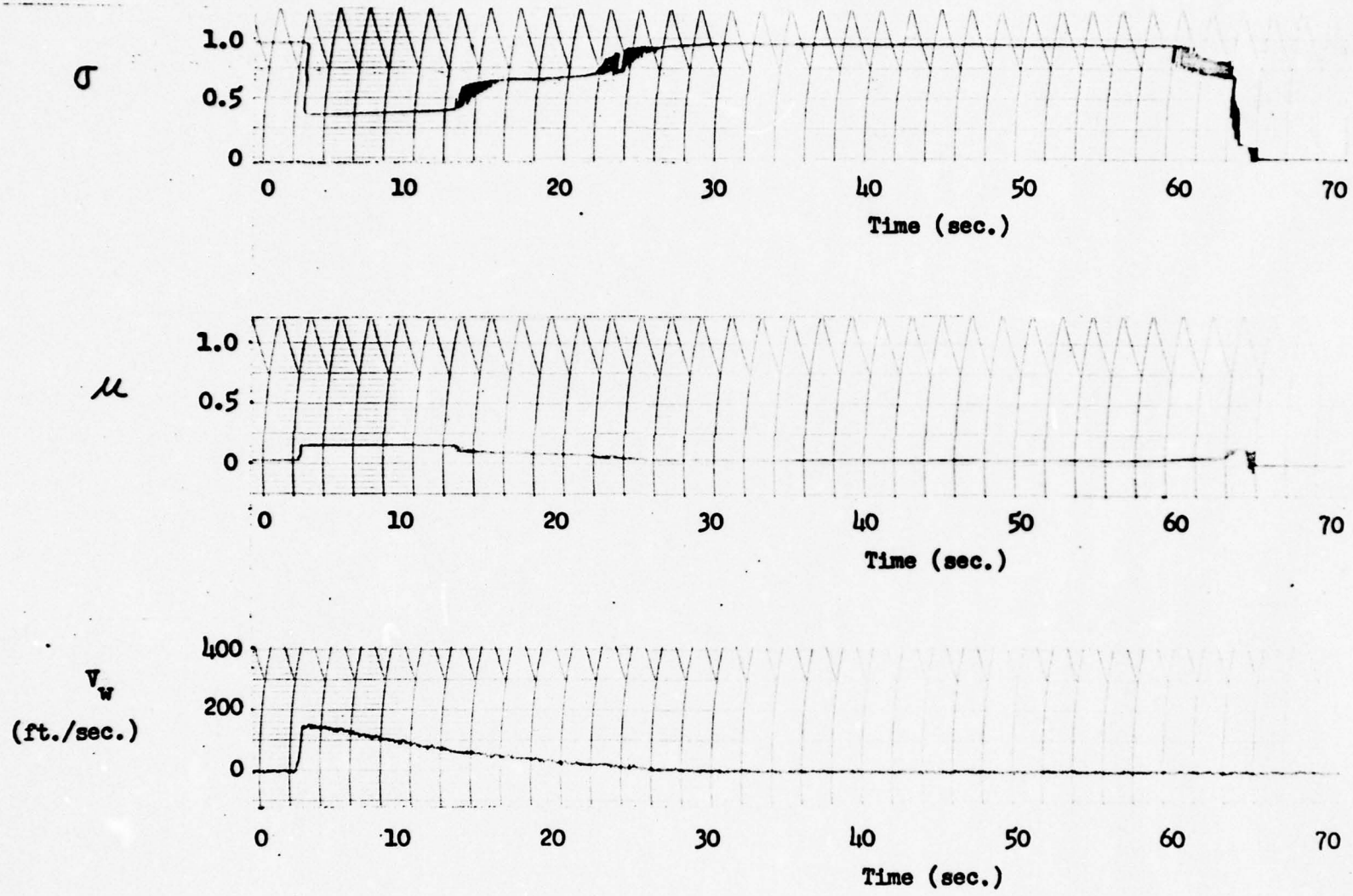

Fig. 51. σ, μ, and V_w vs. Time for 35,000 lb. F-4E, Wet Runway

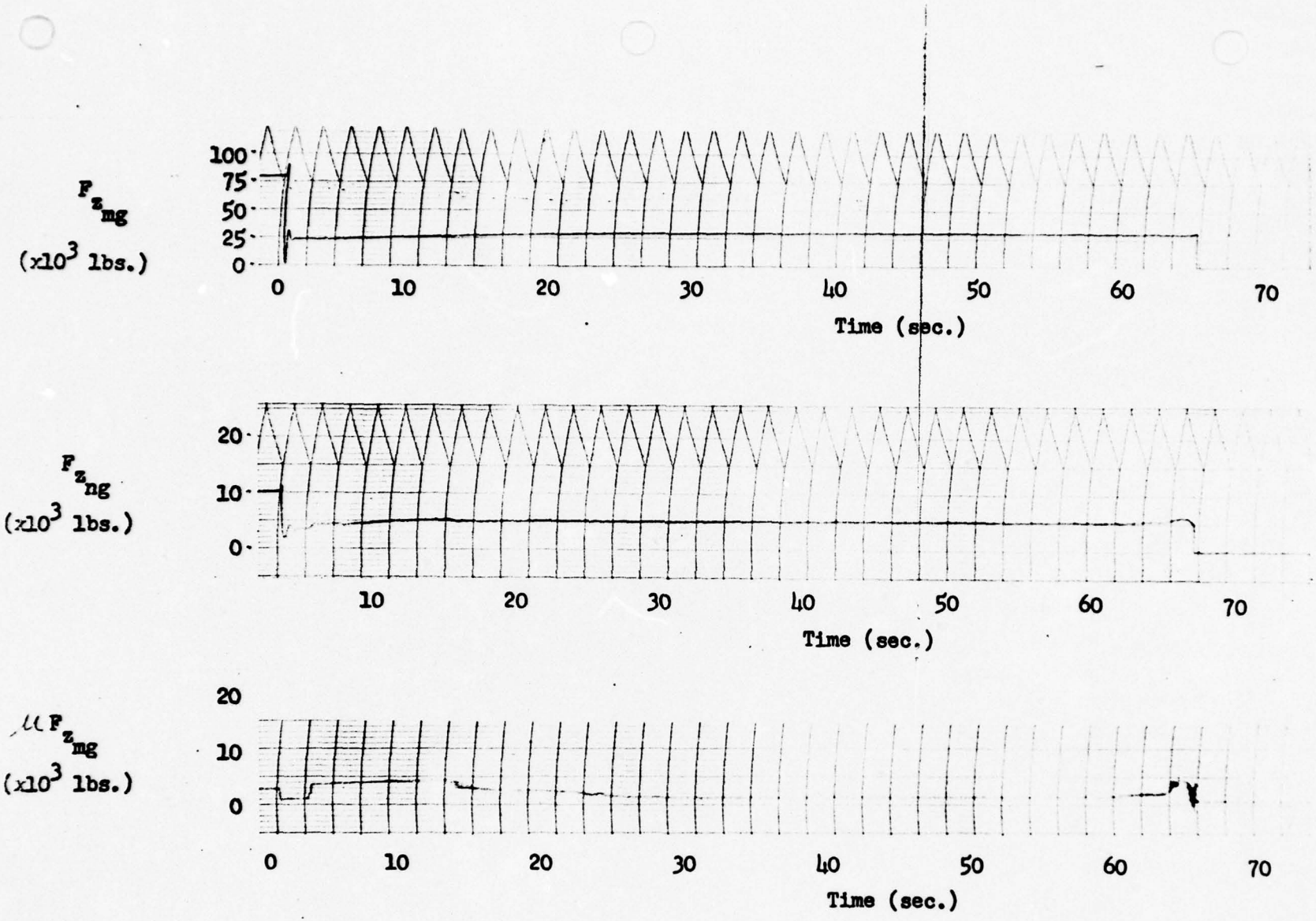

Fig. 52. $F_{z_{mg}}$, $F_{z_{ng}}$, and $\Delta F_{z_{mg}}$ vs. Time for 35,000 lb. F-4E, Wet Runway

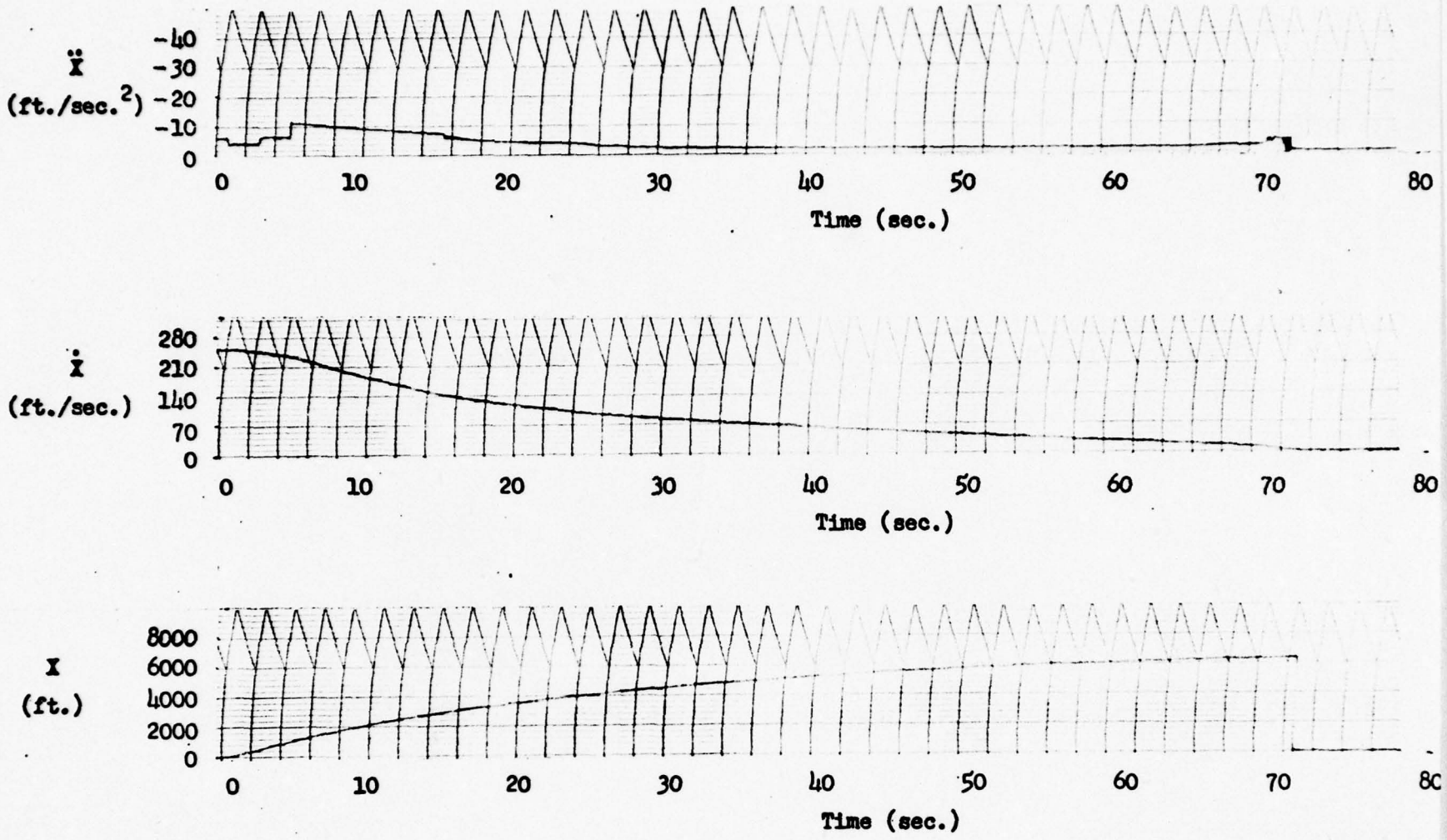

Fig. 53. $\ddot{X}$, $\dot{X}$, and X vs. Time for 40,000 lb. F-4E, Wet Runway

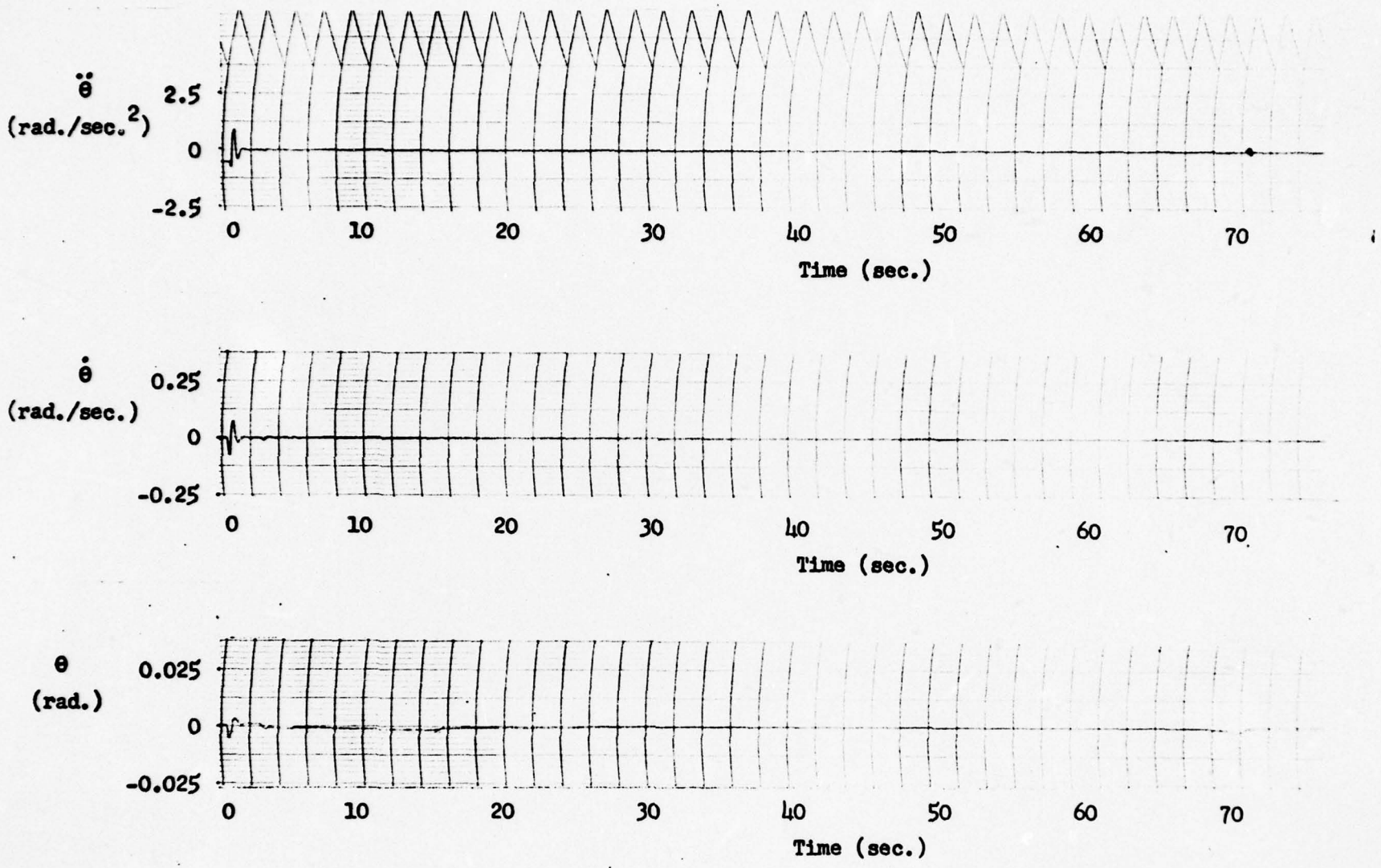

Fig. 54. $\ddot{\theta}$, $\dot{\theta}$, and θ vs. Time for 40,000 lb. F-4E, Wet Runway

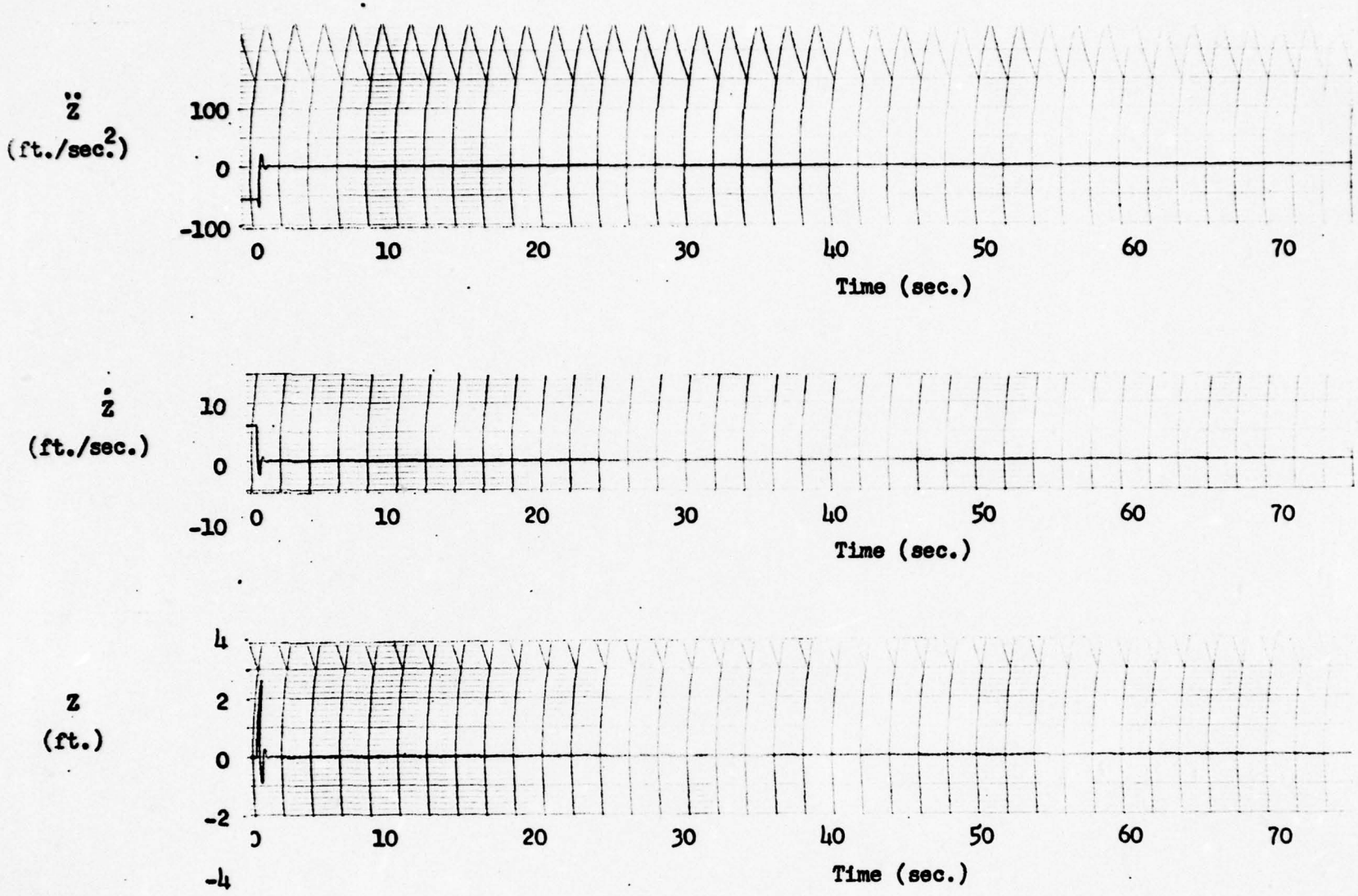

Fig. 55. $\ddot{z}$, $\dot{z}$, and z vs. Time for 40,000 lb. F-4E, Wet Runway

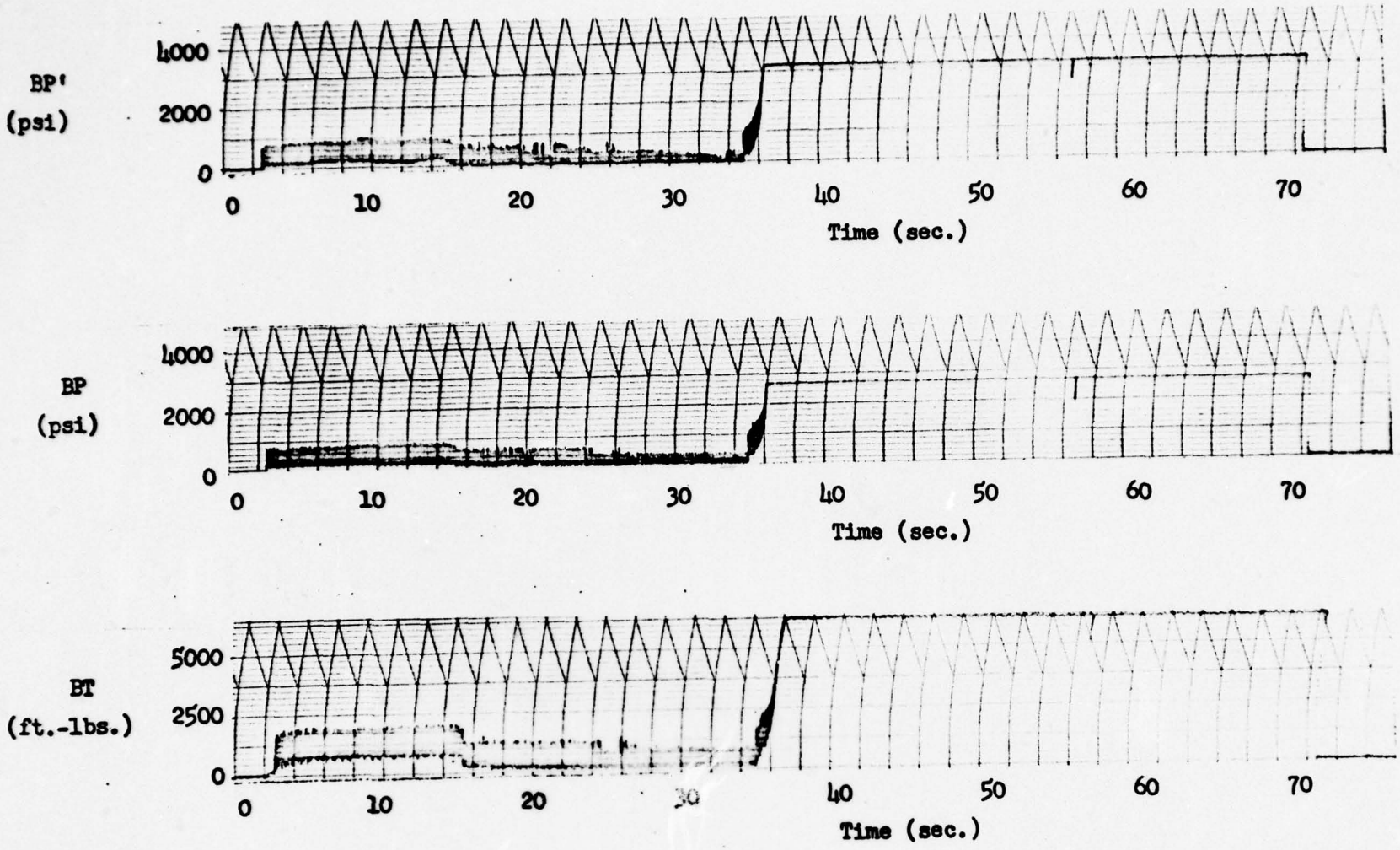

Fig. 56. BP', BP, and BT vs. Time for 40,000 lb. F-4E, Wet Runway

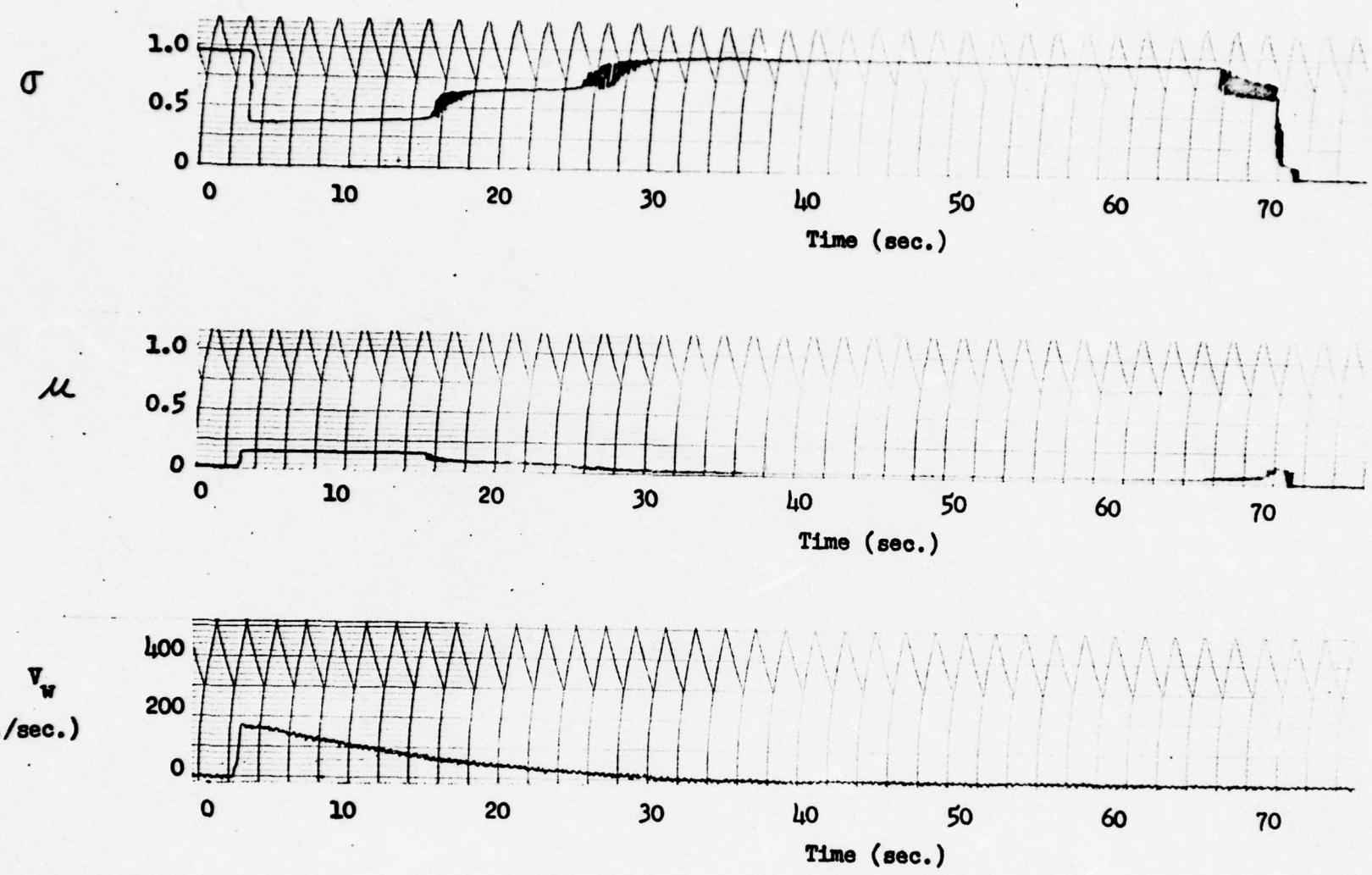

Fig. 57. σ, μ, and V_w vs. Time for 40,000 lb. F-4E, Wet Runway

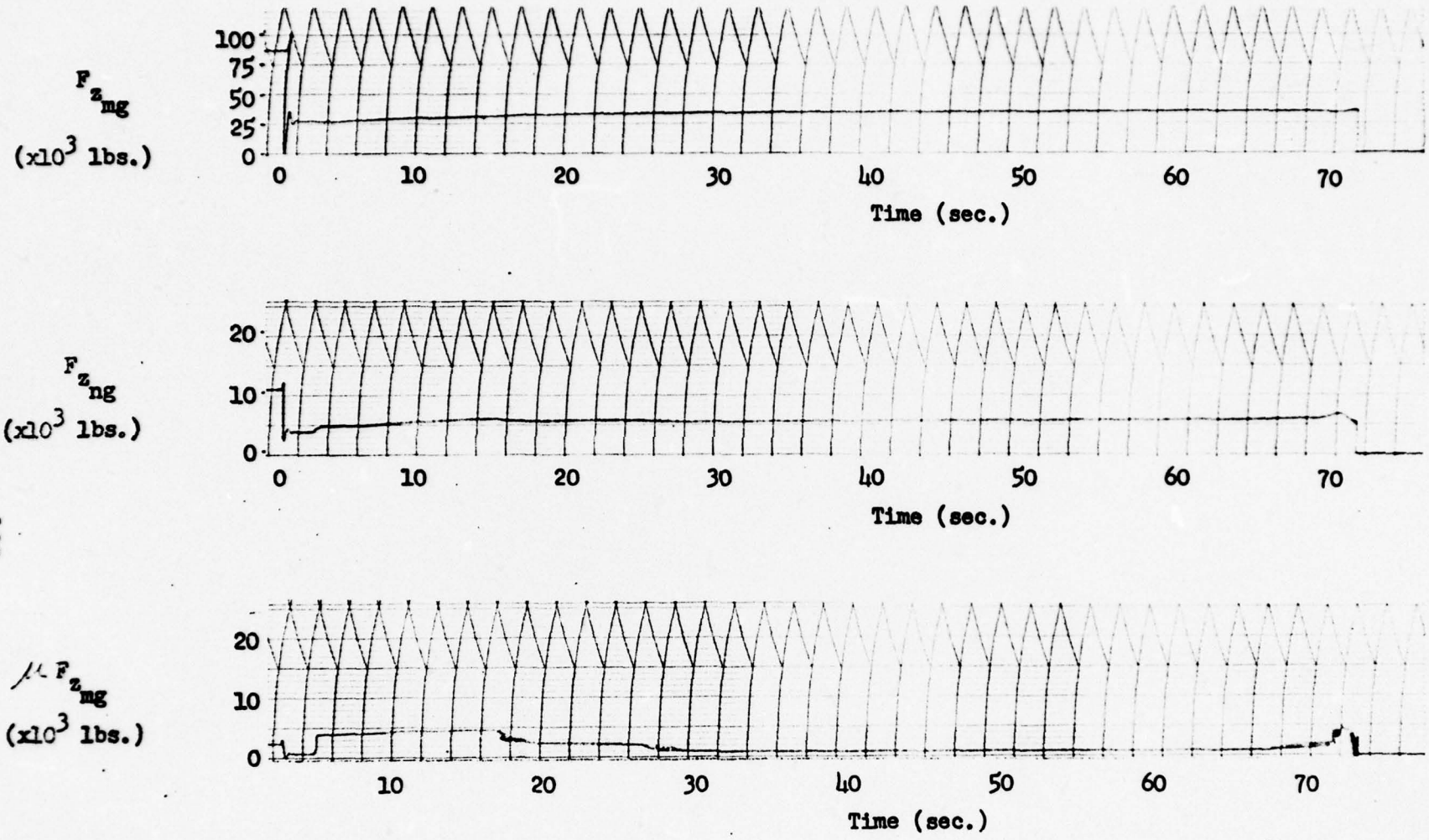

Fig. 58. $F_{z_{mg}}$, $F_{z_{ng}}$, and $\mu F_{z_{mg}}$ vs. Time for 40,000 lb. F-4E, Wet Runway

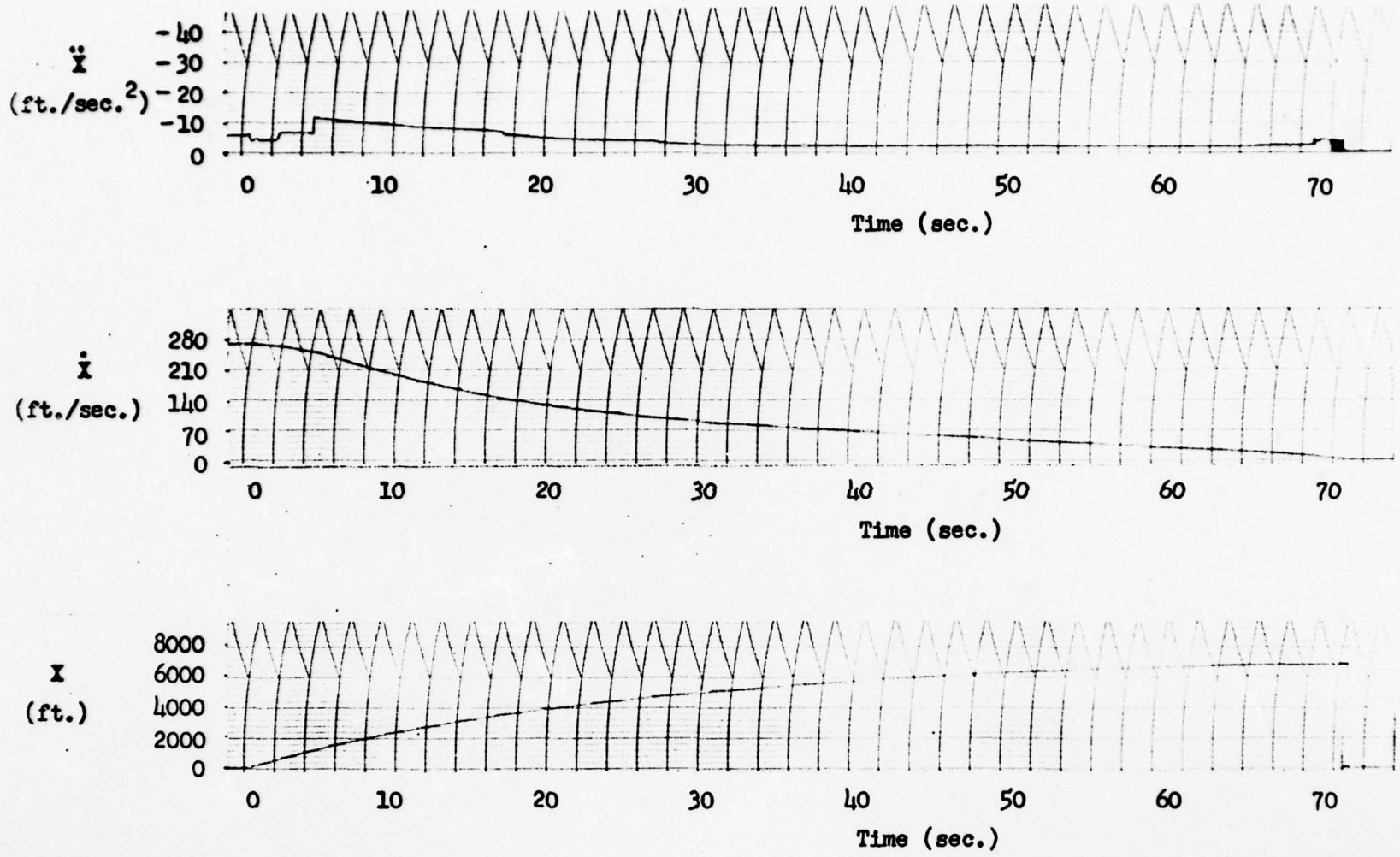

Fig. 59. $\ddot{X}$, $\dot{X}$, and X vs. Time for 45,000 lb. F-4E, Wet Runway

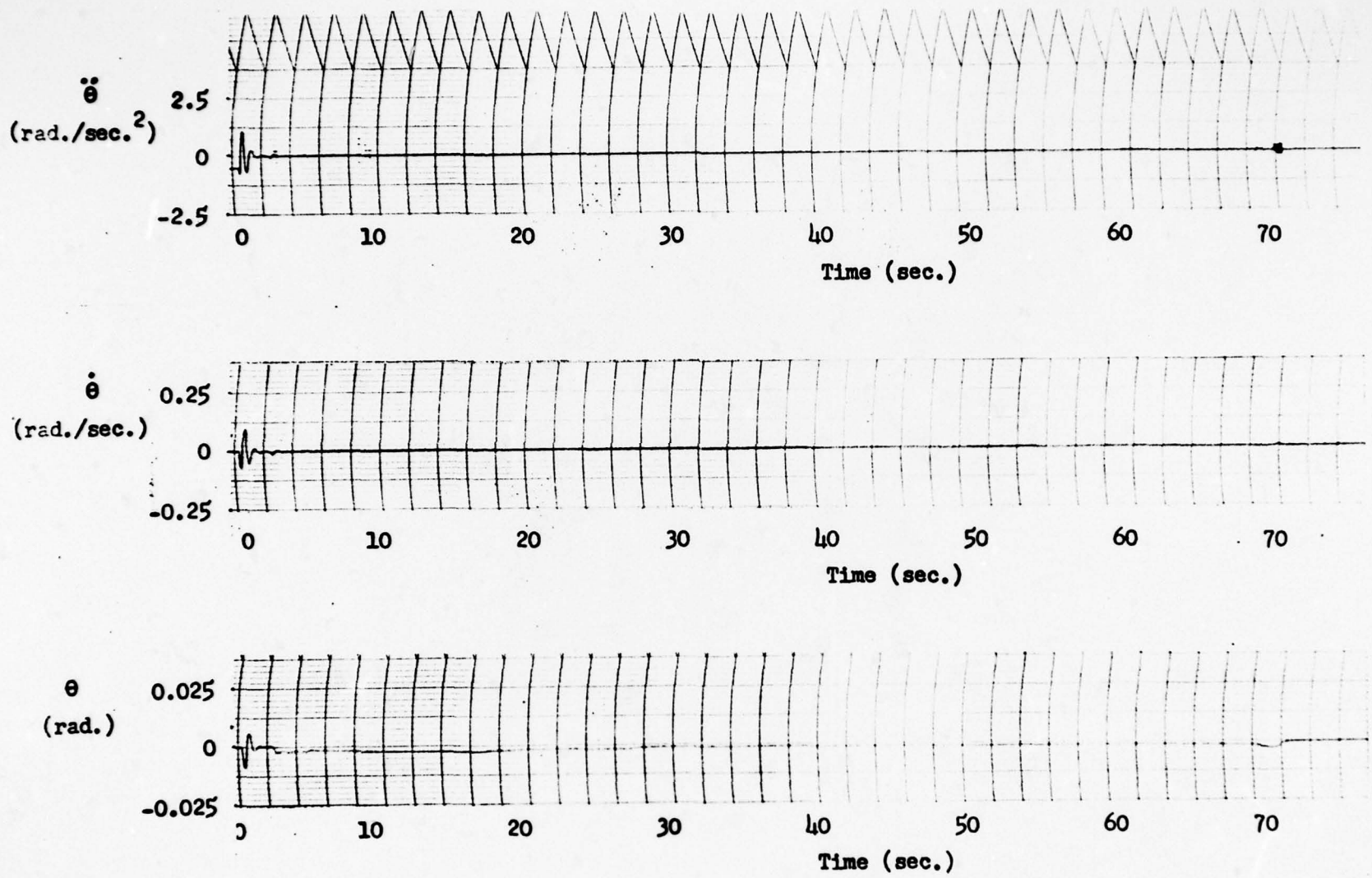

Fig. 60. $\ddot{\theta}$, $\dot{\theta}$, and θ vs. Time for 45,000 lb. F-4E, Wet Runway

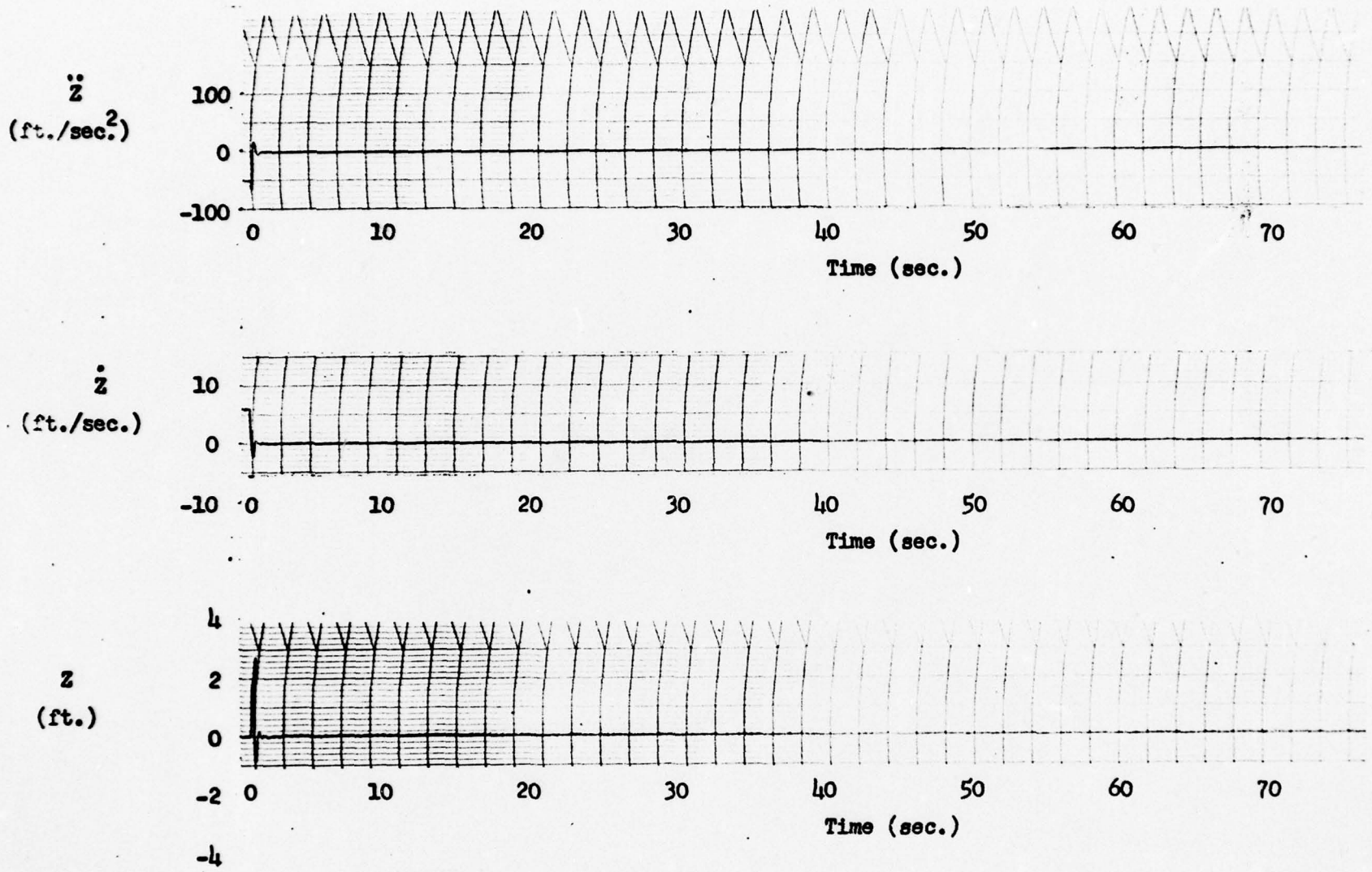

Fig. 61. $\ddot{z}$, $\dot{z}$, and z vs. Time for 45,000 lb. F-4E, Wet Runway

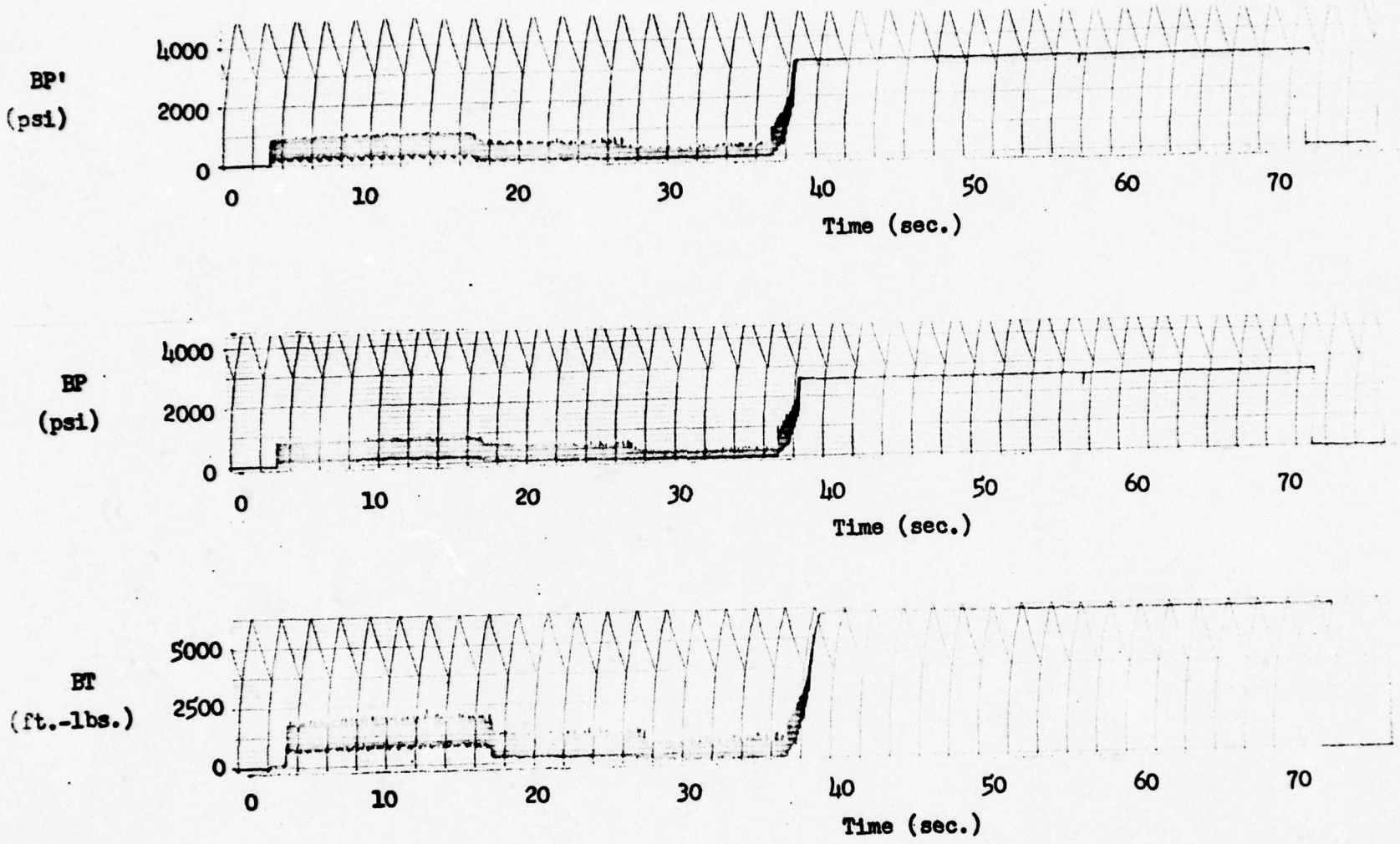

Fig. 62. BP', BP, and BT bs. Time for 45,000 lb. F-4E, Wet Runway

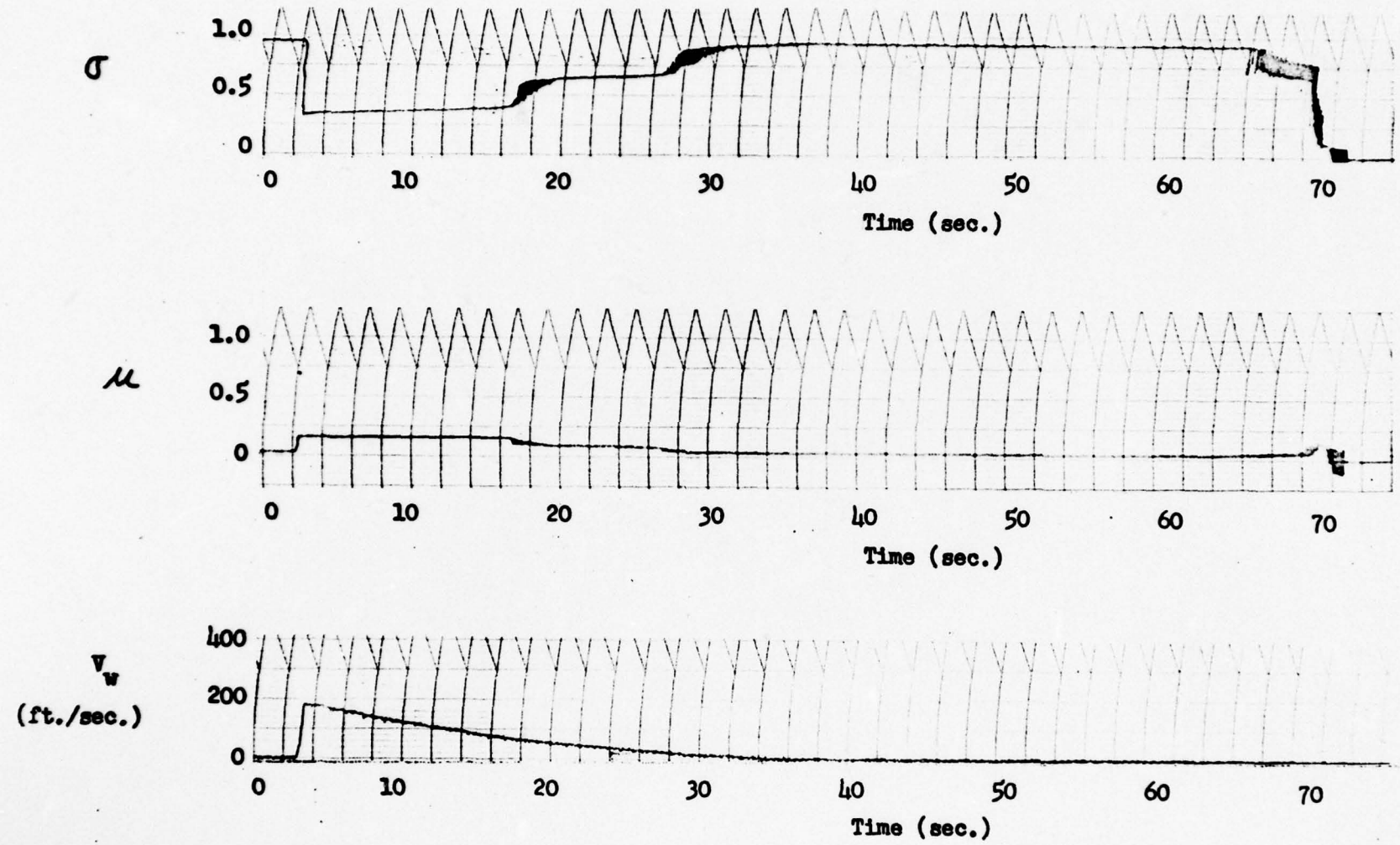

Fig. 63. σ, μ, and $F_{z_{mg}}$ vs. Time for 45,000 lb. F-4E, Wet Runway

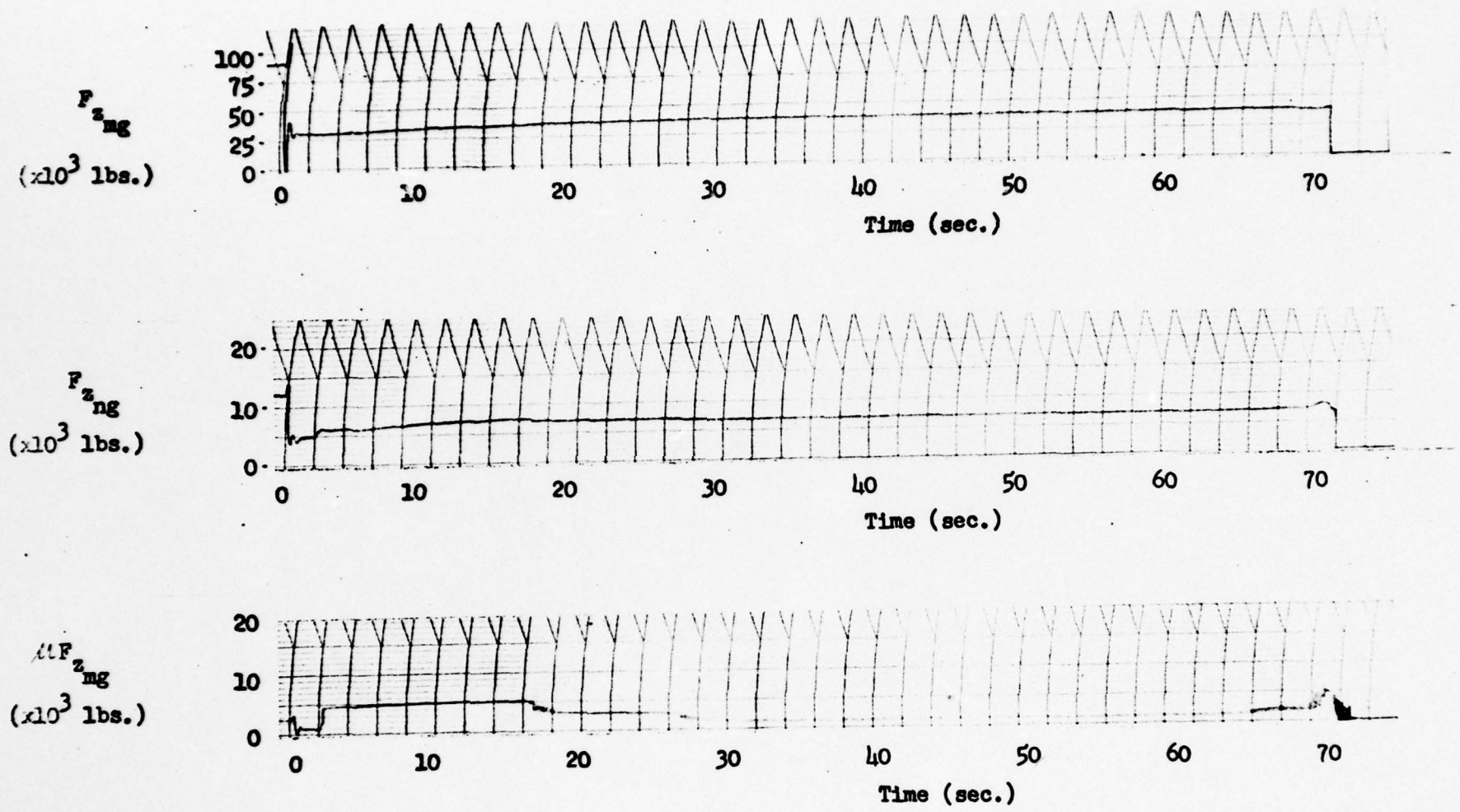

Fig. 64. $F_{z_{mg}}$, $F_{z_{ng}}$, and $\mu F_{z_{mg}}$ vs. Time for 45,000 lb. F-4E, Wet Runway

Appendix C

Source Data

Included herein are the source data for particular relationships, such as brake pressure vs. brake torque, that are essential to the model. They are listed in the following order:

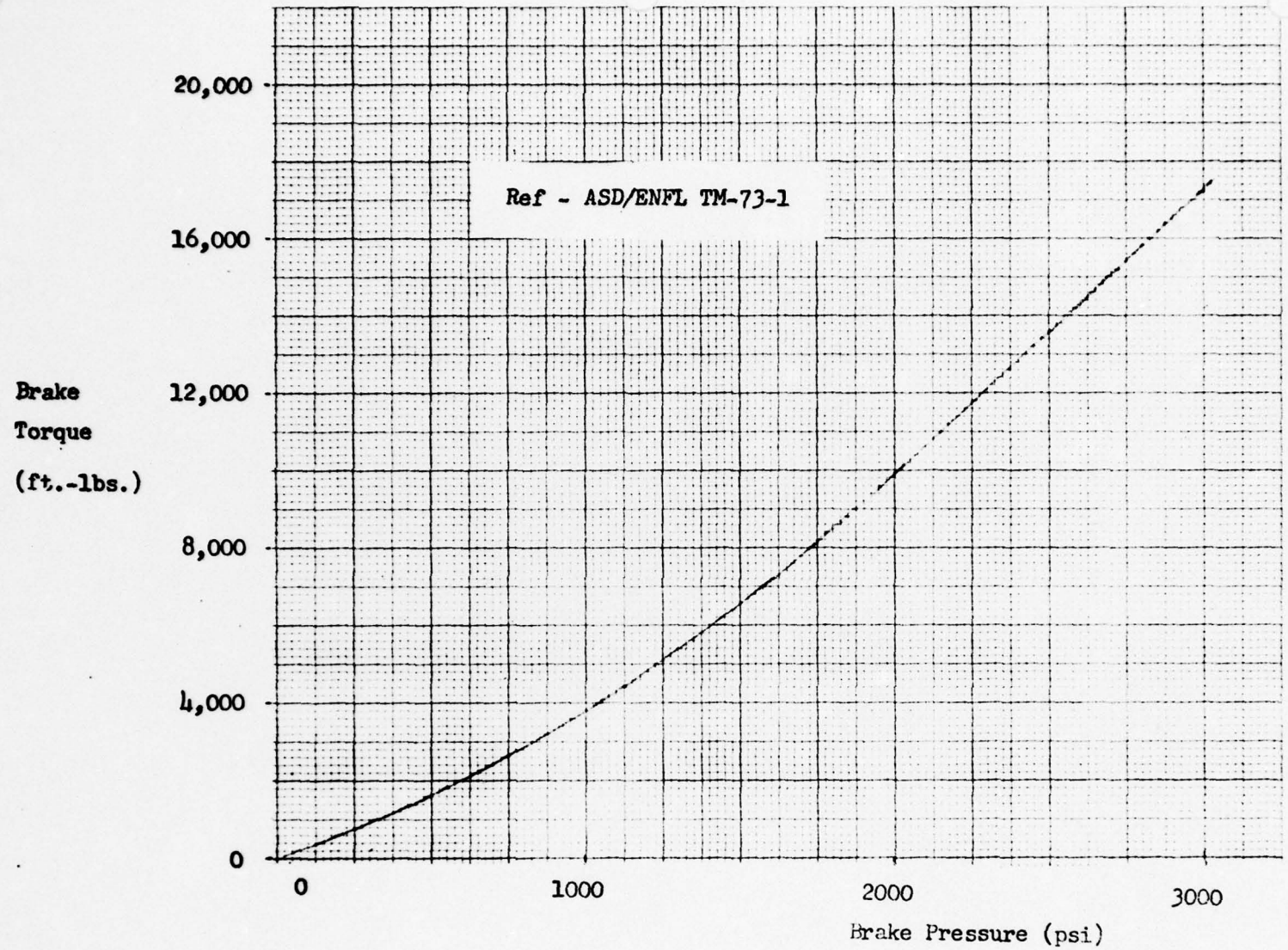

Fig 65 Brake Pressure vs. Brake Torque

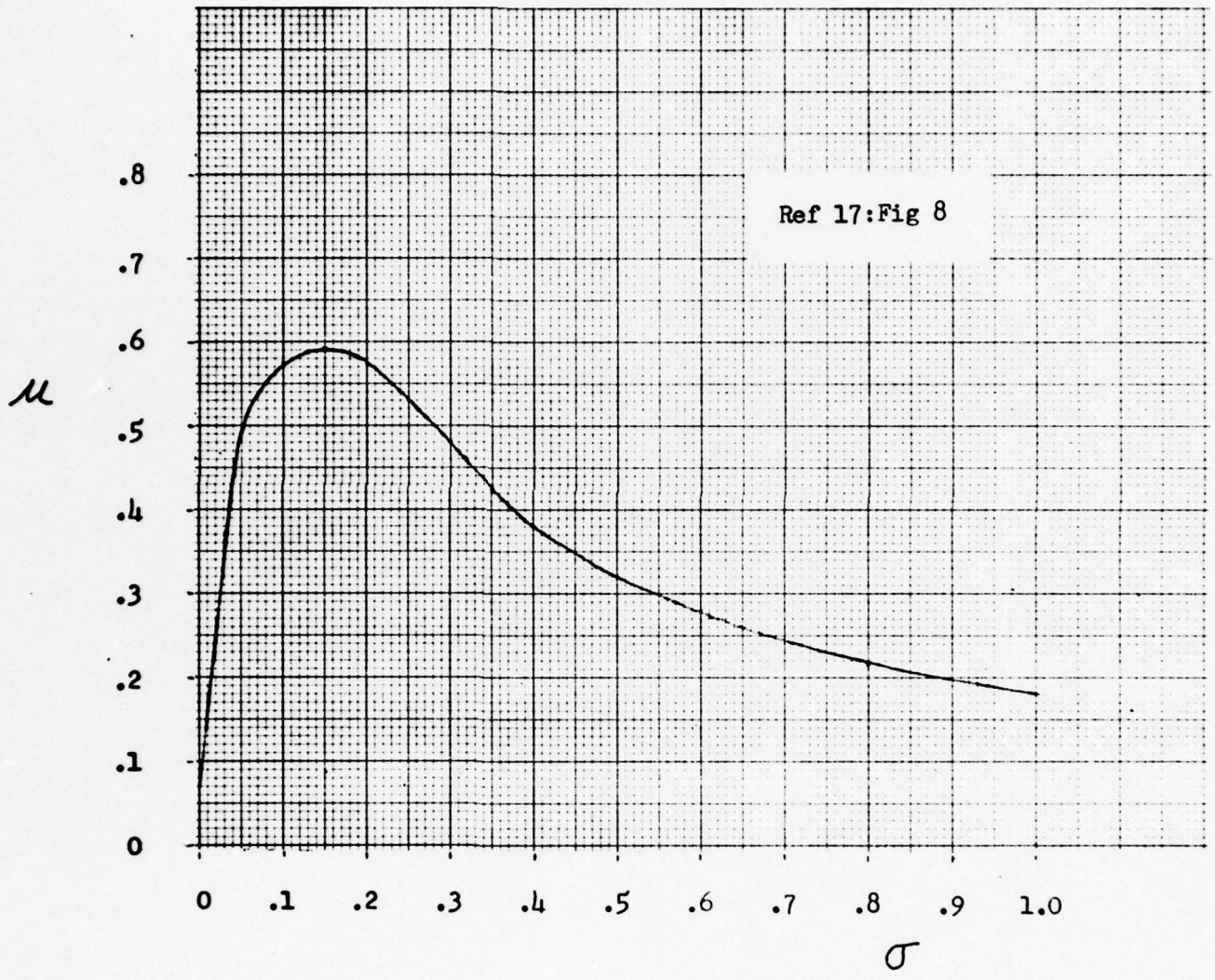

Fig 66 Coefficient of Braking Friction vs. Wheel Slip Ratio , Dry Runway, 75 Knots

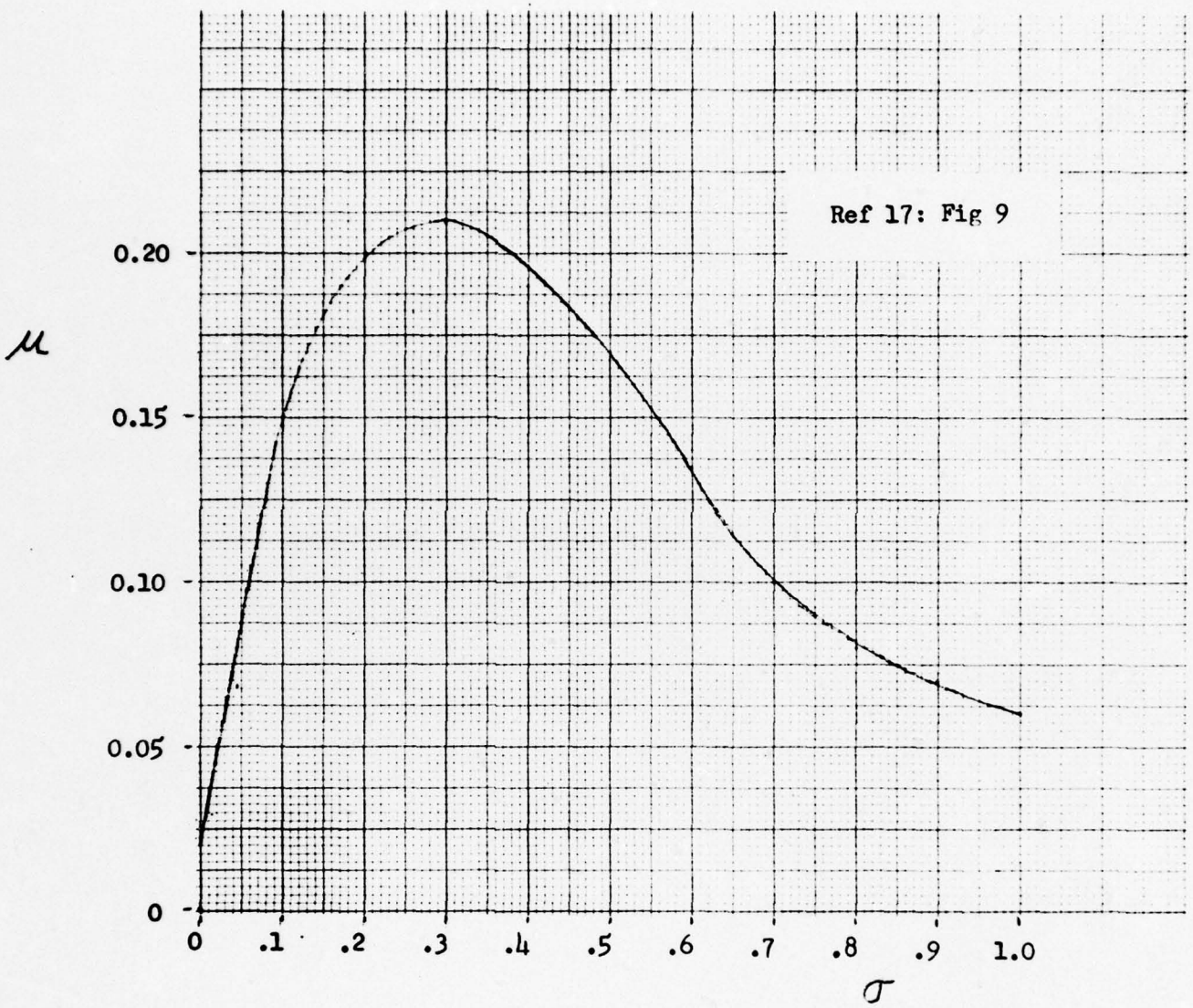

Fig. 67 Coefficient of Braking Friction vs. Wheel Slip Ratio, Wet Runway, 75 Knots

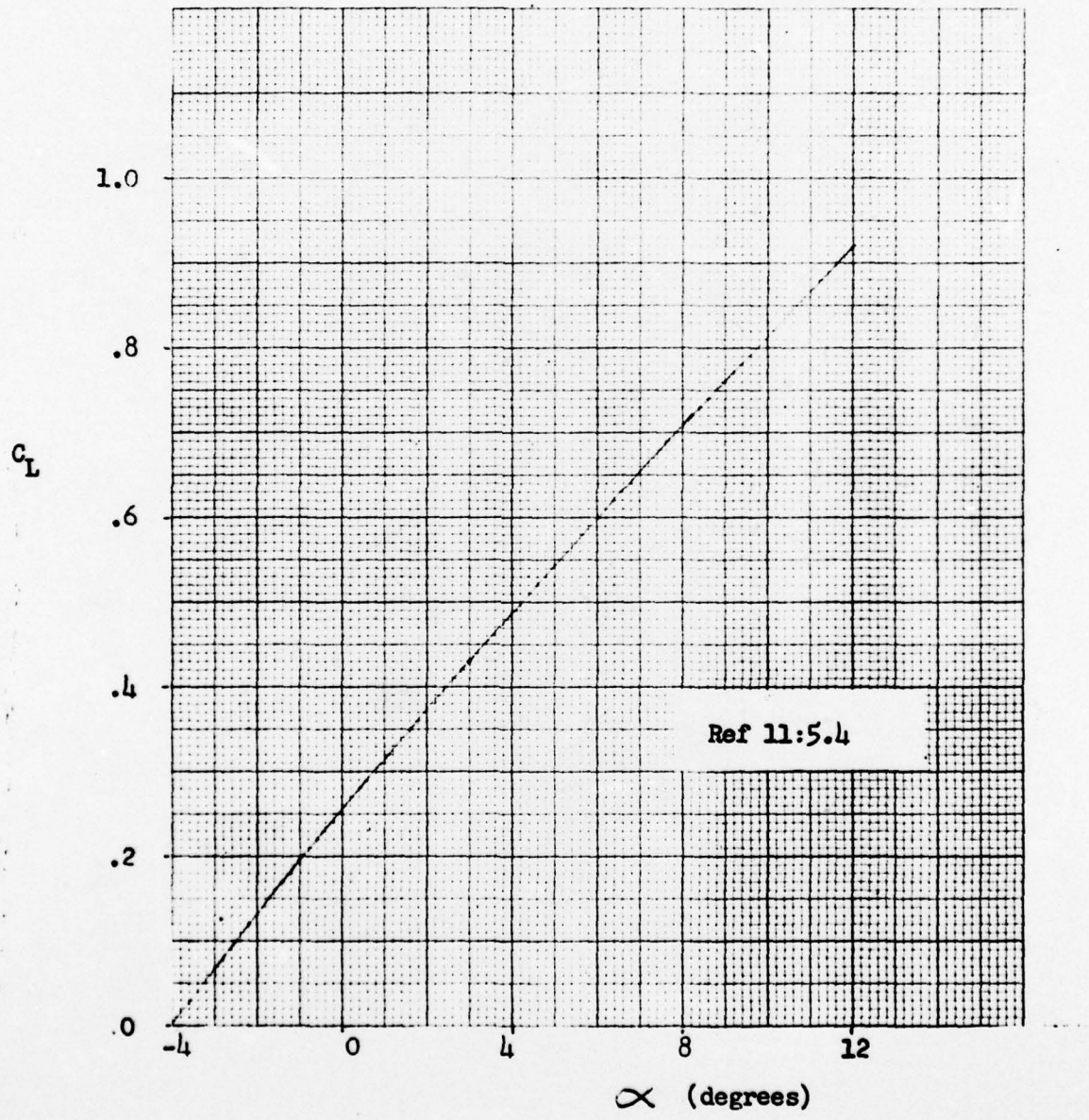

Fig 68 C_L vs. α for F-4E, Approach Configuration

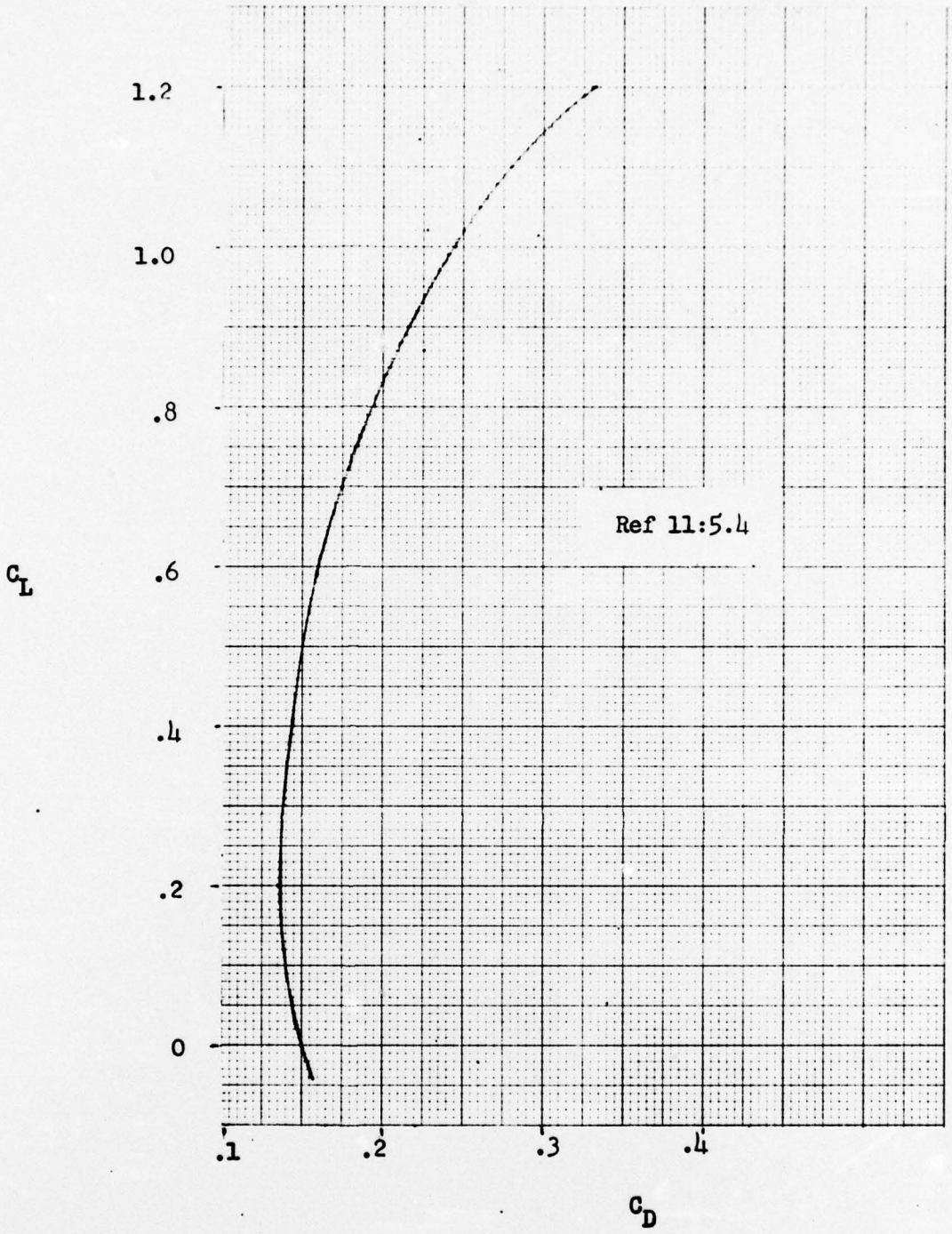

Fig 69 C_L vs C_D for F-4E, Approach Configuration

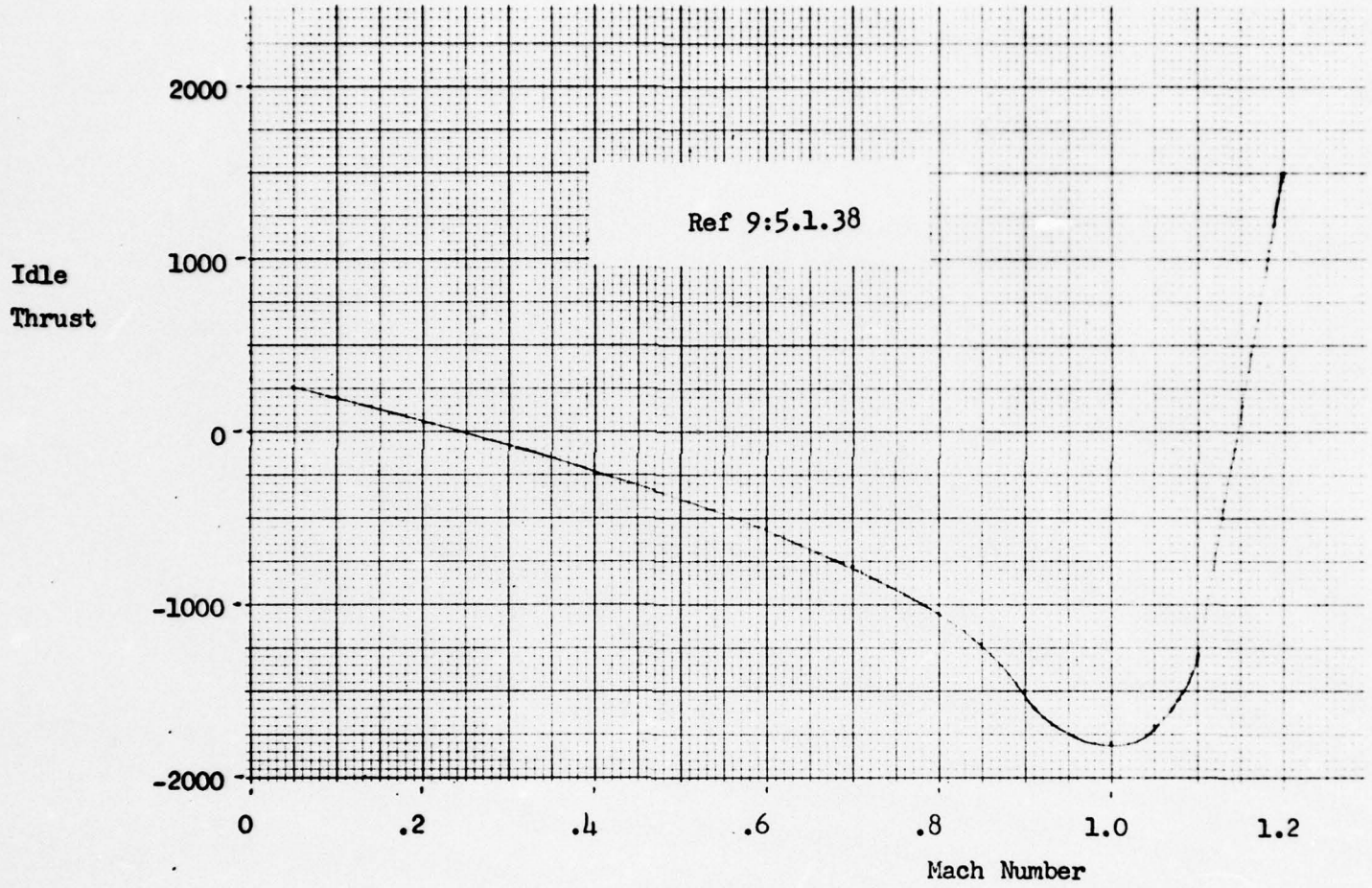

Fig. 70 Idle Thrust vs. Mach Number, One Engine, F-4E, Sea Level, Standard Day

F-4E
FINAL APPROACH SPEEDS

AIRPLANE CONFIGURATION
ALL DRAG INDEXES
GEAR DOWN
FLAPS AS NOTED

REMARKS
ENGINE(S): (2) J79-GE-17
ICAO STANDARD DAY

Note

- DATA IS FOR A CG LOCATION OF 31% MAC. ADD 0.5 KNOTS FOR EACH PERCENT OF CG FORWARD OF 31% MAC.

GUIDE

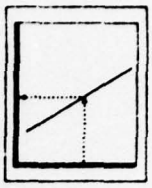

FUEL GRADE: JP-4
FUEL DENSITY: 6.5 LB/GAL

DATE: 1 AUGUST 1973
DATA BASIS: FLIGHT TEST

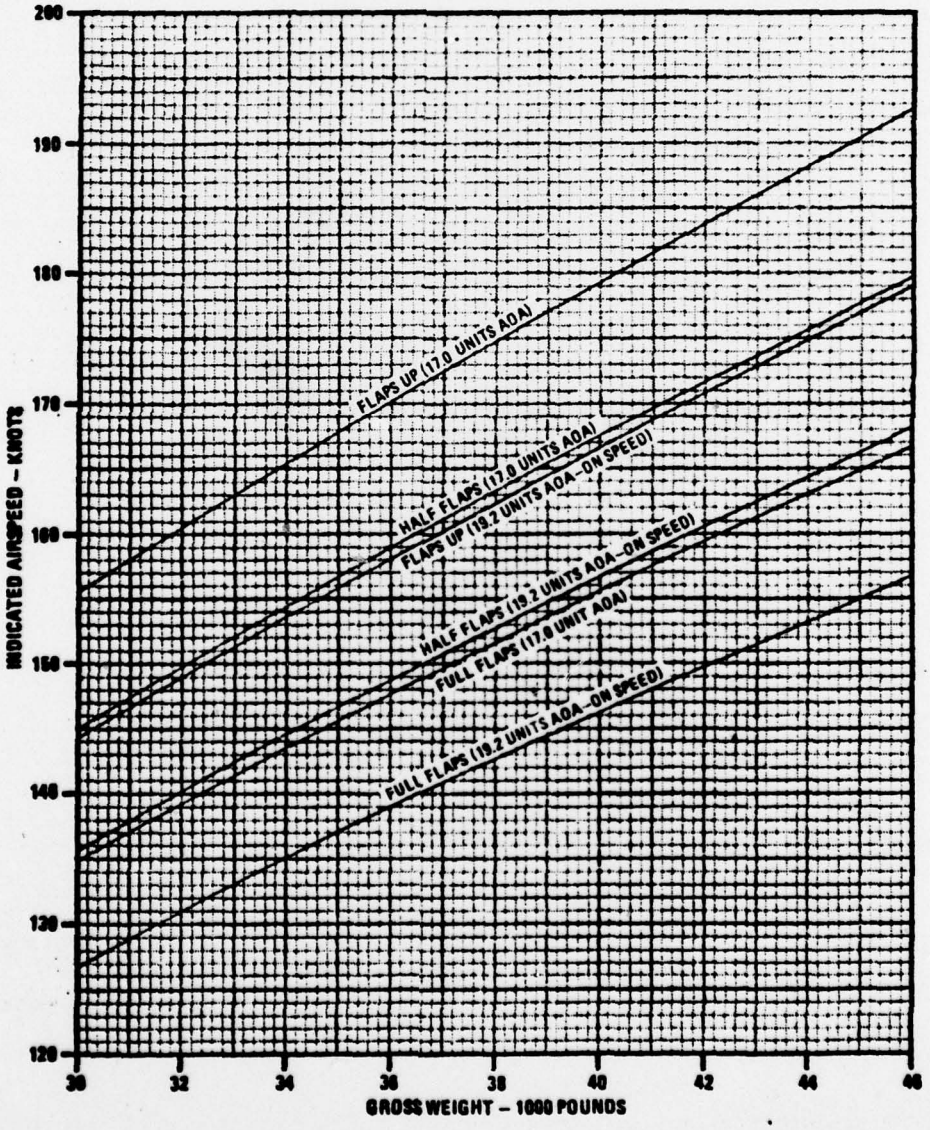

Fig. 71. F-4E Final Approach Speeds

F-4E

MINIMUM LANDING ROLL DISTANCE

IDLE THRUST

AIRPLANE CONFIGURATION
ALL DRAG INDEXES
FLAPS EXTENDED, GEAR DOWN
DRAG CHUTE DEPLOYED

REMARKS
ENGINE(S): (2) J79-GE-17

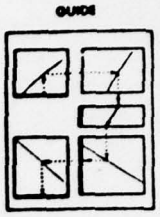

DATE: 1 OCTOBER 1973
DATA BASIS: FLIGHT TEST

FUEL GRADE: JP-4
FUEL DENSITY: 6.5 LB/GAL

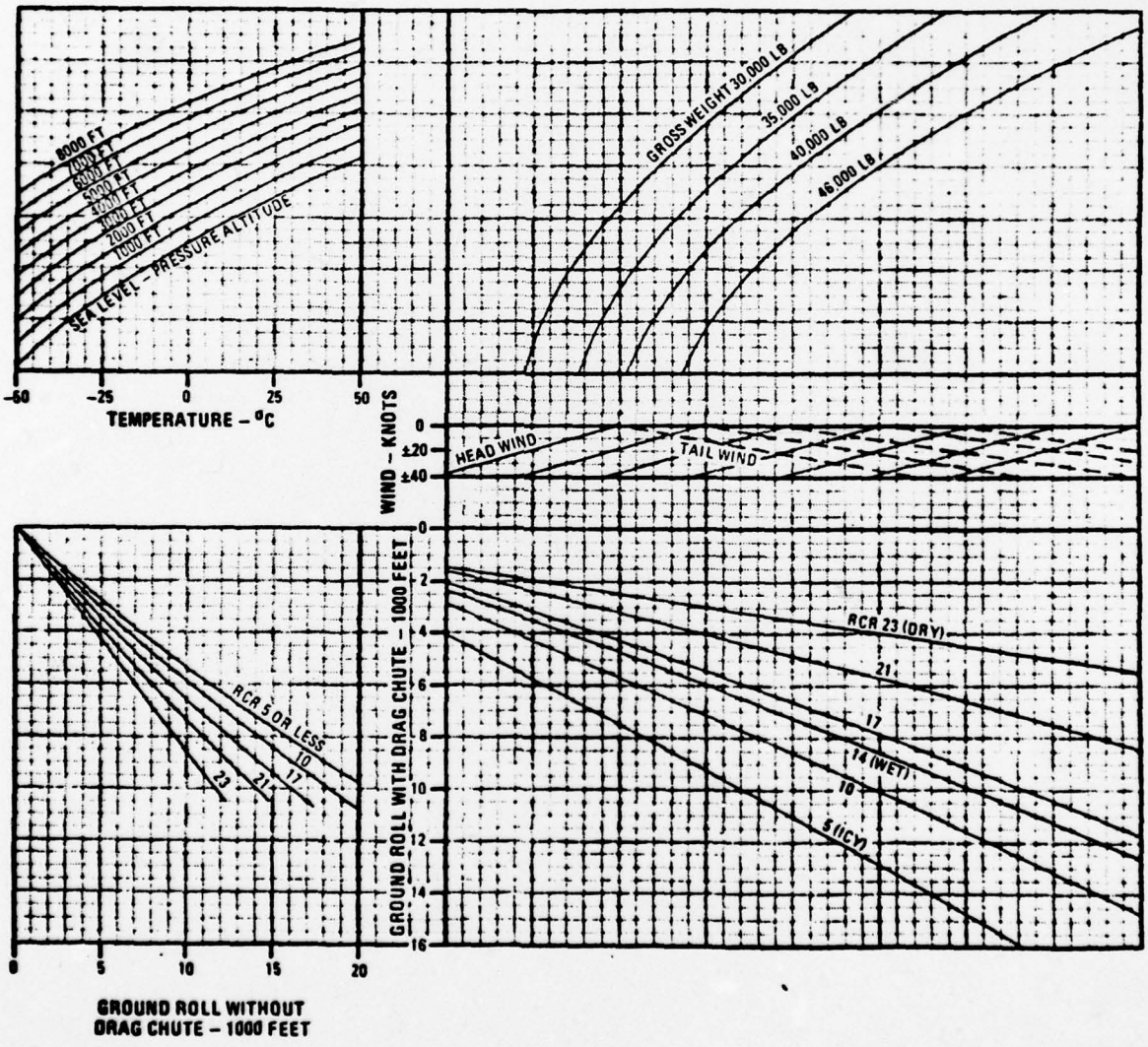

Fig. 72. F-4E Landing Roll Distance

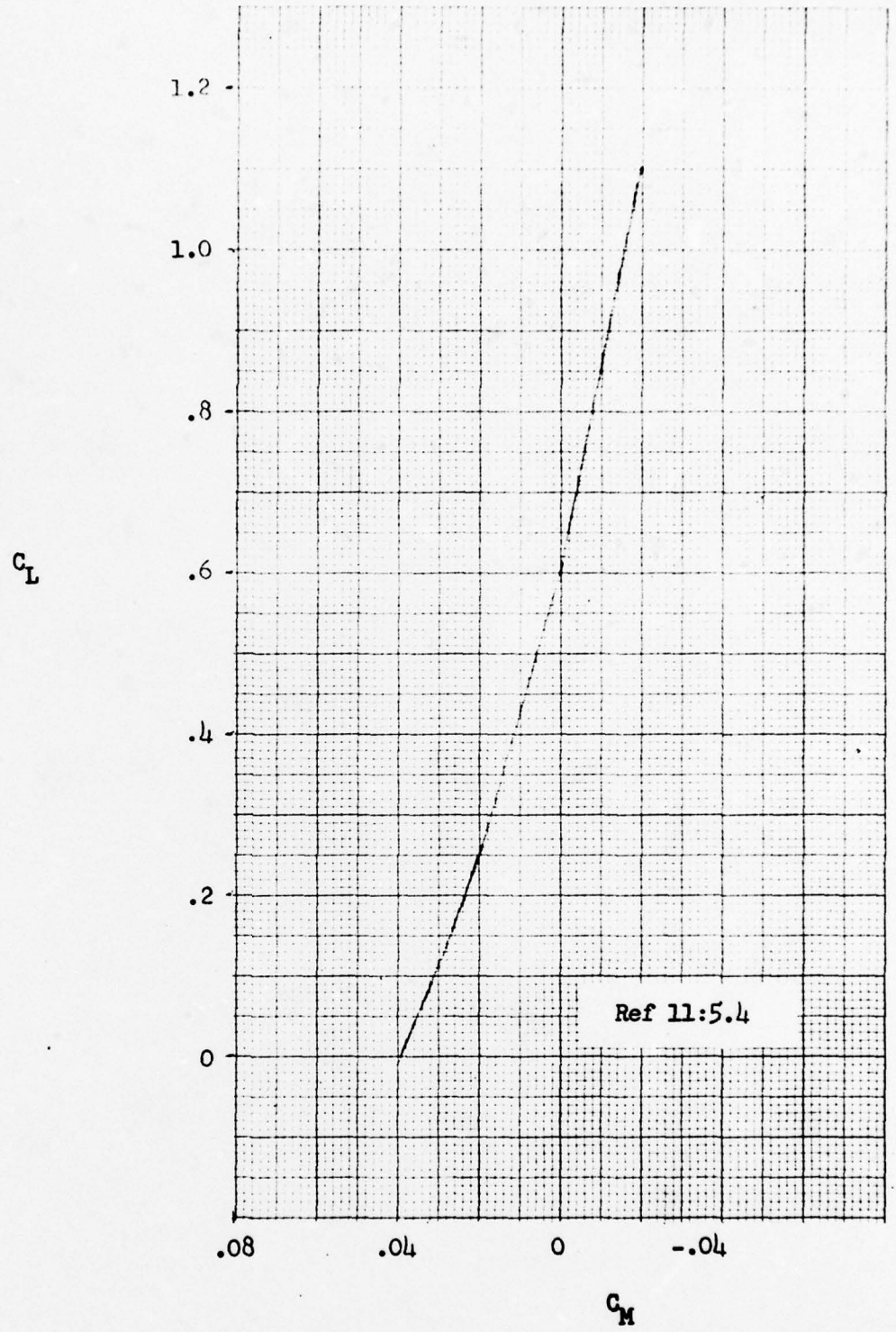

Fig 73 Untrimmed C_M vs. C_L for F-4E, Approach Configuration

Vita

John Anthony Skorupa was born 23 October 1947 in Chester, Pennsylvania. He graduated from high school in Claymont, Delaware, in 1965 and received a Bachelor of Science degree from the USAF Academy in 1969. After pilot training at Williams AFB, Arizona, he was assigned to the 37th Tactical Airlift Squadron at Langley AFB, Virginia. While at Langley he accumulated 2000 hours in the C-130E while upgrading to instructor pilot and flying such varied missions as diplomatic support in South America, logistic support in Egypt for clearing the Suez Canal, Airborne Command and Control Center for joint NATO exercises, flare drop for night attack missions, and P.O.W. exchange in North Vietnam. Accomplishments at Langley include an additional duty tour with the Director of Airlift Systems, Headquarters Tactical Air Command, during which time he authored several statements of Required Operational Capability to upgrade C-130 communications and air drop capability. In 1975 he entered the School of Engineering, Air Force Institute of Technology.

UNCLASSIFIED

SECURITY CLASSIFICATION OF THIS PAGE *(When Data Entered)*

REPORT DOCUMENTATION PAGE		READ INSTRUCTIONS BEFORE COMPLETING FORM
1. REPORT NUMBER GAE/MC/76D-7	2. GOVT ACCESSION NO.	3. RECIPIENT'S CATALOG NUMBER
4. TITLE *(and Subtitle)* System Simulation in Aircraft Landing Gear and Tire Development		5. TYPE OF REPORT & PERIOD COVERED 6. PERFORMING ORG. REPORT NUMBER
7. AUTHOR(s) John A. Skorupa Captain USAF		8. CONTRACT OR GRANT NUMBER(s)
9. PERFORMING ORGANIZATION NAME AND ADDRESS Air Force Institute of Technology Wright-Patterson AFB, Ohio 45433		10. PROGRAM ELEMENT, PROJECT, TASK AREA & WORK UNIT NUMBERS
11. CONTROLLING OFFICE NAME AND ADDRESS Air Force Institute of Technology Wright-Patterson AFB, Ohio 45433		12. REPORT DATE December 1976 13. NUMBER OF PAGES 137
14. MONITORING AGENCY NAME & ADDRESS *(if different from Controlling Office)*		15. SECURITY CLASS. *(of this report)* UNCLASSIFIED 15a. DECLASSIFICATION/DOWNGRADING SCHEDULE

16. DISTRIBUTION STATEMENT *(of this Report)*

Approved for Public Release; Distribution Unlimited

17. DISTRIBUTION STATEMENT *(of the abstract entered in Block 20, if different from Report)*

18. SUPPLEMENTARY NOTES

Approved for Public Release; IAW AFR/190-17.

Jerral F. Guess, Captain, USAF
Director of Information

19. KEY WORDS *(Continue on reverse side if necessary and identify by block number)*

Landing Gear
Tire
System Simulation

20. ABSTRACT *(Continue on reverse side if necessary and identify by block number)*

Main gear load vs. time is predicted for an F-4E aircraft through the use of subsystem modeling and analog computation. Subsystems modeled are the aerodynamics, engine dynamics, vertical strut dynamics, fore-aft strut dynamics, tire/wheel dynamics, brake dynamics, and anti-skid dynamics. The problem is restricted to a landing sequence with three degrees of freedom permitted for the

DD FORM 1 JAN 73 1473 EDITION OF 1 NOV 65 IS OBSOLETE

UNCLASSIFIED

SECURITY CLASSIFICATION OF THIS PAGE *(When Data Entered)*

Block 20.

aircraft. Aerodynamics are based on constant coefficients of lift, drag, and pitching moment. A drag chute is also employed. Engine dynamics are based on a linear thrust vs. velocity schedule. The strut dynamics are modeled by a mass-spring-damper system. The tire/wheel dynamics subsystem applies Newton's Second Law to derive the wheel velocity, and calculates the wheel slip ratio and ground-tire coefficient of friction. Brake dynamics are based on a schedule of brake torque vs. brake pressure. Antiskid dynamics model the Hytrol Mark II antiskid system. Stopping distances from simulation are compared to flight test data to verify the model.

Results from the simulation agree with flight test data. A schedule of main gear load vs. velocity is proposed as an alternative to current tire testing practice.